Mechanistic Studies of Radical-Driven Peptide Tandem Mass Spectrometry: Implications for Tyrosine Sulfation Analysis and Higher Order Protein Structural Characterization

by

Eunju Jang

A dissertation submitted in partial fulfillment
of the requirements for the degree of
Doctor of Philosophy
(Chemistry)
in the University of Michigan
2022

Doctoral Committee:

Professor Kristina I. Håkansson, Chair
Professor Robert T. Kennedy
Professor Alexey Nesvizhskii
Professor Brandon T. Ruotolo

Eunju Jang

jangej@umich.edu

ORCID iD: 0000-0002-2034-3110

My greatest treasure is, was, and always will be my family

Acknowledgements

I would like to express my sincere appreciation to all people who supported and guided me toward my Ph.D thesis.

First, I would like to thank my research advisor, Dr. Kristina Håkansson for her guidance and support throughout my graduate research. Her patient and positive attitude always inspired me and her advice, and support guided me to overcome the challenges during my research. I would like to thank Professor Robert T. Kennedy, Professor Alexey Nesvizhskii, and Professor Brandon T. Ruotolo for serving as my committee members. From the candidacy exam to the defense, their insightful comments and suggestions helped me to complete the graduation requirements.

I want to thank all my previous and current lab mates: Dr. Hye Kyong Kweon, Dr. Nick Borotto, Dr. Isaac Agyekum, Dr. Qingyi Wang, Nhat Le, Carson Szot, Josh Salem, LeeAnne Wang, and James Brunemann. I am happy that I could work with smart, kind, and wonderful lab mates during my time in graduate school and they inspired me over the many years. I have so many precious memories and stories.

My research was funded by NIH and NSF grants, a Winter departmental fellowship, a Rackham Travel Grant, and a Rackham Research Grant. I would like to thank these funding sources for allowing me to continue research and broaden my insights through attending several conferences. Also, I would like to thank the Chemistry Department for providing professional development programs such as mentoring and teaching opportunities. These programs greatly helped me develop myself.

I also want to thank the mass spectrometry group at Merck South San Francisco. Especially, I greatly appreciate Dr. Fengfei Ma for great mentorship and support during my internship. I learned more about industrial research as well as the inner workings of a pharmaceutical company.

To all my friends in South Korea and the US, I am deeply grateful that I could meet you all and spend a wonderful time together. I'll never forget your willingness to help me, to encourage me, to cheer me on. I want to express special thanks to my Ann Arbor friends, Federica, Lexie, Paola, Yeori, Minsik, and SungJin. We went through hard times together, and celebrated each accomplishment. Let's keep in touch!

Finally, I express my sincere gratitude to my family members for their emotional support. Family members are my motivation and everything. I deeply thank my parents, Jongbung Jang and Heeja Yang for their unconditional love. Thank you for always being there and encouraging me. I couldn't have completed this dissertation without your endless support. I also thank my younger brother, Hojin Jang, for his quiet encouragement.

Eunju Jang

3/23/2022

Ann Arbor, Michigan

Table of Contents

List of Tables

List of Figures

List of Abbreviations

CCS	Collisional Cross Section
CEM	Charge Ejection Model
CI	Chemical ionization
CID	Collision Induced Dissociation
CRM	Charge Residue Model
DABCO	1,4-diazabicyclo[2.2.2]octane
DMSO	Dimethyl Sulfoxide
ECD	Electron Capture Dissociation
EDD	Electron Detachment Dissociation
ESI	Electrospray Ionization
ETciD	Electron Transfer with Collision Induced Dissociation
ETD	Electron Transfer Dissociation
EThcD	Electron Transfer with Higher Energy Collision Dissociation
FRIPS	Free Radical Initiated Peptide Sequencing
FT-ICR	Fourier Transform-Ion Cyclotron Resonance
H/D	Hydrogen/Deuterium
HCD	High-Energy Collision Dissociation
HDX	Hydrogen Deuterium Exchange

HPCA	1H-pyrazole-1-carboxamidine hydrochloride
HPLC	High Performance Liquid Chromatography
HX	Hydrogen Exchange
IAM	Iodoacetamide
IEM	Ion Ejection Model
IM	Ion Mobility
IMAC	Immobilized Metal Affinity Chromatography
IR	Infrared
IRMPD	Infrared Multiphoton Dissociation
iTRAQ	Isobaric Tags for Relative and Absolute Quantitation
IVR	Intramolecular Vibrational-energy Redistribution
LC	Liquid Chromatography
LTQ	Linear Trap Quadrupole
m/z	Mass-to-Charge Ratio
MOAC	Metal Oxide Affinity Chromatography
MS	Mass Spectrometry
MS/MS	Tandem mass spectrometry
NEM	N-ethylmaleimide
nESI	Nano Electrospray ionization
nETD	Negative-Ion Electron Transfer dissocitaion
nFRIPS	Negative-Ion Free Radical Initiated Peptide Sequencing
NHS	N-Hydroxysuccinimide
niECD	Negative-Ion Electron Capture Dissociation

NMR	Nuclear Magnetic Resonance
nUVPD	Negative-Ion Ultravioloet Photo Dissocitation
PAPS	3'-phosphoadenosine 5'-phosphosulfate
PTM	Posttranslational Modification
Q	Quadrupole
RF	Radio Frequency
RPLC	Reversed-Phase Liquid Chromatography
SCX	Strong Cation Exchange
TEA	Triethylamine
TEAB	Triethylaminei bicarbonate
TEMPO	2,2,6,6-tetramethylpiperidine- 1-oxy
TFA	Trifluoroacetic Acid
TMT	Tandem Mass Tag
TOF	Time-of-Flight
TPST1	Tyrosylprotein Sulfotransferase1
UVPD	Ultraviolet Photodissociation
VP	1-Methyl-2-vinylpyridinium

Abstract

Three-dimensional structure, established by the amino acid sequence, determines protein function. The amino acid sequence can be identified via tandem mass spectrometry (MS/MS) whereas hydrogen/deuterium exchange (HDX)-liquid chromatography/MS is widely used for determination of protein conformation. In this dissertation, mechanistic studies of radical-driven peptide MS/MS are presented for improved identification of the highly labile, biologically important posttranslational modification (PTM) tyrosine sulfation, and for enhanced structural resolution in HDX-MS.

The generalizability of the alternative MS/MS method free radical initiated peptide sequencing (FRIPS) is explored in Chapter 2. We show that competition between desired radical-driven fragmentation pathways and undesired mobile proton-driven pathways appears dependent on the peptide charge state. Lower charge states promote radical-driven dissociation with high sequence coverage. Alternative positive ion mode charge carriers, including sodium and calcium ions, are shown to restore radical-driven fragmentation for peptides lacking basic amino acid residues.

Tyrosine sulfation is particularly challenging to characterize in positive ion mode MS. In Chapter 3, the influence of basic amino acid residues and peptide chemical modifications on sulfopeptide stability are examined. We show that guanidination increases sulfopeptide stability during electrospray ionization and improves sulfate retention during MS/MS. We hypothesize that such groups may stabilize sulfate groups via salt bridge formation and/or by sequestering protons.

Cysteine modifications also affect sulfopeptide stability. In particular, alkylation with fixed positive charge-containing vinyl pyridine resulted in several sulfate-retaining fragment ions following electron transfer dissociation (ETD). Such sulfated fragments allow direct sulfotyrosine identification within a peptide, a feat that has been elusive to date.

Even more challenging is the determination of a sulfation site in peptides containing multiple tyrosine residues. In Chapter 4, the insights from Chapter 3 were applied towards sulfation site determination in a tyrosylprotein sulfotransferase 1 (TPST1) singly sulfated peptide containing three tyrosines. This peptide was previously detected in a proteomic analysis of rat liver Golgi; however, complete desulfation was observed upon higher energy collision dissociation (HCD) MS/MS. Both ETD and electron capture dissociation (ECD) allowed sulfation site determination in a synthetic, unmodified TPST1 tryptic peptide sulfated on the third tyrosine Guanidination resulted in the observation of sulfated fragment ions for the other two sulfopeptide isomers; however, lack of characteristic fragments precluded unambiguous identification of the sulfation site in these two sulfopeptides. By contrast, negative ion mode FRIPS was explored and enabled sulfation site determination in these two sulfopeptide isomers.

Chapter 5 probes the degree of hydrogen/deuterium scrambling prior to ECD (which does not incur H/D scrambling) as a function of peptide size. “Soft” ion source/transfer conditions were previously shown to prevent scrambling for a 12-mer model peptide; however, such conditions typically significantly reduce ion abundance. We hypothesized that larger peptides may be more tolerant to typical ion source/transfer conditions, thus allowing wider implementation of ECD for enhancing structural resolution. Indeed we found that a shorter, 10-mer, peptide showed a higher degree of scrambling under the same “soft” conditions. By contrast, under “harsh” conditions where signal abundance is higher and the 12-mer peptide undergoes nearly compete scrambling, a

longer, 16-mer, peptide showed moderate scrambling. Overall, the mechanistic studies and chemical derivatization strategies described in this dissertation will allow implementation of improved radical driven MS/MS methods to enable deeper insights into protein structure.

Chapter 1

Introduction

1.1 Mass Spectrometry Based Protein Structural Characterization

Proteins are important biological molecules in living cells, involved in cellular structure, activity, signaling, and catalysis [1]. The ribosome synthesizes proteins based on mRNA templates, a process termed translation, and each protein has a unique amino acid sequence or primary structure [2]. Protein folding is determined by their amino acid sequence and the complexity of this higher order structure can be classified into secondary, tertiary, and quaternary structures [3]. The secondary structure is defined as the local spatial conformation of amino acids in the forms of alpha helices, beta sheets, and turns [3,4]. Protein tertiary structure is composed of the coordination of secondary structures and all amino acid functional groups to form a distinct three-dimensional shape. Finally, quaternary structure is the arrangement of several proteins into a complex [3].

Depending on the biological function in the cell, proteins translated from the ribosome may require further chemical modification, termed posttranslational modification (PTM) [2]. PTM involves enzymatic or non-enzymatic addition or removal of chemical moieties to amino acid residues. PTMs include, e.g., phosphorylation, glycosylation, sulfation, and acetylation, and these chemical alterations play important roles in regulation, immunity, cellular recognition, etc. [5]. Peptide and protein structural information can be obtained by measuring molecular weights of

intact analytes and their fragments through mass spectrometry (MS). A mass spectrometer consists of three main parts: an ionization source, a mass analyzer, and a detector [6]. Gas phase analyte ions are generated by the ionization source, and the mass-to-charge (m/z) ratios of these ions are measured by the mass analyzer and the detector [6,7]. MS is well established as a method of choice for analyzing complex protein samples due to high sensitivity, high accuracy, and rapid acquisition speed [6,8]. With the advancement in mass spectrometry instrumentation, improved sample preparation methods, and availability of sequenced genomes, MS-based proteomics enables insight into complex biological samples, including, e.g., organelles, membranes, biofluids, cells, tissues, organs, and microbial communities [9,10].

1.1.1 Bottom-up, Top-down, and Middle-down Proteomics Approaches

The bottom-up and top-down approaches are commonly employed in proteomics research. The bottom-up approach, or shotgun proteomics, refers to the characterization of proteins following digestion into peptides via proteolytic enzymes [1,10]. Typically these peptide mixtures are subjected to liquid chromatography (LC) separation coupled with MS. The bottom-up approach is universally adopted for proteomics because peptides have high solubility, are readily separated with reverse phase liquid chromatography (RPLC), and yield structurally informative fragmentation in tandem MS (MS/MS) (see below) [11]. Trypsin has become the gold standard for protein digestion due to its high specificity [12]. Also, because trypsin cleaves the protein backbone at the C-terminal side of arginine and lysine residues, [13] each peptide will contain at least two basic sites for MS ionization (the peptide N-terminus is the second site). For highly complex samples, multiple chromatographic methods can be combined with a popular approach being strong cation exchange (SCX) followed by RPLC [14]. Sequence informative peptide fragment ions allow peptide identification via sequence databases and bioinformatics tools [15,16].

Unlike the bottom-up approach, the top-down approach does not involve proteolytic cleavage prior to MS analysis, i.e., intact proteins or protein complexes are directly analyzed. This approach includes a number of advantages, including improved characterization of proteoforms and global PTM analysis. However, the top-down approach presents several analytical challenges, including lower ionization efficiency of intact proteins, more challenging chromatography, and lower fragmentation efficiency [17]. The middle-down approach incorporates features from both the bottom-up and the top-down approaches. Similar to the bottom-up strategy, the middle-down approach involves proteolytic cleavage of proteins, but the resulting peptides are longer (2.5 kDa to 10 kDa) than in the bottom-up approach (0.8 kDa to 2 kDa) [18]. Unlike the top-down strategy, the middle-down approach is not limited by protein size. The generation of larger peptides reduces the sample complexity due to the lower number of resulting peptides from the proteolysis step. Other advantages of this approach are the improved detection of post-translational modifications, and the improved sequence coverage compared with the top-down approach [19].

1.1.2 Protein Tyrosine Sulfation

Tyrosine sulfation is a PTM that is enzymatically introduced by tyrosylprotein sulfotransferases (TPSTs) from the donor molecule 3'-phosphoadenosine 5'- phosphosulfate (PAPS) to form tyrosine O-sulfate esters [20,21] (Fig. 1.1). It has been reported that up to 1% of tyrosine residues can be sulfated in eukaryotic organisms [22].

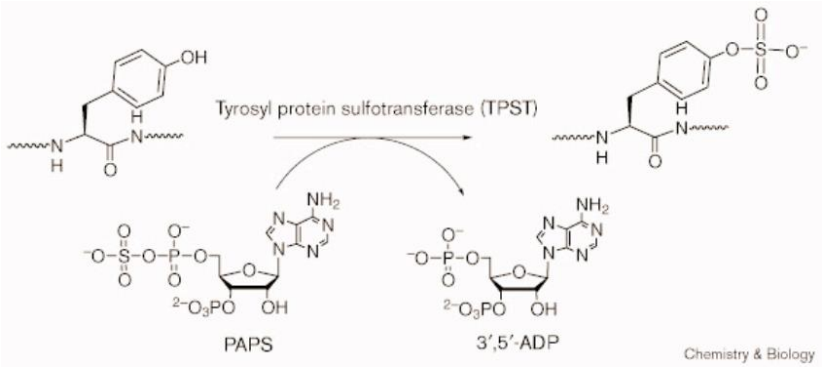

Figure 1.1 Enzymatic sulfonate transfer from 3'-phosphoadenosine 5'- phosphosulfate (PAPS) to the hydroxyl group of tyrosine [23].

Tyrosine sulfation occurs in the trans-Golgi network [22,23] with the TPST active site being luminally oriented. This PTM has a lack of reversibility in vivo, thus protein desulfation is unlikely to occur during transport to the cell surface or in secretory granules [22]. Tyrosine sulfation plays important role in protein-protein interactions such as receptor binding [23]. This PTM can be found in secretory and transmembrane proteins, such as P-selection glycoprotein ligand-1, hirudin, G-protein-coupled receptor, chemokine receptor, HIV-co-receptor, and antibodies [20,24]. However, there are limitations in the analysis of tyrosine sulfation through MS. Positive ion mode MS is typically used for proteomics workflows. However, facile loss of SO_3 during both ESI and tandem MS fragmentation occurs due to the high lability of sulfate group [25,26], thus often precluding sulfation site determination. Improved localization of sulfation can be achieved by using adducts, such as metal ions [25], and guanidinium ions [27]. Another challenge to the sulfation analysis is the small mass difference between sulfation and phosphorylation (HPO_3), only 9.5 mDa [28]. Thus high resolution FT-based instruments are required to confidently annotate this modification.

1.2 Mass Spectrometry Instrumentation

1.2.1 Electrospray Ionization

The soft ionization method electrospray ionization (ESI; Fig. 1.2) was introduced by Fenn and co-workers [29]. ESI is soft enough to even preserve weak noncovalent interactions during ionization and gas-phase transfer [30]. An intrinsic trait of ESI for large biomolecules is the generation of multiply charged ions, which allow the corresponding m/z values to fall into the effective mass range of any mass analyzer [31]. ESI is directly compatible with HPLC and has become an invaluable analytical tool for the analysis of small and large molecules in complex sample mixtures [32].

Under typical ESI conditions, sample solution flows into an ESI emitter at microliter per minute flow rates, and a high voltage (up to 6 kV) is applied between this spray needle tip and the entrance to the mass spectrometer, e.g., a heated capillary [33]. The strong electric field at the emitter tip results in Coulomb destabilization at the meniscus, generating an aerosol of charged droplets. The production of these charged droplets is an electrochemical process with the electron flow depending on the polarity of the electric field. In positive ion mode, oxidation reactions occur at the liquid/metal interface of the spray capillary, releasing electrons through the contact that supplies the electric potential [32,34]. This oxidation reaction can be summarized as:

Equation 1.1

$$Metal(s) \rightarrow Metal^{2+}(aq) + 2e^{-}$$

$$4OH^{-}(aq) \rightarrow O_2(g) + 2H_2O + 4e^{-}$$

Water and methanol are commonly used ESI solvents and the oxidation reaction results in the production of excess protons (H^+) inside the solution[35]. In the presence of the applied electric field, excess positive charges accumulate at the emitter tip [32], leading to the surface destabilization, and formation of a Taylor cone at the emitter tip [36]. Under the high electric field, charged droplets are ejected as a fine jet of liquid from the Taylor cone and move towards the

typically heated inlet of the mass spectrometer. Micrometer size droplets are initially formed [37]. Sheath gas (usually N_2) can be used for improved nebulization and drying gas is often applied to enhance solvent evaporation from the charged droplets, resulting in decreased droplet size [38]. With the assistance of drying gas and/or a heated inlet, the droplet size keeps decreasing until it reaches the Rayleigh limit [39]. At this limit, Coulomb repulsion exceeds surface tension, resulting in droplet fission into smaller droplets [40]. These offspring droplets continue to shrink and divide, thus generating even smaller droplets with the higher charge to mass ratio than the original droplets [32].

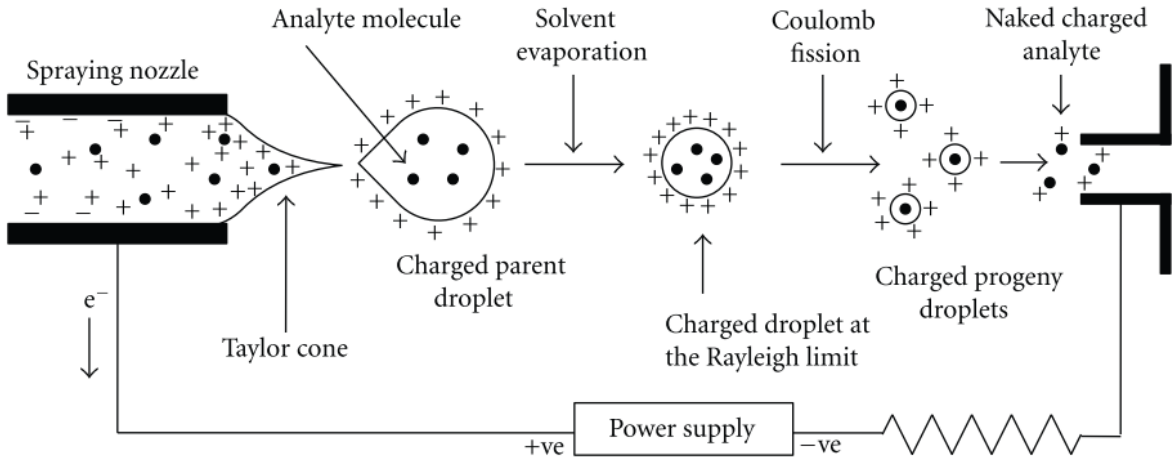

Figure 1.2 Positive ion mode electrospray ionization process [32].

Nano-electrospray ionization (nESI) uses lower flow rates at the nL/min scale and lower spray voltages are applied compared with conventional ESI [41]. Because nESI involves a smaller emitter diameter, the initial droplet size is smaller, in the nanometer range, and, therefore, a lower number of evaporation and fission events occurs [42]. The advantages of nESI are low sample consumption, increased sensitivity, and enhanced ionization efficiency [32].

1.2.2 Fourier Transform Ion Cyclotron Resonance Mass Spectrometry

Fourier transform ion cyclotron resonance (FT-ICR) mass spectrometry [43,44] was introduced by Comisarow and Marshall in 1974. FT-ICR MS provides high resolution, high accuracy, ion storage, and multi-tandem mass spectrometric capability [45,46], which provides great advantages in organic, inorganic, physical, and biotechnological research [47]. An FT-ICR mass analyzer consists of three main components: a superconductive magnet, an ultrahigh vacuum system, and an analyzer cell [47]. Higher magnetic field strength has several advantages, including improved upper mass limit, maximum ion kinetic energy, the maximum number of trapped ions, maximum ion trapping duration, and mass resolving power [48]. Magnetic field strengths of 7 Tesla (T) – 15 T are commercially available through Bruker, and the world's highest magnetic field strength for FT-ICR MS, 21 T, is available at the National High Magnetic Field Laboratory [49] and the Environmental Molecular Sciences Laboratory [50]. An ultrahigh vacuum system, in the range of 10^{-9} – 10^{-10} Torr, is required for FT-ICR MS because ions travel significant distances during typical detection times (milliseconds to seconds) required for high mass resolution [51]. To achieve such low pressure, multiple turbomolecular pumps are typically employed in stages. The ICR analyzer cell stores and detects ions. Several cell designs, such as cubic or cylindrical, have been used with the open-ended cylindrical cell being popular. The "infinity cell" [46] is a closed cylindrical design composed of two excitation plates, two detection plates, and two trapping plates located at the two ends of the cell. The magnetic field confines ions radially inside the cell whereas the trapping plates confine the ions axially via an applied weak electrostatic field (Figure. 1.3).

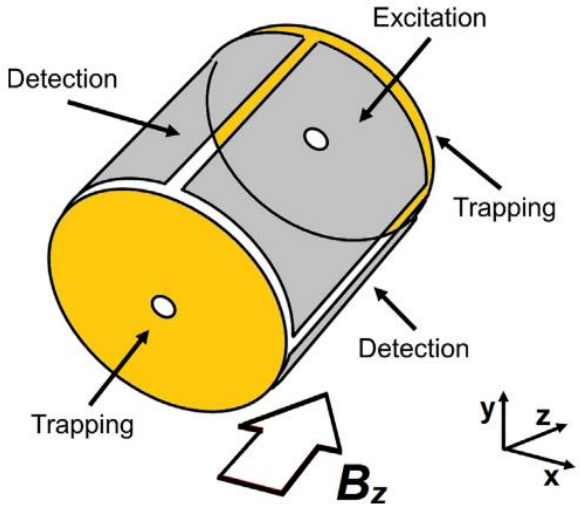

Figure 1.3 Schematic representation of a closed cylindrical cell. The magnetic field axis is parallel with the trapping axis (z-axis). The trapping electrodes are located at the front and the end of the cell [52].

The latest development in ICR cell technology, the harmonized cell, for example, the so-called "ParaCell" from Bruker [53], allows further improved resolving power and excitation range.

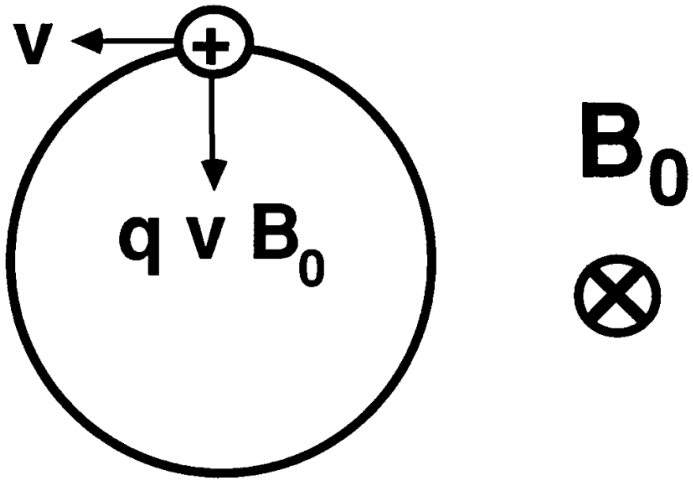

Figure 1.4 Ion cyclotron motion of a positively charged ion having a velocity, v [54].

Ions trapped within the ICR cell are affected by the magnetic and electric fields, resulting in three major motions: cyclotron motion, magnetron motion, and trapping motion [55]. Ion cyclotron motion is illustrated in Figure 1.4. When ions with a velocity component, *v*, in the xy-

plane (assuming the magnetic field is along the z axis) enter the ICR cell, they experience the Lorentz force, perpendicular to the field, resulting in circular orbits at characteristic cyclotron frequencies [55]. This angular cyclotron motion, ω, can be described as:

Equation 1.2

$$\omega = \frac{q}{m} B_0$$

where q is the analyte charge, B_0 is the magnetic field strength, and m is the analyte mass. The radius of this cyclotron orbit depends on the ion's kinetic energy; however, the angular frequency does not, thus yielding high resolution.

In addition to the cyclotron motion (Fig. 1.3), ions undergo axial oscillation due to the trapping electric field[56]. The combination of this electric field and the magnetic field also cause ion magnetron motion [57]. This motion causes the center of the cyclotron motion to precess around the ICR cell and defines the detectable, reduced cyclotron frequency [55].

Ions with different m/z values can be detected simultaneously in the ICR cell by applying an external radiofrequency (RF) frequency sweep to the excitation plates [57]. When the externally amplified RF frequency matches the ion cyclotron frequency, ions absorb energy and move in a larger cyclotron orbit [47]. This increasing cyclotron radius causes ions to move closer to the detection plates, thus attracting electrons in a periodic manner with a frequency equal to their cyclotron frequency. The resulting alternating electrical current, i.e., the image current [58], is recorded in the time domain. The corresponding signal is then converted to the frequency domain through Fourier transformation to yield the corresponding mass spectrum, per equation 1.2. [58].

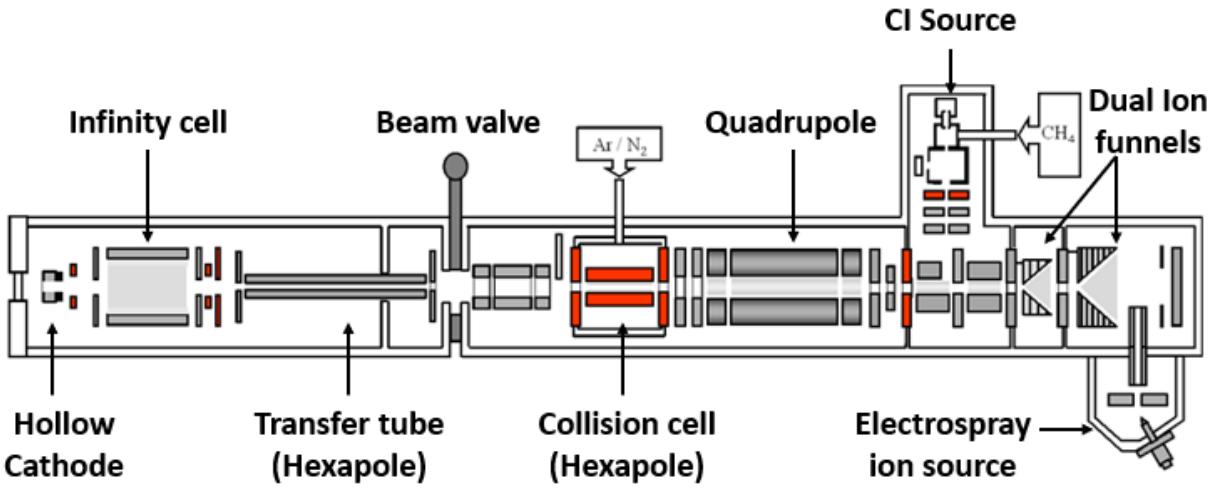

Figure 1.5 Schematic diagram of a 7T SolariX quadrupole FT-ICR mass spectrometer (Bruker Daltonics) in the Håkansson lab.

A diagram of a 7T FT-ICR mass spectrometer, available in the Håkansson lab, is shown in Figure 1.5. This instrument comprises an Apollo II ESI source, dual ion funnels for improved focusing and transmission, a chemical ionization (CI) source for the generation of reagent for electron transfer dissociation (ETD, see below), a quadrupole mass filter (Q) for m/z selection, a hexapole collision cell for beam-type collision induced dissociation (CID), a transfer hexapole, an ICR Infinity cell, a hollow dispenser cathode for ion-electron reactions, and a CO_2 infrared laser for infrared multiphoton dissociation (IRMPD). Ions are generated via ESI and pass through an inlet glass capillary and the ion funnels as well as multiple ion guides before reaching the ICR cell. This instrument provides diverse tandem mass spectrometric methods in both positive and negative polarities, including CID, ECD, ETD, negative ion electron capture dissociation (niECD), electron detachment dissociation (EDD), and IRMPD, thus allowing state-of-the-art protein structure analysis capabilities.

1.2.3 Orbitrap Fourier Transform Mass Spectrometry

The Orbitrap is the newest mass analyzer developed by Makarov [59]. The first commercial instrument, a hybrid design that couples a linear quadrupole ion trap (LTQ) [60] and Orbitrap, was introduced in 2006 [61]. Since then this hybrid instrument design has received significant attention because of the high mass resolution, high space charge capacity, high mass accuracy, high dynamic range, and rapid MS/MS scan speed [62]. Orbitrap MS employs several features from conventional mass analyzers. Similar to FT-ICR MS, ion detection occurs through time-domain image current followed by Fourier transformation, and ion packets are pulsed into the Orbitrap, similar to time-of-flight (TOF) mass analyzers [62]. This pulsing occurs through a so called C-trap, which ensures ion packets have narrow axial distributions. However, the Orbitrap design is unique with two outer cup-shaped electrodes and a spindle-like central electrode [59]. Orbitrap MS exclusively uses an electrostatic field with no RF or magnetic field required to trap ions [63]. Ions inside the analyzer exhibit three types of motions, including rotational motion, radial motion, and axial oscillation, which combine to generate an overall spiral motion [62]. Ions are trapped around the central electrode by the radial electric field, but ion m/z values are determined by the oscillation frequency along the electric field axis [64]. The frequency of axial oscillation, ω, is described as:

Equation 1.3

$$\omega = \sqrt{\frac{e}{(m/z)}k}$$

where e is the elementary charge (1.602×10^{-19} C), and k is the field curvature. This equation demonstrates that the frequencies of ion axial oscillation are governed by the shape and geometry of the Orbitrap electrodes. The detected image current is generated between the two outer electrodes when ion packets oscillate along the axial direction [65].

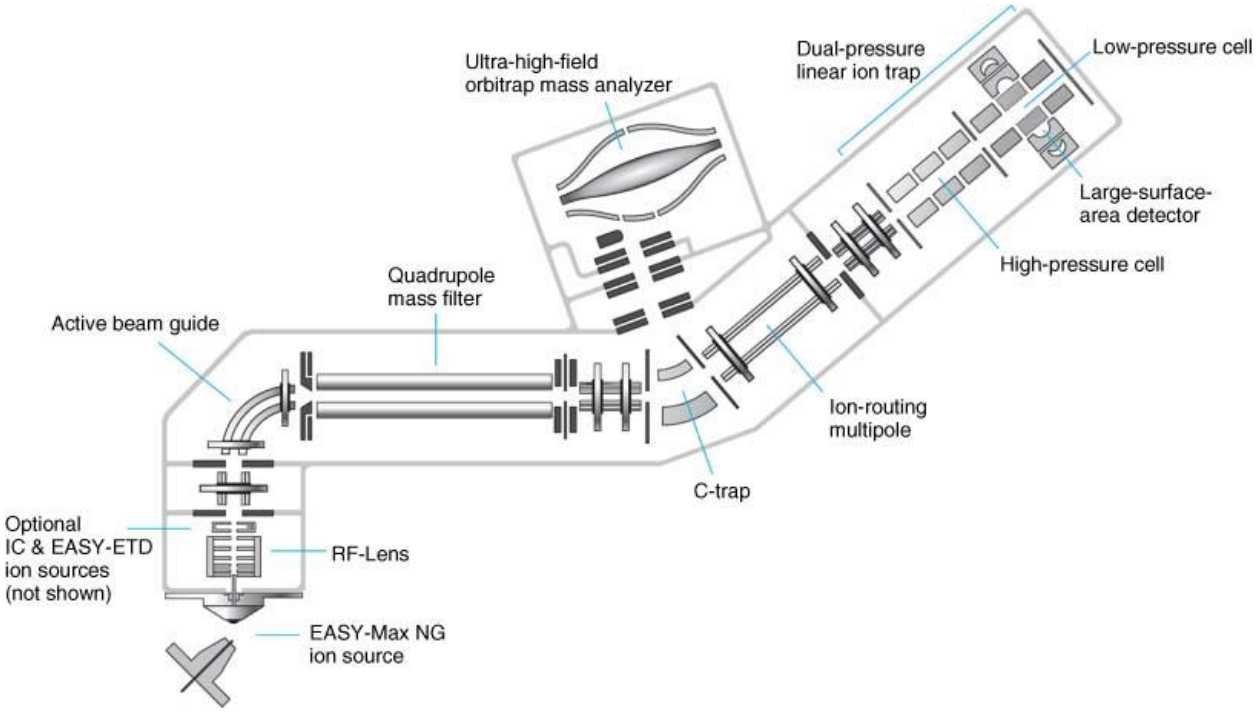

Figure 1.6 Schematic diagram of an Orbitrap Fusion Lumos mass spectrometer (Thermo Scientific).

Figure 1.6 shows a schematic diagram of an Orbitrap Fusion Lumos Tribrid instrument, which, in addition to the Orbitrap and linear ion trap, also contains a quadrupole mass filter. This instrument is equipped with a nano ESI source, an RF lens for reducing chemical noise, an ETD reagent ion source, an ion routing multipole for directing ions to the Orbitrap or ion trap, and for performing higher energy collision dissociation (HCD, a trade name for beam-type CID), and a dual pressure linear ion trap. This instrument has also been custom modified to include a CO_2 IR laser for IRMPD. Thus, similar to FT-ICR, various tandem mass spectrometry methods are available, including HCD, ion trap-type CID, ETD, and IRMPD. Additionally, supplemental activation can be combined with ETD, i.e., ETD followed by HCD (EThcD) [66], and ETD followed by CID [67].

1.3 Tandem Mass Spectrometry Methods

Tandem mass spectrometry provides structural information through gas-phase bond cleavages to yield structurally informative fragment ions for a variety of molecules, including pharmaceutical drugs, proteins, and nucleic acids [68]. In MS/MS, a precursor ion is first selected by, e.g., a quadrupole mass filter, and then energy is applied to activate the precursor ions and generate fragment ions. For peptides and proteins, backbone bond cleavage is desired to generate fragment ions differing in mass by the mass of the various amino acids, thus allowing sequence determination. The fragment ions nomenclature for such backbone fragmentation was first proposed by Roepstorff and Fohlman [69], and later replaced with the Biemann system [70]. Peptide backbone C_α-C, C-N, and N-C_α bonds can be cleaved by tandem mass spectrometry. Fragments containing the N-terminus are named *a*, *b*, and *c* ions, respectively; whereas fragments containing the C-terminus are named *x*, *y*, and *z* ions respectively, Fig. 1.7 [71]. Multiple activation methods have been developed that deposit energy into precursor ions based on different physical principles, thus yielding different cleavage preferences [72]. These methods include CID, ECD, ETD, IRMPD, ultraviolet photodissociation (UVPD), niECD, electron detachment dissociation (EDD), and negative ion electron transfer dissociation (nETD). Peptide backbone bond cleavage preferences for most of these methods are shown in Figure 1.7 and the approaches I used in my dissertation work are described in more detail below.

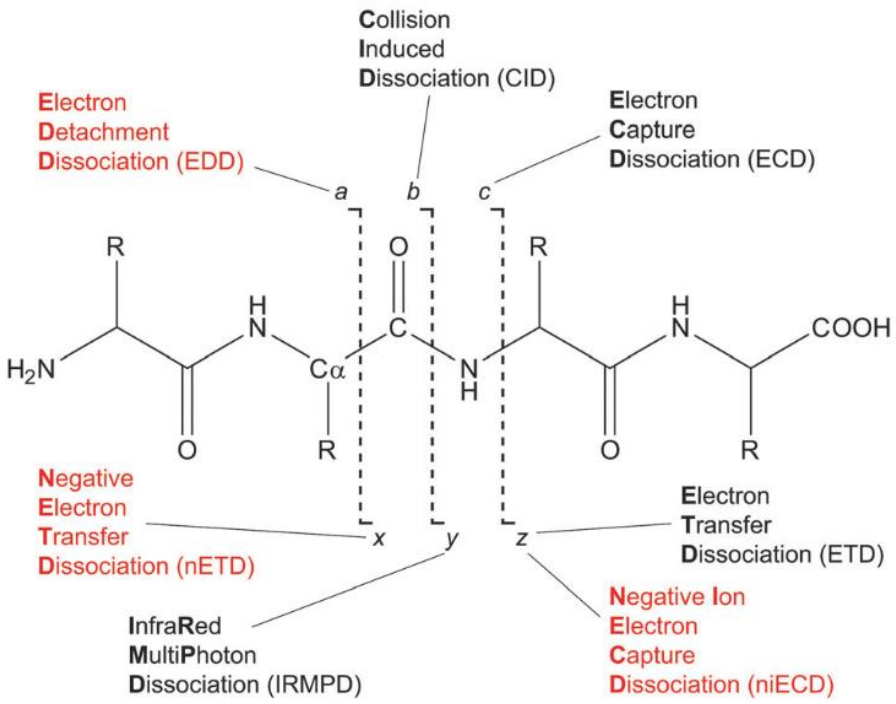

Figure 1.7 Nomenclature of peptide fragment ions and corresponding tandem mass spectrometry techniques [73].

1.3.1 Collision Induced Dissociation (CID)

Collision induced dissociation is the most common MS/MS fragmentation method with utility in a number of applications [74]. In CID, precursor ions are accelerated and collide with neutral gas molecules to increase their internal energy and induce fragmentation. When an ion with high translational energy collides with neutral gas, a portion of the translational energy is converted into internal energy [74]. The amount of translational energy that can be transferred depends on the masses of the precursor ion and the neutral gas, and can be expressed as follows:

Equation 1.4

$$E_{com} = \left(\frac{N}{m_p + N}\right) E_{lab}$$

where E_{lab} is the kinetic energy of the ion, E_{com} is the internal energy increase of the ion, N is the mass of the neutral gas, and m_p is the mass of the precursor ion. Conventionally, up to 100 eV of

laboratory collision energy is utilized in most MS instruments, and N_2 or Ar is used as collision gas [75]. CID is classified as a 'slow heating' method where ion activation occurs on the microsecond to millisecond time scale [76]. CID can be classified into two types: beam type-CID and ion trap type-CID. Beam type-CID, such as higher energy collision dissociation (HCD), is a non-resonant activation CID that occurs in tandem-in-space instruments. The beam of ions are excited and collide with neutral gas by the direct current voltage applied to the collision cell, when the ions axially pass through the collision cell [77]. The dissociation rate of beam type-CID is greater than ~104 /s [78]. On the other hand, ion trap type-CID is a resonant activation CID that involves the activation and deactivation process. Ions that enter the ion trap are deactivated by the collisional cooling process by helium bath gas, followed by the resonant excitation for the dissociation [77]. The time scale for the ion activation and deactivation is range between tens to hundreds of milliseconds, and the dissociation rate is in the range of 1-100 /s [78]. CID cleaves the peptide backbone amide bond, generating sequence informative *b* and *y* fragment ions (Fig. 1.6) along with the loss of small neutral molecules such as water and ammonia. The dissociation of protonated peptides through CID is proposed to occur via the mobile proton model [79]. Initial protonation sites (e.g., basic side chains and the N-terminus) are energetically and kinetically more favorable [80]. However, during collisional activation, protons transfer to the backbone amide nitrogen, which weakens the amide bond and makes it susceptible to nucleophilic attack from a nearby electron rich group, such as the N-terminal carbonyl group [81], yielding the observed *b* and *y*-type ions.

1.3.2 Electron Capture Dissociation(ECD)/Electron Transfer Dissociation (ETD)

Electron capture dissociation was discovered by Zubarev et al. in 1998 [82] via a modified ICR cell and generates *c/z* type peptide fragment ions. In ECD, low-energy, ~1 eV, electrons are

captured by positively charged ions to form radical, charge-reduced cations, which dissociate via peptide N-Cα bond cleavage. ECD has been proposed to be a non-ergodic process involving bond dissociation on a time scale shorter than intramolecular vibrational energy redistribution (IVR) [83]. Thus, labile PTMs and noncovalent interactions can be preserved during activation. An alternative explanation is that addition of a radical site to the peptide backbone weakens backbone bonds to require less energy to fragment than, e.g., a labile PTM [84,85]. In either mechanism, ECD fragmentation is directed by the initial electron capture site rather than bond strength threshold, thus more extensive fragmentation can be achieved [86]. ECD requires multiply-charged precursor ions due to the reduction in charge upon electron capture. The ECD mechanism for peptide fragmentation can be summarized as:

Equation 1.5

$$[M + nH]^{n+} + e^{-}(< 1eV) \rightarrow [M + nH]^{(n-1)+\bullet} \longrightarrow c'/z^{\bullet}$$

where prime(ʻ) denotes the transfer of a hydrogen atom to the *c* fragment, and • denotes a radical site. The Cornell mechanism [82] and the Utah-Washington mechanism [84,85] describe alternative explanations for generation of c' and $z^{\bullet}$-type fragment ions in ECD. In the Cornell mechanism, electrons are proposed to be captured at protonated sites to form a hypervalent radical species. This hypervalent radical releases a hot hydrogen atom that transfers to a nearby backbone carbonyl to yield N-Cα bond cleavage from radical rearrangement. However, this mechanism may not explain generation of *c*- and *z*-type fragment ions from ECD of metal-cationized peptides, and peptides with fixed charge derivatives [87]. The Utah-Washington mechanism [87] instead proposes that electrons are directly captured by backbone amide π* orbitals, Coulomb stabilized by a nearby positively charged site. Intramolecular proton transfer then results in the observed N-C_α bond dissociation. In addition to backbone N-C_α bonds, disulfide bonds are preferentially

cleaved in ECD [88]. ECD is mostly implemented in FT-ICR instruments because the electromagnetic field allows stable electron motion inside the ICR cell, thus providing sufficient reaction time with precursor ions [86]. In early ECD studies, a directly heated filament was used for electron generation [82,89,90]. However, due to the resulting broad electron energy distribution from a filament, the indirectly heated dispenser cathode has replaced the heated filament [91]. Today, implementation of a ring-shaped hollow dispenser cathode allows the combination of ECD and IRMPD, by introducing the IR beam through the center of the dispenser cathode [92].

Electron transfer dissociation uses radical anions as electron donors to transfer electrons to multiply charged positive ions. This MS/MS method was introduced by Syka et al. in 2004 to allow ECD-type fragmentation in ion trap mass analyzers [93]. Similar to ECD, ETD yields *c/z* type fragment ions. The ETD mechanism can be summarized as:

Equation 1.6

$$[M + nH]^{n+} + A^{-\bullet} \rightarrow [M + nH]^{(n-1)+\bullet} \longrightarrow c'/z^{\bullet}$$

While the generated fragment ion types are the same in ECD and ETD, the two methods have major differences in the recombination process and pressure during activation [94]. ECD occurring in an ICR cell where the pressure is very low, results in a recombination energy of 500-800 kJ/mol. On the other hand, ETD, occurring in an ion trap where the pressure is relatively high, involves lower recombination energy and also depend on the electron affinity of the radical anion donor [94]. Thus, the energy deposited to peptide cations upon electron capture/transfer is larger in ECD compared with ETD. This difference can manifest itself through higher fragmentation efficiency. However, ETD is more commonly employed due to its implementation in more widespread ion trap mass spectrometers [73].

1.3.3 Free Radical Initiated Peptide Sequencing (FRIPS)

Free radical promoted peptide fragmentation was first introduced by the Porter group [95]. In their work, lysine side chains were modified to peroxycarbamates and CID of metal adducted modified peptides resulted in radical amine generation through -COOtBu cleavage. This alternative tandem mass spectrometry approach was later termed free radical initiated peptide sequencing (FRIPS) by the Beauchamp group [96]. In their implementation of FRIPS, the free radical initiator Vazo 68 was conjugated to peptide N-termini. A radical site is generated via homolytic bond cleavage within Vazo 68 through collisional activation and this radical is propagated through a subsequent collisional activation step, generating both *c*-/*z*-type and *a*-*x*-type fragments. Later, the amine reactive TEMPO-based radical initiator, *o*-TEMPO-Bz-NHS (ortho-{(2,2,6,6-tetramethylpiperidine-1-oxyl)methyl}benzoic acid N-hydroxysuccinimide ester, Fig. 1.7), was introduced by the Oh group[97]. Due to the ease of conjugation, *o*-TEMPO-Bz-NHS has become more widely used for FRIPS. In MS^2, of *o*-TEMPO-Bz conjugated peptides, homolytic cleavage of the C-O bond via gentle collisional activation releases the highly stable TEMPO radical and generates a radical site on the peptide. Further activation of this radical in MS^3 experiments results in radical-driven fragmentation to yield *a, c, x,* and *z* type ions along with side chain losses[97]. FRIPS can be performed in either positive or negative ion mode with negative ion mode FRIPS (nFRIPS) being shown to be particularly valuable for labile, acidic PTM analysis, including site determination of sulfation and phosphorylation [98]. However, there is a lack of detailed studies on how to drive/optimize the desired radical-driven dissociation pathways in FRIPS.

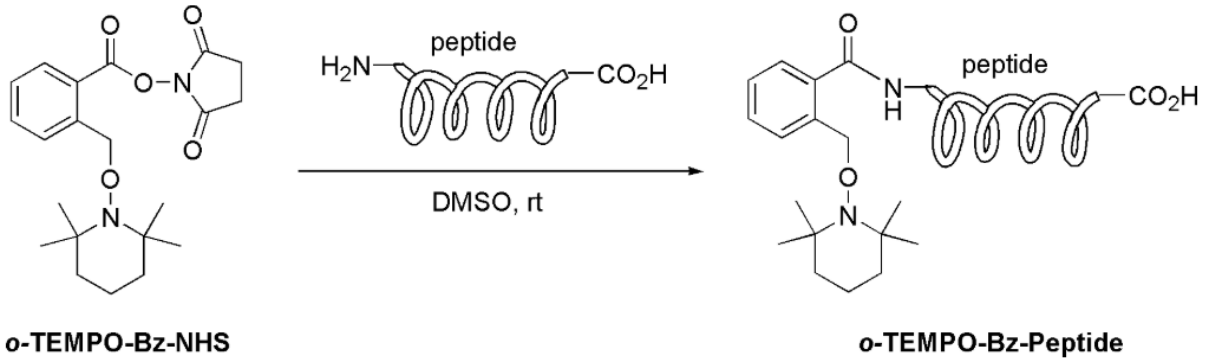

Figure 1.8 Schematic of peptide conjugation reaction with o-TEMPO-Bz-NHS [99].

1.4 Hydrogen/Deuterium Exchange Mass Spectrometry (HDX-MS)

Protein structure can provide the function of proteins involved in biological processes. X-ray crystallography and nuclear magnetic resonance (NMR) spectroscopy are conventional protein structural characterization tools with high spatial resolution. One advantage of X-ray crystallography is its compatibility with large proteins; however it can be limited by crystallization success rate, the requirement for highly pure samples at high concentration [100,101], and limitation in conformational dynamics of macromolecules [102]. NMR spectroscopy allows analysis of protein structure and dynamics in solution, as well as ligand binding, protein-protein interaction, and protein-nucleic acid interaction [102]. However, it is limited by protein size and also requires large sample amounts [100,103]. Mass spectrometry, on the other hand, has emerged as a powerful complementary tool for the characterization of protein conformation and dynamics because it requires much smaller sample amounts (μM), and has less stringent purity requirements [101]. In particular, HDX-MS has been applied to elucidate protein folding, protein-protein-, protein-small molecule-, and protein-membrane interactions [104]. A protein is labeled with deuterium in D_2O and deuterium uptake is measured as a function of exposure time.

Among all the hydrogen atoms in a protein, heteroatom bound hydrogens such as O-H, N-H, and S-H can be exchanged with deuterium atoms under the D_2O buffer [105]. Except for amide

hydrogens, H/D exchange rates are too rapid so the exchange can not be measured by HDX-MS. Unfolded proteins or peptides are influenced by neighboring amino acids effect [106], as well as pH and temperature. Amide hydrogens of folded proteins such as secondary structure reside in core regions that are stabilized through intramolecular hydrogen bonds [107].

1.4.1 Hydrogen/Deuterium Exchange Kinetics

Due to the dynamic nature of proteins, buried or hydrogen bonded backbone amide hydrogens can undergo exchange via exposure to deuterated solvent when proteins are in an 'open' state. The hydrogen exchange of an amide hydrogen in a folded protein can be described as follows [108]:

Equation 1.7

$$NH_{cl} \underset{k_{cl}}{\overset{k_{op}}{\rightleftharpoons}} NH_{op} \xrightarrow[D_2O]{k_{ch}} ND_{op} \underset{k_{op}}{\overset{k_{cl}}{\rightleftharpoons}} ND_{cl}$$

in which NH_{cl}, NH_{op}, ND_{op}, ND_{cl} denotes the amide hydrogen in closed state, and the amide hydrogen in open states, the amide deuteron in open state, and the amide deuteron in closed state, respectively. The rate constant k_{op}, and k_{cl}, represents the rate constant of the opening motion, closing motions, respectively. When proteins are in open state, HDX can occur and the rate constant for HDX is k_{ch}. In native like condition, proteins undergo partial or global opening and closing statuses and the rate constant for HDX can be expressed by the following equation:

Equation 1.8

$$k_{HX} = \frac{k_{op} \cdot k_{ch}}{k_{cl} + k_{ch} + k_{op}}$$

Because stable proteins in the native like condition mostly exist in a closed status $k_{op} << k_{cl}$ and thus, k_{HX} can be simplified as follows:

Equation 1.9

$$k_{HX} = \frac{k_{op} \cdot k_{ch}}{k_{cl} + k_{ch}}$$

HDX behavior can be classified into two exchange regimes, EX1 and EX2[101], based on k_{cl} and k_{ch}. When the hydrogen exchange event occurs faster than the returning to a closed state ($k_{ch} >> k_{cl}$), the EX1 regime applies. Protein motions in EX1 regime can be described as local unfolding, which occurs on milliseconds to days timescale [101]. The rate constant of EX1 hydrogen exchange can be described as:

Equation 1.10

$$k_{HX} = k_{op}$$

When proteins undergo EX1 kinetics, residues participating in unfolding (open state) become deuterated while residues that do not participate in unfolding (closed state) remain unlabled [109,110]. Therefore, a bimodal HDX distribution can be observed [110]. On the other hand, when the reconversion from open to closed state occurs faster than the hydrogen exchange, the EX2 regime applies. Protein motions in the EX2 regime can be described as breathing motions, which occur on microseconds to milliseconds timescale [101]. The rate constant of hydrogen exchange in the EX2 regime is:

Equation 1.11

$$k_{HX} = \frac{k_{op} \cdot k_{ch}}{k_{cl}}$$

Proteins in physiological conditions undergo EX2 kinetics while only a few proteins undergo EX1 kinetics [111].

1.4.2 Bottom up HDX Approach

Bottom-up approaches are typically used for HDX-MS with top-down approaches gaining popularity [112]. The bottom-up approach for HDX-MS (Figure 1.9) involves deuterium labeling, quenching, pepsin digestion (due to low pH requirement for minimizing back exchange), peptic peptide desalting/separation, and mass spectrometry analysis [104].

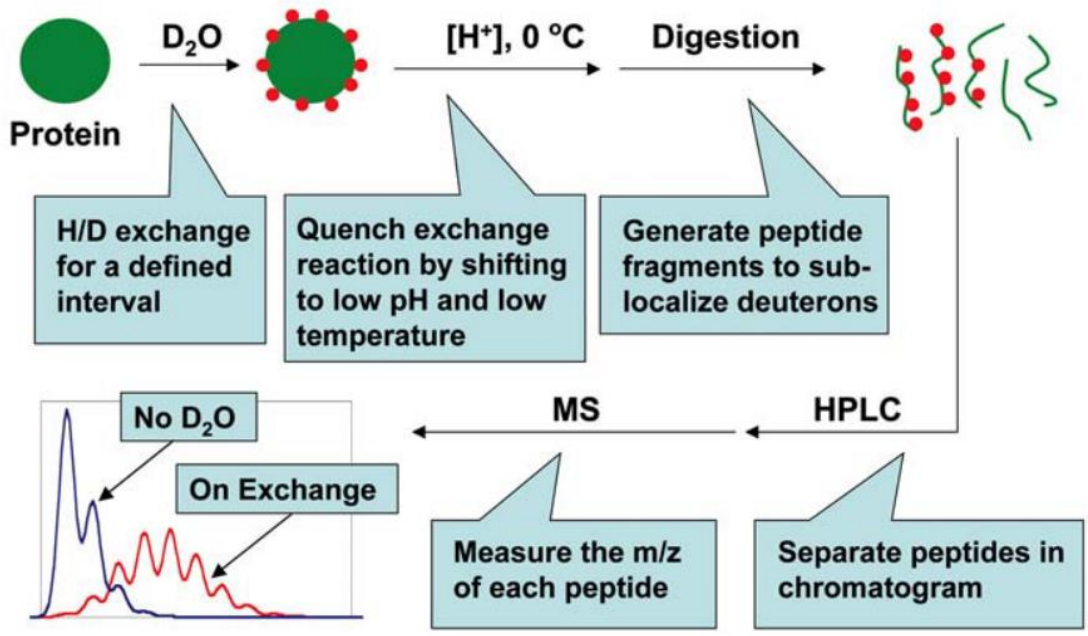

Figure 1.9 General workflow for bottom-up HDX-MS [104].

A protein sample in nondeuterated buffer is diluted into a buffer containing 50-90% D_2O [113]. Following defined incubation times, protein aliquots are subjected to quenching conditions, typically a cold, acidic solution [113]. This quench step is crucial to significantly slow amide H/D back exchange. Pepsin, a non-specific protease, is most widely used for proteolytic cleavage because it is stable and highly active under such quench conditions [114]. Alternatively, other acid proteases such as *Aspergillus saitoi* (type XIII) and *Rhizopus sp*. (type XVIII) can be used. The resulting peptides are subjected to chilled HPLC/UPLC separation, to further prevent loss of deuterium through back-exchange [115]. Separation must also be relatively fast, around 5-20 min.

The separated peptides are typically analyzed by MS for determination of overall deuterium content. Radical-driven tandem mass spectrometry methods such as ECD or ETD have been shown to have some utility for obtaining more localized spatial information [115], see below. Due to the proteolysis step, large size proteins can be analyzed via HDX-MS; however, a compromise in resulting peptide size is needed with small peptides (smaller than five amino acids) being difficult to identify via MS/MS and large peptides reducing spatial resolution [107]. Furthermore, the multiple sample handling steps, e.g., digestion and LC separation, increase the risk of undesired back exchange [116].

1.4.3 Top-down HDX Approach

Unlike the bottom-up approach, top-down approaches do not involve digestion. Here, the deuterated protein sample is directly subjected to MS, followed by MS/MS. There are several advantages to the top-down HDX approach, including less back exchange as digestion and proteolytic peptide separation is omitted. However, MS/MS fragmentation efficiency decreases as molecular size increases [117] with folded internal regions being particularly difficult to fragment [118], thus limiting spatial resolution [116]. The mass range that can be covered by the top-down approach is typically 10-30 kDa [19].

1.4.4 Hydrogen/Deuterium Scrambling

Hydrogen/Deuterium (H/D) scrambling refers to multiple reversible proton/deuteron transfers in peptides, resulting in a random distribution of deuterium across all exchangeable sites [119]. Such gaseous peptide H/D scrambling affects spatial resolution in HDX-MS because solution-phase deuterium labeling patterns are erased. The Jørgensen group developed the unique

regioselective model polypeptide (HHHHHHIIKIIK) that can be used for the sensitive detection of H/D scrambling [120].

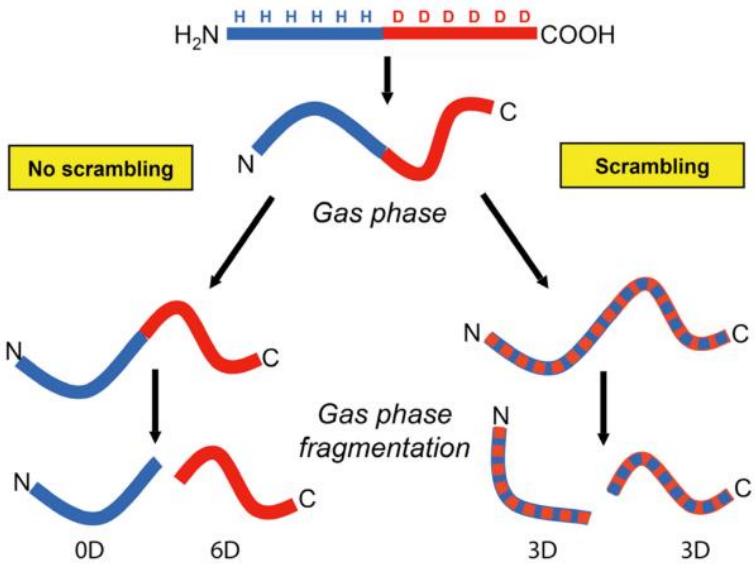

Figure 1.10 Measuring gas phase H/D scrambling using regioselective model peptide (HHHHHHIIKIIK) during the fragmentation [116].

The developed regioselective peptide consists of histidine, isoleucine, and lysine residues with histidines located in the N-terminal half and isoleucines and lysines located in the C-terminal half of the peptide. Due to the side-chain effect, the H/D exchange rate at the C-terminal half of the peptide is slower than the N-terminal half. The branched isoleucine side chain shows a higher degree of protection from intrinsic exchange compared with histidine [106]. The lysines were added to promote charging at different sites than the histidine side chains of this model peptide [120]. Thus, upon deuterium to hydrogen back-exchange, the C-terminal half of the peptide should show a significantly higher retention of deuterium compared with the N-terminal half.

CID is the most common and efficient fragmentation method to study peptide structure, however, it is not a suitable MS/MS method for deuterium localization because it results in extensive hydrogen scrambling, which erases site-specific deuterium labeling [120]. Under collisional activation, there is a displacement and migration of protons along the peptide backbone.

Based on this ‘mobile proton’ model, extensive reversible proton/deuteron trafficking occurs at backbone amide nitrogens and other exchangeable sites [116]. ECD/ETD, on the other hand, can preserve deuterium labeling information [121,122]. In the Cornell mechanism, ECD and ETD fragmentation occurs on a time scale shorter than the intramolecular hydrogen redistribution time scale (<picoseconds) [116] therefore, fragment ions can reflect the correct labeling pattern. In the Utah-Washington mechanism, introduction of a radical site at backbone amides renders backbone cleavage more energetically favorable than hydrogen rearrangement. However, H/D scrambling can also occur prior to MS/MS during ion transfer through a mass spectrometer when peptides gain vibrational energy through collisions. To minimize such H/D scrambling, ion source and transfer parameters must be optimized to “soft” conditions [116]. However, such conditions may results in significant loss of ion signal.

1.5 Dissertation Overview

This dissertation focuses on mechanistic insights into radical-driven peptide tandem mass spectrometry to improve protein structural analysis, particularly for tyrosine sulfation. In addition, conditions that balance reasonable ion transmission with minimum H/D scrambling in HDX-MS/MS experiments are sought.

In Chapter 2, the influence of charge state and charge carriers on FRIPS fragmentation pathways is explored to promote the desired radical driven pathways and prevent unwanted mobile proton pathways. Chapter 3 describes peptide derivatization methods to improve the stability of sulfated peptides in positive ion mode, which has been incompatible with sulfation site determination but is the standard polarity for proteomics experiments. Standard acidic-, synthetic basic-, and synthetic tryptic sulfopeptides are examined. Introduction of fixed positive charges and higher proton affinity groups, such as guanidinium, are explored. Chapter 4 examines the

feasibility of tyrosine sulfation site determination for peptides with multiple tyrosine residues via radical driven tandem mass spectrometry methods. Specifically, the MS/MS behavior of three isobaric tyrosylprotein sulfotransferase 1 (TPST1) sulfopeptides, based on a peptide previously identified from Rat liver Golgi membrane are characterized. ECD, ETD, EThcD, and nFRIPS results are discussed. Furthermore, the degree of hydrogen/deuterium scrambling as a function of peptide length is described in Chapter 5. Regioselective model peptides, developed around the Jørgensen peptide described in section 1.4.4 but varying in length from 10 to 16 amino acid residues, were examined under three different ion source condition. Finally, a summary of all research results along with future directions are discussed in Chapter 6. Chapters 2 through 5 are written in multiple manuscript format.

1.6 References

[1] Timp, W.; Timp, G. Beyond Mass Spectrometry, the next Step in Proteomics. *Sci. Adv.*, **2020**, *6*, 1–17.

[2] Wu, Y.; Engen, J.R. What Mass Spectrometry Can Reveal about Protein Function. *Analyst*, **2004**, *129*, 290–296.

[3] Sun, P.D.; Foster, C.E.; Boyington, J.C. Overview of Protein Structural and Functional Folds. *Curr. Protoc. Protein Sci.*, **2004**, *35*, 1711–171189.

[4] Chait, B.T.; Cadene, M.; Olinares, P.D.; Rout, M.P.; Shi, Y. Revealing Higher Order Protein Structure Using Mass Spectrometry. *J. Am. Soc. Mass Spectrom.*, **2016**, *27*, 952–965.

[5] Larsen, M.R.; Trelle, M.B.; Thingholm, T.E.; Jensen, O.N. Analysis of Posttranslational Modifications of Proteins by Tandem Mass Spectrometry. *Biotechniques*, **2006**, *40*, 790–798.

[6] Aebersold, R.; Mann, M. Mass Spectrometry-Based Proteomics. *Nature*, **2003**, *422*, 198–207.

[7] Yates, J.R. Mass Spectrometry from Genomics to Proteomics. *Trends Genet.*, **2000**, *16*, 5–8.

[8] Nefedov, A. V.; Gilski, M.J.; Sadygov, R.G. Bioinformatics Tools for Mass Spectrometry-Based High Throughput Quantitative Proteomics Platforms. *Curr. Proteomics*, **2011**, *8*, 125–137.

[9] Zhang, G.; Annan, R.S.; Carr, S.A.; Neubert, T.A. Overview of Peptide and Protein Analysis by Mass Spectrometry. *Curr. Protoc. Protein Sci.*, **2010**, *62*, 16.1.1-16.1.30.

[10] Angel, T.E.; Aryal, U.K.; Hengel, S.M.; Baker, E.S.; Kelly, R.T.; Robinson, E.W.; Smith, R.D. Mass Spectrometry-Based Proteomics: Existing Capabilities and Future Directions.

Chem. Soc. Rev., **2012**, *41*, 3912–3928.
[11] Chait, B.T. Mass Spectrometry: Bottom-Up or Top-Down? *Scinece*, **2006**, *314*, 65–66.
[12] Trevisiol, S.; Ayoub, D.; Lesur, A.; Ancheva, L.; Gallien, S.; Domon, B. The Use of Proteases Complementary to Trypsin to Probe Isoforms and Modifications. *Proteomics*, **2016**, *16*, 715–728.
[13] Wysocki, V.H.; Resing, K.A.; Zhang, Q.; Cheng, G. Mass Spectrometry of Peptides and Proteins. *Methods*, **2005**, *35*, 211–222.
[14] Karpievitch, Y. V.; Polpitiya, A.D.; Anderson, G.A.; Smith, R.D.; Dabney, A.R. Liquid Chromatography Mass Spectrometry-Based Proteomics: Biological and Technological Aspects. *Ann. Appl. Stat.*, **2010**, *4*, 1797–1823.
[15] Nesvizhskii, A.I.; Aebersold, R. Interpretation of Shotgun Proteomic Data: The Protein Inference Problem. *Mol. Cell. Proteomics*, **2005**, *4*, 1419–1440.
[16] Zhang, Y.; Fonslow, B.R.; Shan, B.; Baek, M.-C.; Yates, J.R. Protein Analysis by Shotgun/Bottom-up Proteomics. *Chem. Rev.*, **2013**, *113*, 2343–2394.
[17] Cui, W.; Rohrs, H.W.; Gross, M.L. Top-down Mass Spectrometry: Recent Developments, Applications and Perspectives. *Analyst*, **2011**, *136*, 3854–3864.
[18] Pandeswari, P.B.; Sabareesh, V. Middle-down Approach: A Choice to Sequence and Characterize Proteins/Proteomes by Mass Spectrometry. *RSC Adv.*, **2019**, *9*, 313–344.
[19] Cristobal, A.; Marino, F.; Post, H.; van Den Toorn, H.W.P.; Mohammed, S.; Heck, A.J.R. Toward an Optimized Workflow for Middle-Down Proteomics. *Anal. Chem.*, **2017**, *89*, 3318–3325.
[20] Moore, K.L. The Biology and Enzymology of Protein Tyrosine O-Sulfation. *Journal of Biological Chemistry*, **2003**, *278*, 24243–24246.
[21] Moore, K.L. Protein Tyrosine Sulfation: A Critical Posttranslation Modification in Plants and Animals. *Proc. Natl. Acad. Sci. U. S. A.*, **2009**, *106*, 14741–14742.
[22] Huttner, W.B. Tyrosine Sulfation and the Secretory Pathway. *Annu. Rev. Physiol.*, **1988**, *50*, 363–376.
[23] Kehoe, J.W.; Bertozzi, C.R. Tyrosine Sulfation: A Modulator of Extracellular Protein-Protein Interactions. *Chem. Biol.*, **2000**, *7*, 57–61.
[24] Choe, H.; Li, W.; Wright, P.L.; Vasilieva, N.; Venturi, M.; Huang, C.; Grundner, C.; Dorfman, T.; Zwick, M.B.; Wang, L.; Rosenberg, E.S.; Kwong, P.D.; Burton, D.R.; Robinson, J.E.; Sodroski, J.G.; Farzan, M. Tyrosine Sulfation of Human Antibodies Contributes to Recognition of the CCR5 Binding Region of HIV-1 Gp120. *Cell*, **2003**, *114*, 161–170.
[25] Liu, H.; Håkansson, K. Electron Capture Dissociation of Tyrosine O-Sulfated Peptides Complexed with Divalent Metal Cations. *Anal. Chem*, **2006**, *78*, 7570–7576.
[26] Yagami, T.; Kitagawa, K.; Aida, C.; Fujiwara, H.; Futaki, S. Stabilization of a Tyrosine O-Sulfate Residue by a Cationic Functional Group: Formation of a Conjugate Acid-Base Pair. *J. Pept. Res.*, **2000**, *56*, 239–249.
[27] Shih, M.; McLuckey, S.A. Ion/Ion Charge Inversion/Attachment in Conjunction with Dipolar DC Collisional Activation as a Selective Screen for Sulfo- and Phosphopeptides. *Int. J. Mass Spectrom.*, **2019**, *444*, 116–181.
[28] Yang, Y.S.; Wang, C.C.; Chen, B.H.; Hou, Y.H.; Hung, K.S.; Mao, Y.C. Tyrosine Sulfation as a Protein Post-Translational Modification. *Molecules*, **2015**, *20*, 2138–2164.
[29] Fenn, J.B.; Mann, M.; Meng, C.K.A.I.; Wong, S.F.; Whitehouse, C.M. Electrospray Ionization for Mass Spectrometry of Large Biomolecules. *Science (80-.).*, **1989**, *246*, 64–

71.
[30] Veenstra, T.D. Electrospray Ionization Mass Spectrometry in the Study of Biomolecular Non-Covalent Interactions. *Biophys. Chem.*, **1999**, *79*, 63–79.
[31] Covey, T.R.; Bonner, R.F.; Shushan, B.I.; Henion, J.; Boyd, R.K. The Determination of Protein, Oligonucleotide and Peptide Molecular Weights by Ion-spray Mass Spectrometry. *Rapid Commun. Mass Spectrom.*, **1988**, *2*, 249–256.
[32] Banerjee, S.; Mazumdar, S. Electrospray Ionization Mass Spectrometry: A Technique to Access the Information beyond the Molecular Weight of the Analyte. *Int. J. Anal. Chem.*, **2012**, *2012*, 1–40.
[33] Van Berkel, G.J.; Kertesz, V. Electrochemistry of the Electrospray Ion Source. In *Electrospray and MALDI Mass Spectrometry: Fundamentals, Instrumentation, Practicalities, and Biological Applications: Second Edition*; Cole, R.B., Ed.; John Wiley and Sons, Inc, **2012**; pp. 75–122.
[34] Kebarle, P.; Verkerk, U.H. ELECTROSPRAY: FROM IONS IN SOLUTION TO IONS IN THE GAS PHASE, WHAT WE KNOW NOW. *Mass Spectrom. Rev.*, **2009**, *28*, 898–917.
[35] Blades, A.T.; Ikonomou, M.G.; Kebarle, P. Mechanism of Electrospray Mass Spectrometry. Electrospray as an Electrolysis Cell. *Anal. Chem.*, **1991**, *63*, 2109–2114.
[36] Taylor, G. Disintegration of Water Drops in an Electric Field. *Proc. oft he R. Soc. London A*, **1964**, *280*, 383–397.
[37] Bruins, A.P. Mechanistic Aspects of Electrospray Ionization. *J. Chromatogr. A*, **1998**, *794*, 345–357.
[38] Hommerson, P.; Khan, A.M.; de Jong, G.J.; Somsen, G.W. Ionization Techniques in Capillary Electrophoresis-mass Spectrometry: Principles, Design, and Application. *Mass Spectrom. Rev.*, **2011**, *30*, 1096–1120.
[39] Rayleigh, Lord. On the Equilibrium of Liquid Conducting Masses Charged with Electricity. *London, Edinburgh, Dublin Philos. Mag. J. Sci.*, **1882**, *14*, 184–186.
[40] Wilm, M..; Mann, M. Electrospray and Taylor-Cone Theory, Dole's Beam Ofmacromolecules at Last? *Int. J. Mass Spectrom. Ion Process.*, **1994**, *136*, 167–180.
[41] Karas, M.; Bahr, U.; Dülcks, T. Nano-Electrospray Ionization Mass Spectrometry: Addressing Analytical Problems beyond Routine. *Fresenius. J. Anal. Chem.*, **2000**, *366*, 669–676.
[42] Wilm, M.; Mann, M. Analytical Properties of the Nanoelectrospray Ion Source. *Anal. Chem.*, **1996**, *68*, 1–8.
[43] Comisarow, M.B.; Marshall, A.G. Fourier Transform Ion Cyclotron Resonance Spectroscopy. *Chem. Phys. Lett.*, **1974**, *25*, 282–283.
[44] Comisarow, M.B.; Marshall, A.G. The Early Development of Fourier Transform Ion Cyclotron Resonance (FT-ICR) Spectroscopy. *J. Mass Spectrom.*, **1996**, *31*, 581–585.
[45] Allemann, M.; Kellerhals, H.; Wanczek, K.P. A New Fourier-Transform Mass Spectrometer with a Superconducting Magnet. *Chem. Phys. Lett.*, **1980**, *75*, 328–331.
[46] Caravatti, P.; Allemann, M. The 'Infinity Cell': A New Trapped-ion Cell with Radiofrequency Covered Trapping Electrodes for Fourier Transform Ion Cyclotron Resonance Mass Spectrometry. *Org. Mass Spectrom.*, **1991**, *26*, 514–518.
[47] Schmid, D.G.; Grosche, P.; Bandel, H. FTICR-Mass Spectrometry for High-Resolution Analysis in Combinatorial Chemistry. *Biotechnol. Bioenegineering (Comibinatorial Chem.*, **2001**, *71*, 149–161.

[48] Marshall, A.G.; Guan, S. Advantages of High Magnetic Field for Fourier Transform Ion Cyclotron Resonance Mass Spectrometry. *Rapid Commun. Mass Spectrom.*, **1996**, *10*, 1819–1823.
[49] Hendrickson, C.L.; Quinn, J.P.; Kaiser, N.K.; Smith, D.F.; Blakney, G.T.; Chen, T.; Marshall, A.G.; Weisbrod, C.R.; Beu, S.C. 21 Tesla Fourier Transform Ion Cyclotron Resonance Mass Spectrometer: A National Resource for Ultrahigh Resolution Mass Analysis. *J. Am. Soc. Mass Spectrom.*, **2015**, *26*, 1626–1632.
[50] Shaw, J.B.; Lin, T.; Leach III, F.E.; Tolmachev, A. V.; Toli, N.; Robinson, E.W.; Koppenaal, D.W.; Pa, L. 21 Tesla Fourier Transform Ion Cyclotron Resonance Mass Spectrometer Greatly Expands Mass Spectrometry Toolbox. *J. Am. Sociatey Mass Spectrom.*, **2016**, *27*, 1929–1936.
[51] Adamson, J.T.; Håkansson, K. Electrospray Ionization Fourier Transform Ion Cyclotron Resonance Mass Spectrometry for Lectin Analysis. In *Lectins: Analytical Technologies*; Nilson, C.L., Ed.; Elsevier Science, **2007**; pp. 343–371.
[52] Qi, Y.; O'Connor, P.B. Data Processing in Fourier Transform Ion Cyclotron Resonance Mass Spectrometry. Mass. *Mass Spectrom Rev*, **2011**, *33*, 333–352.
[53] Nikolaev, E.N.; Boldin, I.A.; Jertz, R.; Baykut, G. Initial Experimental Characterization of a New Ultra-High Resolution FTICR Cell with Dynamic Harmonization. *J. Am. Soc. Mass Spectrom.*, **2011**, *22*, 1125–1133.
[54] Marshall, A.G.; Verdun, F.R. Fourier Transform Ion Cyclotron Resonance Mass Spectrometry. In *Fourier Transforms in NMR, Optical, and Mass Spectrometry: a user's handbook*; Marshall, A.G.; Verdun, F.R., Eds.; Elsevier Science: Amsterdam, **1990**; pp. 225–278.
[55] Amster, I.J. Fourier Transform Mass Spectrometry. *J. Mass Spectrom.*, **1996**, *31*, 1325–1337.
[56] Marshall, A.G.; Schweikhard, L. Fourier Transform Ion Cyclotron Resonance Mass Spectrometry: Technique Developments. *Int. J. Mass Spectrom. Ion Process.*, **1992**, *118–119*, 37–70.
[57] Marshall, A.G.; Hendrickson, C.L.; Jackson, G.S. FOURIER TRANSFORM ION CYCLOTRON RESONANCE MASS SPECTROMETRY : A PRIMER. *Mass Spectrom. Rev.*, **1998**, *17*, 1–35.
[58] Cho, Y.; Ahmed, A.; Islam, A.; Kim, S. DEVELOPMENTS IN FT-ICR MS INSTRUMENTATION, IONIZATION TECHNIQUES, AND DATA INTERPRETATION METHODS FOR PETROLEOMICS. *Mass Spectrom. Rev.*, **2015**, *34*, 248–263.
[59] Makarov, A. Electrostatic Axially Harmonic Orbital Trapping: A High-Performance Technique of Mass Analysis. *Anal. Chem.*, **2000**, *72*, 1156–1162.
[60] Hager, J.W. A New Linear Ion Trap Mass Spectrometer. *Rapid Commun. Mass Spectrom.*, **2002**, *16*, 512–526.
[61] Makarov, A.; Denisov, E.; Kholomeev, A.; Balschun, W.; Lange, O.; Strupat, K.; Horning, S. Performance Evaluation of a Hybrid Linear Ion Trap/Orbitrap Mass Spectrometer. *Anal. Chem.*, **2006**, *78*, 2113–2120.
[62] Zubarev, R.A.; Makarov, A. Orbitrap Mass Spectrometry. *Anal. Chem*, **2013**, *85*, 5288–5296.
[63] Madeira, P.J.A.; Alves, P.A.; Borges, C.M. High Resolution Mass Spectrometry Using FTICR and Orbitrap Instruments. In *Fourier Transform - Materials Analysis*; Salih, S.,

Ed.; InTech, **2012**; pp. 25–44.
[64] Hecht, E.S.; Scigelova, M.; Eliuk, S.; Makarov, A. Fundamentals and Advances of Orbitrap Mass Spectrometry. *Encyclopedia of Analytical Chemistry*, **2019**, 1–40.
[65] Hu, Q.; Noll, R.J.; Li, H.; Makarov, A.; Hardman, M.; Cooks, R.G. The Orbitrap: A New Mass Spectrometer. *J. Mass Spectrom.*, **2005**, *40*, 430–443.
[66] Frese, C.K.; Altelaar, A.F.M.; Van Den Toorn, H.; Nolting, D.; Griep-Raming, J.; Heck, A.J.R.; Mohammed, S. Toward Full Peptide Sequence Coverage by Dual Fragmentation Combining Electron-Transfer and Higher-Energy Collision Dissociation Tandem Mass Spectrometry. *Anal. Chem.*, **2012**, *84*, 9668–9673.
[67] Swaney, D.L.; McAlister, G.C.; Wirtala, M.; Schwartz, J.C.; Syka, J.E.P.; Coon, J.J. Supplemental Activation Method for High-Efficiency Electron-Transfer Dissociation of Doubly Protonated Peptide Precursors. *Anal. Chem.*, **2007**, *79*, 477–485.
[68] Sleno, L.; Volmer, D.A. Ion Activation Methods for Tandem Mass Spectrometry. *J. Mass Spectrom.*, **2004**, *39*, 1091–1112.
[69] Roepstorff, P.; Fohlman, J. Proposal for a Common Nomenclature for Sequence Ions in Mass Spectra of Peptides. *Biomed. Mass Spectrom.*, **1984**, *11*, 601–605.
[70] Biemann, K. Nomenclature for Peptide Fragment Ions (Positive Ions). *Methods Enzym.*, **1990**, *193*, 886–887.
[71] Chu, I.K.; Siu, C.-K.; Lau, J.K.-C.; Tang, W.K.; Mu, X.; Lai, C.K.; Guo, X.; Wang, X.; Li, N.; Xia, Y.; Kong, X.; Oh, H. Bin; Ryzhov, V.; Tureček, F.; Hopkinson, A.C.; Siu, K.W.M. Proposed Nomenclature for Peptide Ion Fragmentation. *Int. J. Mass Spectrom.*, **2015**, *390*, 24–27.
[72] Wysocki, V.H.; Cheng, G.; Zhang, Q.; Herrmann, K.A.; Beardsley, R.L.; Hilderbrand, A.E. Pepetide Fragmentation Overview. In *Principles of Mass Spectrometry Applied to Biomolecules*; Laskin, J.; Lifshitz, C., Eds.; John Wiley and Sons: New York, **2006**; pp. 279–300.
[73] Zhurov, K.O.; Fornelli, L.; Wodrich, M.D.; Laskay, Ü.A.; Tsybin, Y.O. Principles of Electron Capture and Transfer Dissociation Mass Spectrometry Applied to Peptide and Protein Structure Analysis. *Chem. Soc. Rev.*, **2013**, *42*, 5014–5030.
[74] Mitchell Wells, J.; McLuckey, S.A. Collision-Induced Dissociation (CID) of Peptides and Proteins. *Methods Enzymol.*, **2005**, *402*, 148–185.
[75] McLuckey, S.A. Principles of Collisional Activation in Analytical Mass Spectrometry. *J. Am. Soc. Mass Spectrom.*, **1992**, *3*, 599–614.
[76] Mcluckey, S.A.; Goeringer, D.E. *Slow Heating Methods in Tandem Mass Spectrometry*; **1997**; Vol. 32.
[77] Ichou, F.; Schwarzenberg, A.; Lesage, D.; Alves, S.; Junot, C.; MacHuron-Mandard, X.; Tabet, J.C. Comparison of the Activation Time Effects and the Internal Energy Distributions for the CID, PQD and HCD Excitation Modes. *J. Mass Spectrom.*, **2014**, *49*, 498–508.
[78] Xia, Y.; Liang, X.; McLuckey, S.A. Ion Trap versus Low-Energy Beam-Type Collision-Induced Dissociation of Protonated Ubiquitin Ions. *Anal. Chem.*, **2006**, *78*, 1218–1227.
[79] Dongré, A.R.; Jones, J.L.; Somogyi, Á.; Wysocki, V.H. Influence of Peptide Composition, Gas-Phase Basicity, and Chemical Modification on Fragmentation Efficiency: Evidence for the Mobile Proton Model. *J. Am. Chem. Soc.*, **1996**, *118*, 8365–8374.
[80] Tsaprailis, G.; Nair, H.; Zhong, W.; Kuppannan, K.; Futrell, J.H.; Wysocki, V.H. A Mechanistic Investigation of the Enhanced Cleavage at Histidine in the Gas-Phase

Dissociation of Protonated Peptides. *Anal. Chem.*, **2004**, *76*, 2083–2094.
[81] Paizs, B.; Suhal, S. Fragmentation Pathways of Protonated Peptides. *Mass Spectrom. Rev.*, **2005**, *24*, 508–548.
[82] Zubarev, R.A.; Kelleher, N.L.; McLafferty, F.W. Electron Capture Dissociation of Multiply Charged Protein Cations. A Nonergodic Process. *J. Am. Chem. Soc.*, **1998**, *120*, 3265–3266.
[83] McLafferty, F.W.; Horn, D.M.; Breuker, K.; Ge, Y.; Lewis, M.S.; Cerda, B.; Zubarev, R.A.; Carpenter, B.K. Electron Capture Dissociation of Gaseous Multiply Charged Ions by Fourier-Transform Ion Cyclotron Resonance. *J. Am. Soc. Mass Spectrom.*, **2001**, *12*, 245–249.
[84] Syrstad, E.A.; Tureček, F. Toward a General Mechanism of Electron Capture Dissociation. *J. Am. Soc. Mass Spectrom.*, **2005**, *16*, 208–224.
[85] Sobczyk, M.; Anusiewicz, I.; Berdys-Kochanska, J.; Sawicka, A.; Skurski, P.; Simons, J. Coulomb-Assisted Dissociative Electron Attachment: Application to a Model Peptide. *J. Phys. Chem. A*, **2005**, *109*, 250–258.
[86] Qi, Y.; Volmer, D.A. Eletron-Based Fragmentation Methods in Mass Spectrometry: An Overview. *Mass Spectrom. Rev.*, **2017**, *36*, 4–15.
[87] Jones, A.W.; Cooper, H.J. Probing the Mechanisms of Electron Capture Dissociation Mass Spectrometry with Nitrated Peptides. *Phys. Chem. Chem. Phys.*, **2010**, *12*, 13394–13399.
[88] Zubarev, R.A.; Kruger, N.A.; Fridriksson, E.K.; Lewis, M.A.; Horn, D.M.; Carpenter, B.K.; McLafferty, F.W. Electron Capture Dissociation of Gaseous Multiply-Charged Proteins Is Favored at Disulfide Bonds and Other Sites of High Hydrogen Atom Affinity. *J. Am. Chem. Soc.*, **1999**, *121*, 2857–2862.
[89] Zubarev, R.A.; Horn, D.M.; Fridriksson, E.K.; Kelleher, N.L.; Kruger, N.A.; Lewis, M.A.; Carpenter, B.K.; McLafferty, F.W. Electron Capture Dissociation for Structural Characterization of Multiply Charged Protein Cations. *Anal. Chem*, **2000**, *72*, 563–573.
[90] Kelleher, N.L.; Zubarev, R.A.; Bush, K.; Furie, B.; Furie, B.C.; McLafferty, F.W.; Walsh, C.T. Localization of Labile Posttranslational Modifications by Electron Capture Dissociation: The Case of γ-Carboxyglutamic Acid. *Anal. Chem.*, **1999**, *71*, 4250–4253.
[91] Zubarev, R.A.; Haselmann, K.; Budnik, B.; Kjeldsen, F.; Jensen, F. Towards an Understanding of the Mechanism of Electron- Capture Dissociation: A Historical Perspective and Modern Ideas. *Eur. J. Mass Spectrom.*, **2002**, *8*, 337.
[92] Tsybin, Y.O.; Witt, M.; Baykut, G.; Kjeldsen, F.; Håkansson, P. Combined Infrared Multiphoton Dissociation and Electron Capture Dissociation with a Hollow Electron Beam in Fourier Transform Ion Cyclotron Resonance Mass Spectrometry. *Rapid Commun. Mass Spectrom.*, **2003**, *17*, 1759–1768.
[93] Syka, J.E.P.; Coon, J.J.; Schroeder, M.J.; Shabanowitz, J.; Hunt, D.F. Peptide and Protein Sequence Analysis by Electron Transfer Dissociation Mass Spectrometry. *Proc. Natl. Acad. Sci. U. S. A.*, **2004**, *101*, 9528–9533.
[94] Asakawa, D.; De Pauw, E. Difference of Electron Capture and Transfer Dissociation Mass Spectrometry on Ni2+-, Cu2+-, and Zn2+-Polyhistidine Complexes in the Absence of Remote Protons. *J. Am. Soc. Mass Spectrom.*, **2016**, *27*, 1165–1175.
[95] Masterson, D.S.; Yin, H.; Chacon, A.; Hachey, D.L.; Norris, J.L.; Porter, N.A. Lysine Peroxycarbamates: Free Radical-Promoted Peptide Cleavage. *J. Am. Chem. Soc.*, **2004**, *126*, 720–721.

[96] Hodyss, R.; Cox, H.A.; Beauchamp, J.L. Bioconjugates for Tunable Peptide Fragmentation: Free Radical Initiated Peptide Sequencing (FRIPS). *J. AM. CHEM. SOC*, **2005**, *127*, 12436–12437.
[97] Lee, M.; Kang, M.; Moon, B.; Oh, H. Bin. Gas-Phase Peptide Sequencing by TEMPO-Mediated Radical Generation. *Analyst*, **2009**, *134*, 1706–1712.
[98] Borotto, N.B.; Ileka, K.M.; Tom, C.A.T.M.B.; Martin, B.R.; Håkansson, K. Free Radical Initiated Peptide Sequencing for Direct Site Localization of Sulfation and Phosphorylation with Negative Ion Mode Mass Spectrometry. *Anal. Chem.*, **2018**, *90*, 9682–9686.
[99] Lee, M.; Lee, Y.; Kang, M.; Park, H.; Seong, Y.; Sung, B.J.; Moon, B.; Oh, H. Bin. Disulfide Bond Cleavage in TEMPO-Free Radical Initiated Peptide Sequencing Mass Spectrometry. *J. mass Spectrom.*, **2011**, *46*, 830–839.
[100] Chalmers, M.J.; Busby, S.A.; Pascal, B.D.; He, Y.; Hendrickson, C.L.; Marshall, A.G.; Griffin, P.R. Probing Protein Ligand Interactions by Automated Hydrogen/Deuterium Exchange Mass Spectrometry. *Anal. Chem*, **2006**, *78*, 1005–1014.
[101] Hoofnagle, A.N.; Resing, K.A.; Ahn, N.G. Protein Analysis by Hydrogen Exchange Mass Spectrometry. *Annu. Rev. Biophys. Biomol. Struct.*, **2003**, *32*, 1–25.
[102] Srivastava, A.; Nagai, T.; Srivastava, A.; Miyashita, O.; Tama, F. Role of Computational Methods in Going beyond X-Ray Crystallography to Explore Protein Structure and Dynamics. *Int. J. Mol. Sci.*, **2018**, *19*.
[103] Percy, A.J.; Rey, M.; Burns, K.M.; Schriemer, D.C. Probing Protein Interactions with Hydrogen/Deuterium Exchange and Mass Spectrometry-A Review. *Anal. Chim. Acta*, **2012**, *721*, 7–21.
[104] Hamuro, Y.; Coales, S.J.; Southern, M.R.; Nemeth-Cawley, J.F.; Stranz, D.D.; Griffin, P.R. Rapid Analysis of Protein Structure and Dynamics by Hydrogen/Deuterium Exchange Mass Spectrometry. *J. Biomol. Tech.*, **2003**, *14*, 171–182.
[105] Artigues, A.; Nadeau, O.W.; Rimmer, M.A.; Villar, M.T.; Du, X.; Fenton, A.W.; Carlson, G.M. *Protein Structural Analysis via Mass Spectrometry-Based Proteomics*; **2016**; Vol. 919.
[106] Bai, Y.; Milne, J.S.; Mayne, L.; Englander, S.W. Primary Structure Effects Hydrogen Exchange on Peptide Group. *Proteins Struct. Funct. Genet.*, **1993**, *17*, 75–86.
[107] Gallagher, E.S.; Hudgens, J.W. *Mapping Protein-Ligand Interactions with Proteolytic Fragmentation, Hydrogen/Deuterium Exchange-Mass Spectrometry*; 1st ed.; Elsevier Inc., **2016**; Vol. 566.
[108] Brown, K.A.; Wilson, D.J. Bottom-up Hydrogen Deuterium Exchange Mass Spectrometry: Data Analysis and Interpretation. *Analyst*, **2017**, *142*, 2874–2886.
[109] Fang, J.; Rand, K.D.; Beuning, P.J.; Engen, J.R. False EX1 Signatures Caused by Sample Carryover during HX MS Analyses. *Int. J. Mass Spectrom.*, **2011**, *302*, 19–25.
[110] Weis, D.D.; Wales, T.E.; Engen, J.R.; Hotchko, M.; Ten Eyck, L.F. Identification and Characterization of EX1 Kinetics in H/D Exchange Mass Spectrometry by Peak Width Analysis. *J. Am. Soc. Mass Spectrom.*, **2006**, *17*, 1498–1509.
[111] Wales, T.E.; Engen, J.R. Hydrogen Exchange Mass Spectrometry for the Analysis of Protein Dynamics. *Mass Spectrom. Rev.*, **2006**, *25*, 158–170.
[112] Pan, J.; Han, J.; Borchers, C.H.; Konermann, L. Hydrogen/Deuterium Exchange Mass Spectrometry with Top-down Electron Capture Dissociation for Characterizing Structural Transitions of a 17 KDa Protein. *J. Am. Chem. Soc.*, **2009**, *131*, 12801–12808.
[113] Hamuro, Y.; Coales, S.J.; Woods, V. Protein-Targeting Drug Discovery Guided by

Hydrogen/Deuterium Exchange Mass Spectrometry (DXMS). *Mass Spectrom. Med. Chem.*, **2007**, *36*, 377–398.
[114] Wei, H.; Tymiak, A.A.; Chen, G. Introduction Hydrogen/Deuterium Exchange Mass Spectrometry for Protein Higher-Order Structure Characterization. In *Characterization of Protein Therapeutics using Mass Spectrometry*; Chen, G., Ed.; Springer: New York, **2013**; pp. 305–341.
[115] Masson, G.R.; Jenkins, M.L.; Burke, J.E. An Overview of Hydrogen Deuterium Exchange Mass Spectrometry (HDX-MS) in Drug Discovery. *Expert Opin. Drug Discov.*, **2017**, *12*, 981–994.
[116] Rand, K.D.; Zehl, M.; Jørgensen, T.J.D. Measuring the Hydrogen/Deuterium Exchange of Proteins at High Spatial Resolution by Mass Spectrometry: Overcoming Gas-Phase Hydrogen/Deuterium Scrambling. *Acc. Chem. Res.*, **2014**, *47*, 3018–3027.
[117] Breuker, K.; Jin, M.; Han, X.; Jiang, H.; McLafferty, F.W. Top-Down Identification and Characterization of Biomolecules by Mass Spectrometry. *J. Am. Soc. Mass Spectrom.*, **2008**, *19*, 1045–1053.
[118] Han, X.; Jin, M.; Breuker, K.; McLafferty, F.W. Extending Top-Down Mass Spectrometry to Proteins with Masses Greater Than 200 Kilodaltons. *Science (80-.).*, **2006**, *314*, 109–113.
[119] Jørgensen, T.J.D.; Gårdsvoll, H.; Ploug, M.; Roepstorff, P. Intramolecular Migration of Amide Hydrogens in Protonated Peptides upon Collisional Activation. *J. Am. Soc. Mass Spectrom.*, **2005**, *127*, 2785–2793.
[120] Rand, K.D.; Jørgensen, T.J.D. Development of a Peptide Probe for the Occurrence of Hydrogen (1 H/ 2 H) Scrambling upon Gas-Phase Fragmentation. *Anal. Chem.*, **2007**, *79*, 8686–8693.
[121] Rand, K.D.; Adams, C.M.; Zubarev, R.A.; Jørgensen, T.J.D. Electron Capture Dissociation Proceeds with a Low Degree of Intramolecular Migration of Peptide Amide Hydrogens. *J. Am. Soc. Mass Spectrom.*, **2008**, *130*, 1341–1349.
[122] Zehl, M.; Rand, K.D.; Jensen, O.N.; Jørgensen, T.J.D. Electron Transfer Dissociation Facilitates the Measurement of Deuterium Incorporation into Selectively Labeled Peptides with Single Residue Resolution. *J. Am. Chem. Soc*, **2008**, *130*, 17453–17459.

Chapter 2

Charge State and Charge Carrier Effects in Free Radical Initiated Peptide Sequencing (FRIPS)

2.1 Introduction

Mass spectrometry-based proteomics provides invaluable insights into protein structure and function [1]. Typically, proteins are enzymatically digested into peptides for more efficient ionization and tandem mass spectrometry (MS/MS) fragmentation. Peptide identification is achieved by matching such gas-phase fragments from peptide backbone cleavage to in silico digestion of proteins in genome-derived databases. This approach is effective when MS/MS activation results in inter-residue cleavage across a peptide for maximum sequence coverage [2]. Collision induced dissociation CID is the most common approach to MS/MS. In CID, precursor ion kinetic energy is increased through acceleration in an electric field and their internal energy is elevated via inelastic collisions with an inert buffer gas, e.g., nitrogen or argon [3]. For protonated peptide cations, protons will migrate from more basic sites to backbone amide nitrogens, thus weakening and cleaving backbone amide bonds to yield N-terminal *b*-type and C-terminal *y*-type fragment ions [4]. CID is widely available in most mass spectrometers and has higher fragmentation efficiency [5]. However, because preferential cleavage of the weakest chemical bonds occurs, identification of labile posttranslational modifications (PTMs) is challenging as

these modifications are preferentially lost [6]. Electron capture/transfer dissociation (ECD/ETD) were developed as alternative MS/MS activation approaches that can circumvent this issue. In ECD/ETD, electrons are either captured or transferred to precursor ions, resulting in radical-driven fragmentation that shows preference for peptide backbone C-N bond cleavage to yield N-terminal *c*′-type and C-terminal *z*•-type ions with retention of labile PTMs [7,8] However, ECD/ETD have low fragmentation efficiency [9], require at least doubly positively charged precursor ions, and need specialized instrumentation to introduce electrons or generate ETD reagent [10,11].

To overcome the drawbacks of the aforementioned activation methods, alternative radical-based MS/MS approaches have been introduced. Porter and co-workers modified lysine side chains to peroxycarbonates through *p*-nitrophenylchloroformate with tert-butyl hydroperoxide reaction [12]. Collisional activation of Li-adducted peroxycarbamate-containing peptides resulted in homolytic bond cleavage to form an amine-centered radical. Further radical rearrangement yielded side chain loss and peptide backbone dissociation. Beauchamp and co-workers later employed Vazo 68 (DuPont) as a free radical initiator conjugated with peptide N-terminal free amines [13]. CID of such conjugated peptides also resulted in homolytic bond cleavage to form an azo group free radical. Further collisional activation of this peptide radical generated N-terminal *a*- and C-terminal *z*-type fragments. This MS/MS approach was termed free radical initiated peptide sequencing, FRIPS [13]. More recently, Oh and co-workers introduced a thermodynamically stable TEMPO (2,2,6,6-tetramethylpiperidine-1-oxy)-based radical initiator for FRIPS, *o*-TEMPO-Bz-NHS [14]. Sinz, Schäfer and co-workers also developed a TEMPO-based crosslinker for FRIPS-based analysis of crosslinked peptides [15].

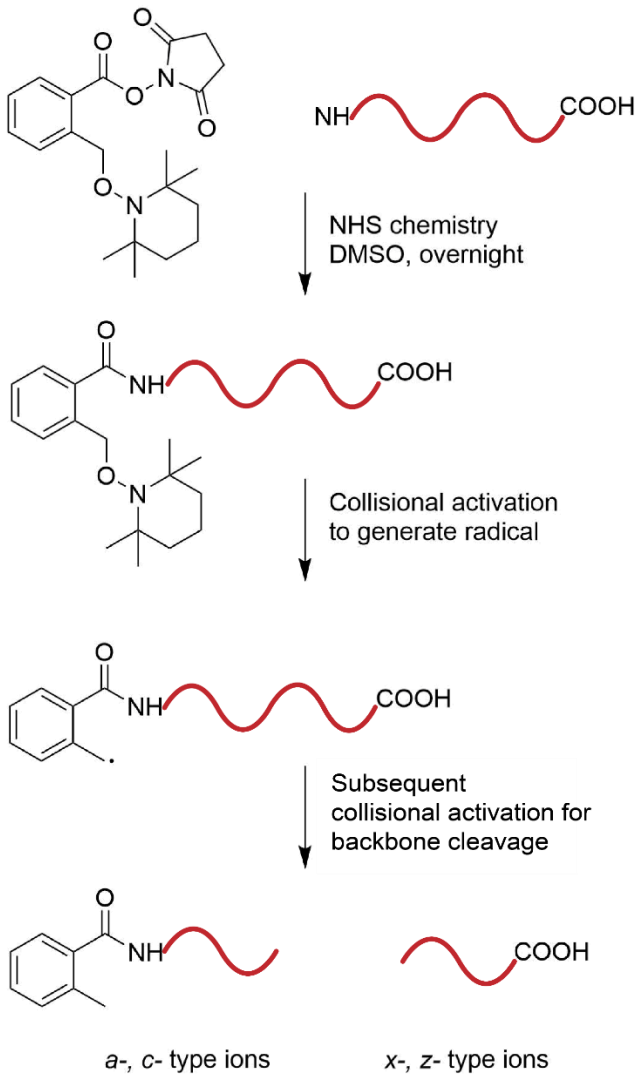

Figure 2.1 Experimental workflow of TEMPO-assisted free radical initiated peptide sequencing.

In TEMPO-assisted FRIPS, conjugated peptides are collisionally activated to generate a free radical through homolytic cleavage of the radical initiator C-O bond (see Figure 2.1). Subsequent collisional activation, preferably in an MS^3 implementation, of this radical-containing conjugated peptide leads to peptide backbone cleavage to yield *a*-, *c*-, *x*-, and *z*- type fragment ions [14]. FRIPS can be implemented in any CID-enabled mass spectrometer although MS^n-capable instruments yield cleaner spectra. In addition, both multiply- and singly-charged precursor ions are compatible with FRIPS, as is either positive or negative ion mode analysis. Similar to ECD/ETD, selective

disulfide bond cleavage has been reported to occur in FRIPS [16] as well as radical and neutral side chain loss that allow determination of specific amino acid residues [17]. Because the energy barrier for homolytic C-O bond cleavage is low [14], limited loss of labile PTMs in FRIPS has been noted: partial retention of phosphorylation was observed in both positive and negative ion mode [18,19] and highly labile sulfation analysis was feasible in negative ion mode [18]. Furthermore, differentiation of aspartic and iso-aspartic acid was demonstrated in positive ion mode FRIPS [20].

Despite these promising applications,, there are remaining challenges in FRIPS experiments. Because FRIPS involves collisional activation to generate and propagate the radical site, competition between radical-driven and mobile proton-driven pathways can occur [21]. Specifically, Oh and co-workers reported that the absence of arginine residues, which sequester protons due to their high proton affinity, can predominantly yield *b*- and *y*-type fragment ions from mobile proton pathways, i.e., the success of FRIPS appears sequence dependent [21]. Sinz and co-workers speculated that heterolytic C-O bond cleavage can occur in their crosslinking FRIPS tag when the overall analyte charge state exceeds the number of basic sites in TEMPO-Bz-derivatized peptides [15]. These authors also demonstrated that an alternative charge carrier, i.e., a sodium cation, reinstated radical-driven fragmentation [15]. However, there is a lack of detailed studies on how to optimize desired radical-driven dissociation pathways and limit mobile proton-driven dissociation pathway in FRIPS. Here, we further examine such charge state and charge carrier effects.

2.2 Experimental

2.2.1 Materials

ACTH 1-10 (SYSMEHFRWG) as well as the synthetic peptides YFYLIPLEYLQ and YFYLIPLSYLR were obtained from Genscript Corp (Piscataway, NJ). Angiotensin I (DRVYIHPFHL), triethylamine bicarbonate (TEAB), dimethyl sulfoxide (DMSO), sodium acetate, and calcium acetate were purchased from Sigma Aldrich (St. Louis, MO). Water, methanol, and formic acid of LC-MS grade were purchased from Fisher chemical (Fair Lawn, NJ). *o*-TEMPO-Bz-C(O)-NHS was acquired from FutureChem (Seoul, Korea).

2.2.2 Conjugation

For peptide N-terminal conjugation with *o*-TEMPO-Bz-C(O)-NHS, 100 µL, 1 mM peptide solution was added to 100 µL of DMSO. The solution pH was adjusted to 8-9 with 100 mM TEAB buffer. This solution was vortexed for 1 min and incubated at room temperature overnight after adding 20 mM of *o*-TEMPO-Bz-C(O)-NHS dissolved in DMSO. This reaction solution was desalted with a C18 reverse phase solid phase extraction Vac cartridge (Sep-Pak C18 1 cc Vac Cartridge: Waters Corp., Milford, MA, USA) and dried using a SpeedVac.

2.2.3 Mass Spectrometry

FRIPS MS^3, CID, and higher energy collision dissociation (HCD) experiments were performed with an Orbitrap Fusion Lumos mass spectrometer (Thermo Fisher Scientific, San Jose, CA, USA). Nanoelectrospray ionization (nanoESI) was performed by directly infusing the sample solution (~1-5 µM conjugated peptide in methanol:water (50:50, v/v) with 0.1% formic acid) through a stainless steel emitter, with sweep gas of 1 arb unit, a positive ion spray voltage of 1800-2000 V, and an ion transfer tube temperature of 250-280 °C. A syringe pump flow rate of 0.5

μL/min was used. For charge carrier effect experiments, metal/conjugated peptide complex was prepared by adding sodium acetate to 1 μM, or calcium acetate to 10 μM in methanol:water (50:50, v/v), respectively.

Data analysis was performed manually using Thermo Xcalibur Qual Browser. Theoretical fragment ion masses were determined by the MS product function in Protein prospector (http://prospector.ucsf.edu/prospector/cgi-bin/msform.cgi?form=msproduct) The FRIPS experimental data were manually analyzed by an in-house Excel macro.

2.3 Results and Discussion

2.3.1 FRIPS Charge State Effect

N-terminally *o*-TEMPO-Bz-C(O) conjugated peptides at varying precursor ion charge states were subjected to FRIPS MS^3. CID in the linear ion trap of an Orbitrap Fusion Lumos mass spectrometer was employed with the goal to generate a radical site through preferential homolytic cleavage of the *o*-TEMPO-Bz C-O bond (Figure 2.1). CID was chosen for this MS^2 step to favor the desired low energy pathway for radical initiation. HCD was then used for MS^3 activation of the truncated radical species to propagate the radical and yield peptide backbone dissociation. The HCD voltage was carefully adjusted to achieve maximum FRIPS efficiency and to minimize mobile-proton pathways that result in *b*- and *y*- type ions. Optimum HCD energy was between 15 and 20 (arbitrary unit).

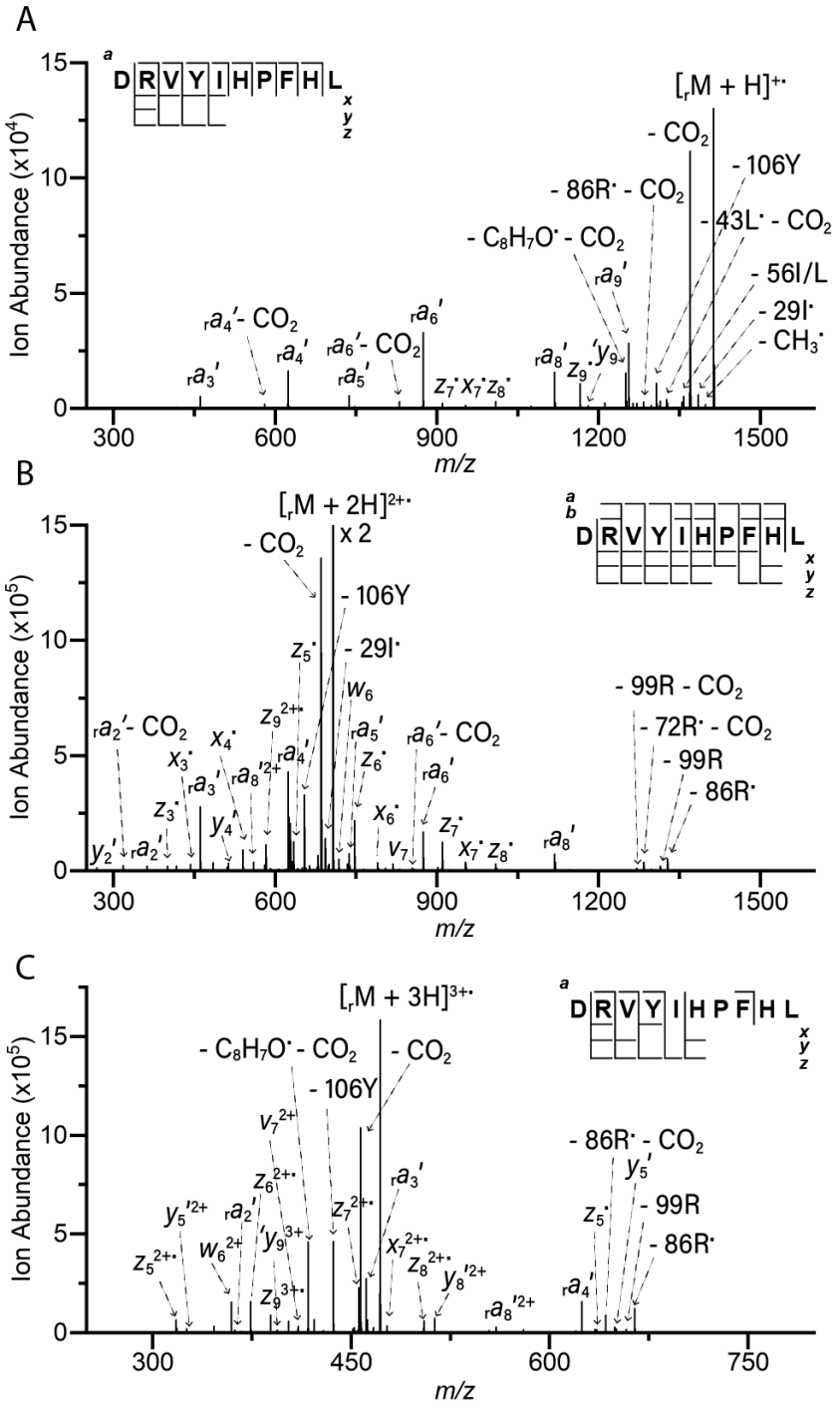

Figure 2.2 FRIPS MS^3 spectra of singly protonated (A), doubly protonated (B), and triply protonated (C) angiotensin I.

Figure 2.2 shows the FRIPS MS^3 spectra of singly- (Fig. 2.2A), doubly- (Fig. 2.2B), and triply- (Fig. 2.2C) protonated, conjugated angiotensin I (DRVYIHPFHL), which contains three basic

amino acid residues; one arginine, and two histidines. The subscript "r" in, e.g., $[_rM + H]^{+\bullet}$ and $_ra_5'$denotes the truncated radical initiator at the peptide N-terminus, corresponding to a mass increase of 117 Da compared with the non-modified peptide (Fig. 2.1, bottom panels) [14]. The fragment ion nomenclature follows the Zubarev nomenclature in which "•" denotes a hydrogen atom, as opposed to "H", which denotes a proton [22]. Sidechain losses are annotated according to Julian and co-workers' proposed system [23]. FRIPS-MS^3 of singly protonated angiotensin I (Fig. 2.2A) shows preferred CO_2 loss, followed by side chain losses and radical *a*- type ion formation. The dominance of N-terminal fragment ions is likely due to the arginine residue in the second position being the likely protonation site, i.e., complementary C-terminal fragments would be neutral and thus not detected. This spectrum is similar to the original work by Oh and co-workers [14]. However, the dominance of neutral CO_2 loss has not previously been explained. We note the similar behavior in radical-driven negative ion mode MS/MS techniques such as electron detachment dissociation (EDD) [24] and negative ETD [25] in which dominant CO_2 loss is proposed to occur following preferred electron detachment from a carboxylate group. In positive ion mode FRIPS, abstraction of a hydrogen radical from a neutral carboxylic acid would generate a similar intermediate. Angiotensin I contains two carboxylic acids that could serve as the site for such hydrogen abstraction. The FRIPS-MS^3 spectrum of doubly protonated angiotensin I in Figure 2.2B also shows preferential CO_2 loss, several side chain losses, and *a*-, *x*-, and *z*- type fragment ion peaks. The side chain losses in the m/z 600 to 800 region are doubly protonated and the side chain losses between m/z 1200 and 1400 are singly protonated. In addition to this radical-driven fragmentation *b*- and *y*- type ions, presumably from mobile proton-driven pathways are found in MS^3 of doubly protonated angiotensin I; however, these ions are of relatively low abundance compared to fragment ions from radical-driven pathways (low abundance ions are not labeled but

indicated in the sequence coverage in Figure 2.2). This spectrum is also similar to that reported in the original work by Oh and co-workers except they did not detect fragments above m/z 1,000. Furthermore, they did not examine triply charged angiotensin I. FRIPS-MS^3 of triply protonated angiotensin I is shown in Figure 2.2C. Similar to the lower charge states, side chain losses, CO_2 loss, *a*- and *z*- type ions are observed. Side chain loss peaks in the m/z 600 to 700 region are doubly charged while sidechain losses in the m/z 400 to 500 region are triply charged. For this higher charge state, *b*- type ions are surprisingly not observed. However, presumably mobile proton-based *y*- type ions are detected at somewhat higher abundance compared with doubly protonated angiotensin I. Overall, side chain losses were dominant, particularly the 106 loss from tyrosine, similar to doubly protonated angiotensin I. Interestingly, a previously unreported 163 Da loss from the precursor ion was observed for all three charge states of angiotensin I with particular prominence for the triply protonated precursor ion. We propose that this neutral loss is a combination of the truncated FRIPS tag ($C_8H_7O^{\bullet}$;119 Da) and CO_2 loss (44 Da). Preferential loss of the radical tag for the 3+ charge state may explain the lower sequence coverage compared with the 2+ charge state. This loss may be due to a more elongated confirmation, preventing hydrogen abstraction and accompanying radical propagation within the peptide. Nevertheless, radical-driven fragmentation to yield relatively abundant *a*-, *x*-, and *z*- type fragment ions persisted for all three examined charge states of angiotensin I.

Figure 2.3 displays FRIPS MS^3 spectra of singly-, doubly-, and triply protonated ACTH 1-10 (SYSMEHFRWG), a peptide containing two (rather than three) basic amino acids; arginine and histidine. For singly protonated ACTH 1-10, several *z*-type fragment ions are observed (Figure 2.3A). The higher number of C-terminal fragments is likely due to the arginine residue near the C-terminus being the preferred protonation site. Likewise, the abundant N-terminal $_r a_9'$ fragment ion

contains the arginine residue. Overall, *a*-, *x*-, and *z*- type fragment ions as well as side chain losses are prevalent, whereas *y*-type fragment ions, e.g., y_9', are observed with low abundance.

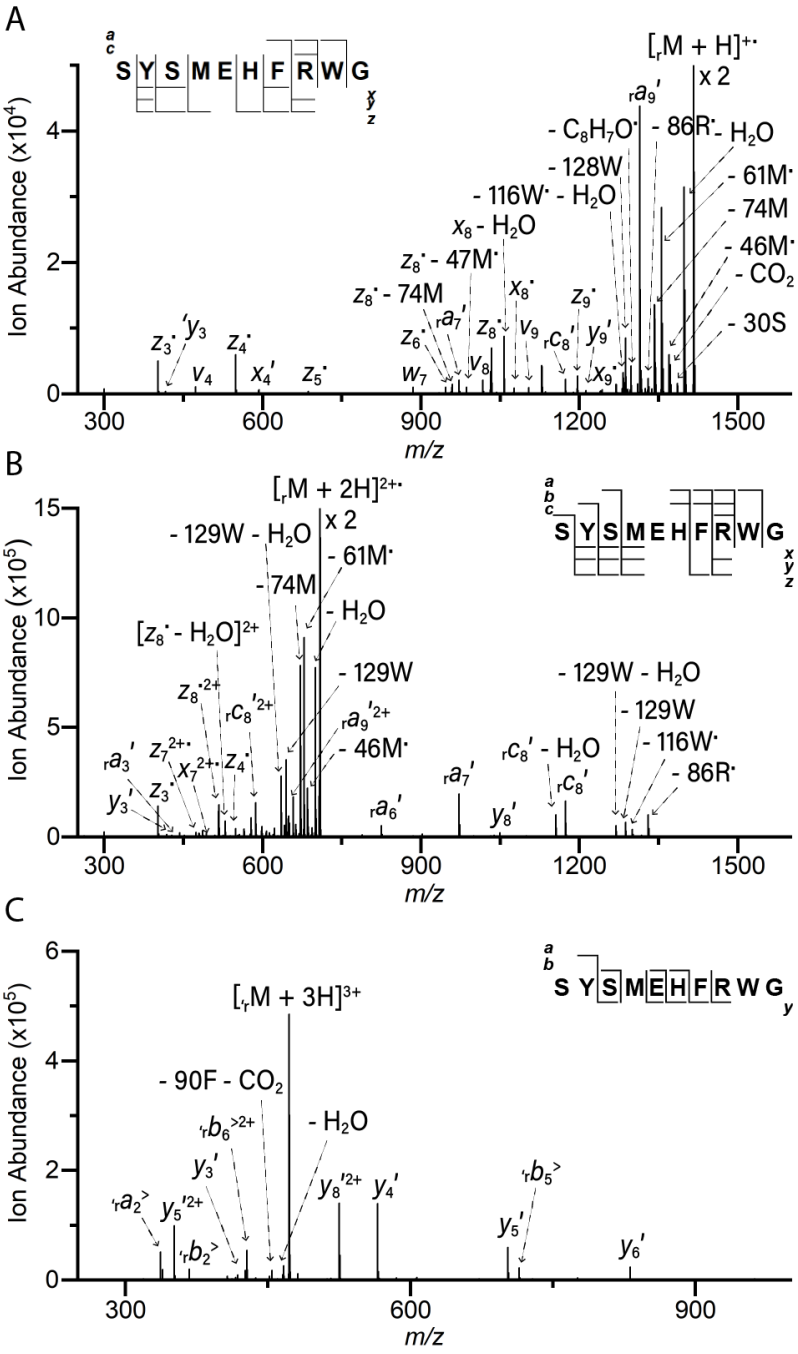

Figure 2.3 FRIPS MS^3 spectra of singly protonated (A), doubly protonated (B), and triply protonated (C) ACTH 1-10.

Similar to the singly protonated peptide, FRIPS MS^3 of doubly protonated ACTH 1-10 shows predominant side chain losses and *a*-, *x*-, and *z*- type fragment ions (Figure 2.3B). Side chain loss peaks between *m/z* 600 and 800 region are doubly charged, and side chain losses in the *m/z* 1200 to 1400 region are singly charged. However, unlike the singly protonated species (Figure 2.3A), *b*- type ions are also found at low ion abundance. By contrast, FRIPS MS^3 of triply protonated ACTH 1-10 (Figure 2.3C) shows a markedly different fragmentation pattern. In addition, the calculated *m/z* value for the desired precursor ion following initial homolytic cleavage of the *o*-TEMPO-Bz-C(O) tag, $[_rM + 3H]^{3+\bullet}$, is 472.87 while the experimentally observed precursor ion showed an m/z value of 472.53, i.e., one hydrogen too light, thus indicating heterolytic rather than homolytic cleavage. This undesired hydrogen atom loss is indicated by the "$['_rM + 3H]^{3+}$" label. HCD voltage of 15-20 (arbitrary unit) was applied for MS^3 of singly- and doubly protonated peptides. However, the triply protonated peptide did not show any fragment ions in this voltage range. By contrast, at higher HCD voltage (28 arbitrary units), the $['_rM + 3H]^{3+}$ species yielded even-electron *b*- and *y*- type fragment ions only. A similar outcome was reported by Sinz and co-workers in FRIPS of crosslinked peptides when the number of ionizing protons exceeded the number of basic amino acid residues [15]. These authors proposed that heterolytic cleavage of the *o*-TEMPO-Bz-C(O)label occurred following protonation of the tag itself to yield a linear truncated tag structure with positive charge on the methyl group (Figure 2.4A). As an alternative explanation, we propose that the peptide N-terminal nitrogen, linked to the *o*-TEMPO-Bz-C(O) tag via an amide bond, can be protonated when the third proton is added, thus promoting cyclization to form a cyclic truncated tag (Figure 2.4B) as a primary carbocation is highly unstable [26].

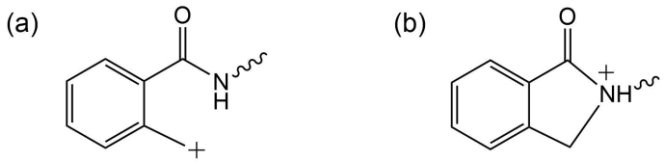

Figure 2.4 Proposed truncated Bz-C(O) tag structures (linear structure [15] (a) and ring structure (b)) from heterolytic cleavage of o-TEMPO-Bz-C(O) in CID when the number of ionizing protons exceeds the number of basic amino acid residues.

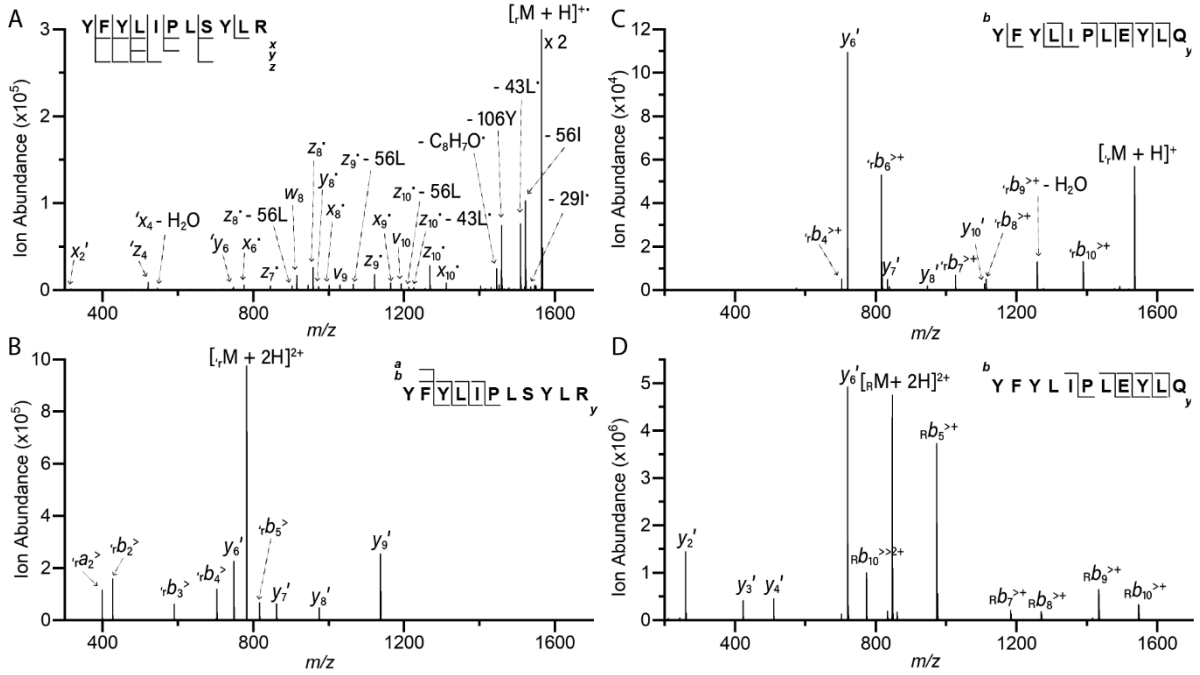

Figure 2.5 FRIPS MS^3 spectra of singly protonated P20 (A), doubly protonated P20 (B), singly protonated P6 (C) and FRIPS MS^2 spectrum of doubly protonated P6 (D).

Next, we explored FRIPS MS^3 of the peptides P20 (YFYLIPLSYLR) and P6 (YFYLIPLSYLQ), which contain one and zero basic amino acid residues, respectively. FRIPS MS^3 of singly protonated P20 shows relatively abundant side-chain losses and *x*-, *y*-, and *z*- type ions (Figure 2.5A). *a*- type ions are absent for this peptide, likely due to the C-terminal arginine residue being the preferred protonation site. Similar to triply protonated ACTH 1-10, adding a proton to P20 to exceed the number of basic residues resulted in heterolytic cleavage of the *o*-TEMPO-Bz-C(O) tag and MS^3 of the resulting even-electron species, $[{}^{\cdot}_{T}M + 2H]^{2+}$, only yielded *b*- and *y*-type fragment ions (Figure 2.5B) at an HCD voltage of 26 arbitrary units. This result

shows that mobile proton-driven pathways are dominant for doubly protonated P20. FRIPS MS^3 of singly protonated P6 (Figure 2.5C) also showed only even-electron *b*- and *y*- type fragment ions, i.e., not even the lowest possible charge state generated radical-driven fragmentation for this peptide lacking basic residues. Figure 2.5D shows the MS^2 behavior for the doubly protonated *o*-TEMPO-Bz-C(O)-labeled P6 peptide. When the number of protons exceeded the number of basic amino acid residues by two, mobile proton-driven peptide backbone cleavage occurred prior to cleavage of the radical initiator, thus leaving the intact radical initiator on the N-terminus of the peptide, as indicated by the subscript "R" in $[_{R}M + 2H]^{2+}$.. For that reason, further MS^3 was unfeasible.

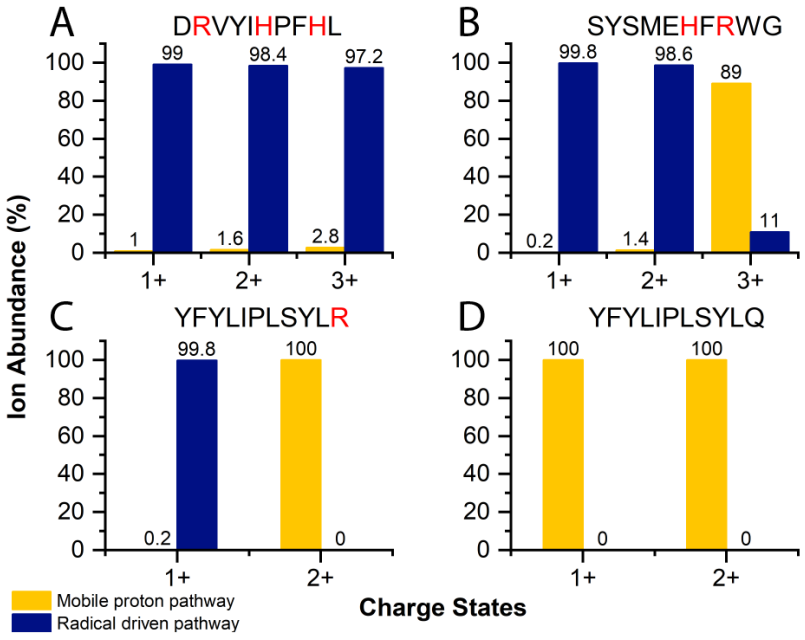

Figure 2.6 Bar chart showing charge state dependent FRIPS dissociation pathways for angiotensin I (A), ACTH 1-10 (B), P20 (C), and P6 (D). Basic amino acids are colored red in the peptide sequences.

The aforementioned results are summarized in Figure 2.6, illustrating how competition between desired radical-driven fragmentation pathways and undesired mobile proton-driven pathways appears dependent on peptide charge state with higher charge states yielding increasingly non-radical-based fragmentation. To generate these graphs, observed fragment ions were classified into

two groups based on the FRIPS dissociation pathways defined by Oh and co-workers [17]: fragments from radical-driven and mobile proton-driven pathways, respectively. Fragment ion abundances were summed and plotted as a function of charge state for each of the examined peptides. As shown in Figure 2.6, fragment ions generated by mobile proton-driven pathways increase in abundance as charge state increases. Mobile proton-driven fragmentation was extensively observed when the number of ionizing protons exceeded the number of basic amino acid residues, in good agreement with previous findings by the Sinz and Oh groups [15,21]

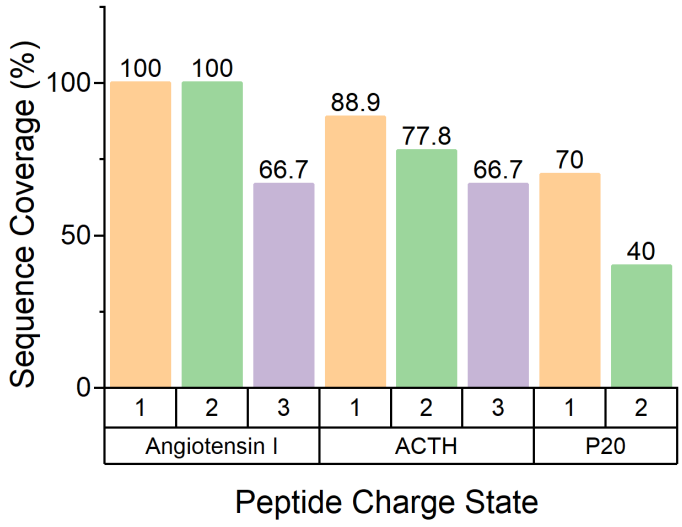

Figure 2.7 Sequence coverage for angiotensin I, ACTH 1-10, and P20 peptides as a function of charge state.

We further examined FRIPS peptide sequence coverage at each charge, as shown in Figure 2.7. The sequence coverage for P6 is not included because no radical-driven fragmentation was observed for neither the singly-, nor the doubly protonated peptide. The highest sequence coverage was obtained for singly protonated peptides. FRIPS of triply protonated angiotensin I and doubly protonated ACTH 1-10 still showed extensive radical-driven dissociation; however, the resulting

sequence coverage was lower than for the lower charge states. Overall, the lower the charge state, the higher quality FRIPS data.

2.3.2 FRIPS Charge Carrier Effect

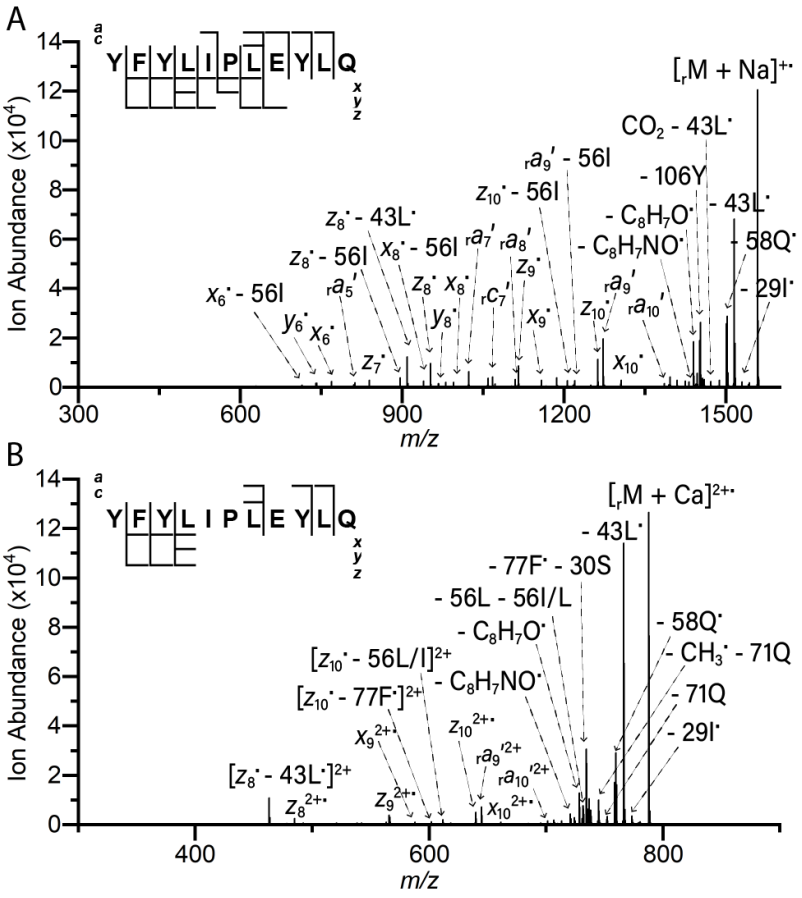

Figure 2.8 FRIPS MS^3 spectra of Na-adducted singly charged- (A), and Ca-adducted doubly charged (B) synthetic peptide YFYLIPLEYLQ. All fragment ions carry metal adducts.

Previous research for crosslinked peptides [15] showed that radical-driven dissociation can be restored by using sodium cation adducts as an alternative charge carrier. Other work showed that the presence of arginine residues with higher proton affinity also improves radical-driven fragmentation [21]. We applied sodium cationization to the peptide P6 (YFYLIPLSYLQ), which did not show any radical-driven fragmentation in its protonated state due to the lack of basic amino

acid residues. Previously our group has shown that abundant multiply charged peptide cations can be generated via complexation with alkaline-earth and other multivalent metal ions [27]. This multivalent metal adduction strategy has also been employed by Chan and co-workers as well as Williams and co-workers to alter fragmentations outcomes in electron capture dissociation [28–30]. We hypothesized that replacing the proton (H^+) charge carrier with multivalent metal ions would also restore radical-driven dissociation in FRIPS.

FRIPS MS^3 of singly sodiated P6 is shown in Figure 2.8A. Unlike protonated P6, the major fragment ions generated in FRIPS of sodiated P6 are *a*-, *c*-, *x*-, and *z*- type ions along with side-chain losses from the precursor ions. By contrast, *b*- and *y*- type ions were predominantly observed in FRIPS MS^3 of singly protonated P6. No *b*- ions were found in the FRIPS MS^3 spectrum of sodium ion-adducted P6. All fragment ions were observed with Na+ as the charge carrier (Figure 2.8A). The desired radical-driven pathways achieved a sequence coverage of 100%.

Calcium ion (Ca^{2+}) adduction allowed us to also further examine the fragmentation behavior of doubly charged P6. Interestingly, homolytic *o*-TEMPO-Bz-C(O) cleavage occurred in MS^2 of the calcium adducted, conjugated P6 peptide without peptide backbone dissociation. Furthermore, radical-driven fragmentation was achieved in MS^3 of the generated radical precursor ion, including side chain losses and *a*-, *z*- type ions, as shown in Figure 2.8B. No *b*- ions were observed following MS^3. FRIPS MS^3 of calcium-adducted P6 generated larger fragment ions, and resulted in fewer backbone cleavage compared with sodiated P6. The sequence coverage in FRIPS MS^3 of the calcium-adducted peptide was 60%. All observed fragment ions were metalated.

2.4 Conclusion

We demonstrated charge state and charge carrier effects upon FRIPS dissociation pathways. The existence of basic amino acid residues that can partially sequester mobile protons is important

to promote radical-driven dissociation pathways. In such radical-driven dissociation, side chain losses are abundant, including the combination of two side chain losses from the precursor ion and the fragment ions. Because FRIPS radical-driven dissociation pathways compete with mobile proton-driven dissociation pathways, the higher the protonation state, the more *b*- and *y*-type ions were generated. The highest sequence coverage from radical-driven dissociation was obtained for singly protonated peptides. Thus, a low charge state is preferred. Peptides lacking basic amino acid residues can be compatible with FRIPS when proton charge carriers are replaced with metal ions. FRIPS MS3 spectra of metalated P6 exhibit the side chain loss peaks as well as metalated fragment ions. Comparison between Na^+ and Ca^{2+}-adducted peptides showed that the highest sequence coverage was obtained when sodium ions were used as charge carrier, presumably due to the overall lower charge state enabling more gentle ion-neutral collisions in CID. These findings are valuable for optimizing information content in FRIPS, particularly for acidic peptides.

2.5 Acknowledgement

This work was supported by the National Science Foundation CHE 1609840 and the University of Michigan. The Thermo Scientific Orbitrap Fusion Lumos was acquired via National Institutes of Health grant S10 OD021619. I would like to thank Dr. Borotto for his guidance.

2.6 References

[1] Aebersold, R.; Mann, M. Mass-Spectrometric Exploration of Proteome Structure and Function. *Nature*, **2016**, *537*, 347–355.
[2] Aebersold, R.; Mann, M. Mass Spectrometry-Based Proteomics. *Nature*, **2003**, *422*, 198–207.
[3] McLuckey, S.A. Principles of Collisional Activation in Analytical Mass Spectrometry. *J. Am. Soc. Mass Spectrom.*, **1992**, *3*, 599–614.
[4] Bythell, B.J.; Suhai, S.; Somogyi, Á.; Paizs, B. Proton-Driven Amide Bond-Cleavage Pathways of Gas-Phase Peptide Ions Lacking Mobile Protons. *J. Am. Chem. Soc.*, **2009**, *131*, 14057–14065.
[5] Tsai, Y.S.; Scherl, A.; Shaw, J.L.; Mackay, C.L.; Shaffer, S.A.; Langridge-smith, P.R.R.;

Goodlett, D.R. Precursor Ion Independent Algorithm for Top-Down Shotgun Proteomics. *J. Am. Soc. Mass Spectrom.*, **2009**, *20*, 2154–2166.
[6] Siuti, N.; Kelleher, N.L. Decoding Protein Modifications Using Top-down Mass Spectrometry. *Nat. Methods*, **2007**, *4*, 817–821.
[7] Zubarev, R.A.; Horn, D.M.; Fridriksson, E.K.; Kelleher, N.L.; Kruger, N.A.; Lewis, M.A.; Carpenter, B.K.; McLafferty, F.W. Electron Capture Dissociation for Structural Characterization of Multiply Charged Protein Cations. *Anal. Chem*, **2000**, *72*, 563–573.
[8] Wiesner, J.; Premsler, T.; Sickmann, A. Application of Electron Transfer Dissociation (ETD) for the Analysis of Posttranslational Modifications. *Proteomics*, **2008**, *8*, 4466–4483.
[9] Adamson, J.T.; Håkansson, K. Electrospray Ionization Fourier Transform Ion Cyclotron Resonance Mass Spectrometry for Lectin Analysis. In *Lectins: Analytical Technologies*; Nilson, C.L., Ed.; Elsevier Science, **2007**; pp. 343–371.
[10] Zubarev, R.A.; Kelleher, N.L.; McLafferty, F.W. Electron Capture Dissociation of Multiply Charged Protein Cations. A Nonergodic Process. *J. Am. Chem. Soc.*, **1998**, *120*, 3265–3266.
[11] Syka, J.E.P.; Coon, J.J.; Schroeder, M.J.; Shabanowitz, J.; Hunt, D.F. Peptide and Protein Sequence Analysis by Electron Transfer Dissociation Mass Spectrometry. *Proc. Natl. Acad. Sci. U. S. A.*, **2004**, *101*, 9528–9533.
[12] Masterson, D.S.; Yin, H.; Chacon, A.; Hachey, D.L.; Norris, J.L.; Porter, N.A. Lysine Peroxycarbamates: Free Radical-Promoted Peptide Cleavage. *J. Am. Chem. Soc.*, **2004**, *126*, 720–721.
[13] Hodyss, R.; Cox, H.A.; Beauchamp, J.L. Bioconjugates for Tunable Peptide Fragmentation: Free Radical Initiated Peptide Sequencing (FRIPS). *J. AM. CHEM. SOC*, **2005**, *127*, 12436–12437.
[14] Lee, M.; Kang, M.; Moon, B.; Oh, H. Bin. Gas-Phase Peptide Sequencing by TEMPO-Mediated Radical Generation. *Analyst*, **2009**, *134*, 1706–1712.
[15] Ihling, C.; Falvo, F.; Kratochvil, I.; Sinz, A.; Schäfer, M. Dissociation Behavior of a Bifunctional Tempo-Active Ester Reagent for Peptide Structure Analysis by Free Radical Initiated Peptide Sequencing (FRIPS) Mass Spectrometry. *J. Mass Spectrom.*, **2015**, *50*, 396–406.
[16] Lee, M.; Lee, Y.; Kang, M.; Park, H.; Seong, Y.; Sung, B.J.; Moon, B.; Oh, H. Bin. Disulfide Bond Cleavage in TEMPO-Free Radical Initiated Peptide Sequencing Mass Spectrometry. *J. mass Spectrom.*, **2011**, *46*, 830–839.
[17] Lee, C.S.; Jang, I.; Hwangbo, S.; Moon, B.; Oh, H. Bin. Side Chain Cleavage in TEMPO-Assisted Free Radical Initiated Peptide Sequencing (FRIPS): Amino Acid Composition Information. *Bull. Korean Chem. Soc.*, **2015**, *36*, 810–814.
[18] Borotto, N.B.; Ileka, K.M.; Tom, C.A.T.M.B.; Martin, B.R.; Håkansson, K. Free Radical Initiated Peptide Sequencing for Direct Site Localization of Sulfation and Phosphorylation with Negative Ion Mode Mass Spectrometry. *Anal. Chem.*, **2018**, *90*, 9682–9686.
[19] Jang, I.; Jeon, A.; Lim, S.G.; Hong, D.K.; Kim, M.S.; Jo, J.H.; Lee, S.T.; Moon, B.; Oh, H. Bin. Free Radical-Initiated Peptide Sequencing Mass Spectrometry for Phosphopeptide Post-Translational Modification Analysis. *J. Am. Soc. Mass Spectrom.*, **2019**, *30*, 538–547.
[20] Degraan-Weber, N.; Zhang, J.; Reilly, J.P. Distinguishing Aspartic and Isoaspartic Acids in Peptides by Several Mass Spectrometric Fragmentation Methods. *J. Am. Soc. Mass*

Spectrom., **2016**, *27*, 2041–2053.
[21] Jeon, A.; Lee, J.H.; Kwon, H.S.; Park, H.S.; Moon, B.J.; Oh, H. Bin. Charge-Directed Peptide Backbone Dissociations of o-TEMPO-Bz-C(O)- Peptides. *Mass Spectrom. Lett.*, **2013**, *4*, 71–74.
[22] Kjeldsen, F.; Haselmann, K.F.; Budnik, B.A.; Jensen, F.; Zubarev, R.A. Dissociative Capture of Hot (3–13 EV) Electrons by Polypeptide Polycations: An Efficient Process Accompanied by Secondary Fragmentation. *Chem. Phys. Lett.*, **2002**, *356*, 201–206.
[23] Sun, Q.; Nelson, H.; Ly, T.; Stoltz, B.M.; Julian, R.R. Side Chain Chemistry Mediates Backbone Fragmentation in Hydrogen Deficient Peptide Radicals. *J. Proteome Res.*, **2009**, *8*, 958–966.
[24] Zubarev, R.A.; Nielsen, M.L.; Budnik, B.A. Tandem Ionization Mass Spectrometry of Biomolecules. *Eur. J. Mass Spectrom.*, **2000**, *6*, 235–240.
[25] Coon, J.J.; Shabanowitz, J.; Hunt, D.F.; Syka, J.E.P. Electron Transfer Dissociation of Peptide Anions. *J. Am. Soc. Mass Spectrom.*, **2005**, *16*, 880–882.
[26] Shi, R.; Wang, F.; Tana; Li, Y.; Huang, X.; Shen, W. A Highly Efficient Cu/La2O3 Catalyst for Transfer Dehydrogenation of Primary Aliphatic Alcohols. *Green Chem.*, **2010**, *12*, 108–111.
[27] Liu, H.; Håkansson, K. Divalent Metal Ion-Peptide Interactions Probed by Electron Capture Dissociation of Trications. *J. Am. Soc. Mass Spectrom.*, **2006**, *17*, 1731–1741.
[28] Fung, Y.M.E.; Liu, H.; Chan, T.-W.D. Electron Capture Dissociation of Peptides Metalated with Alkaline-Earth Metal Ions. *J. Am. Soc. Mass Spectrom.*, **2006**, *17*, 757–771.
[29] Chen, X.; Fung, Y.M.E.; Chan, W.Y.K.; Wong, P.S.; Yeung, H.S.; Chan, T.-W.D. Transition Metal Ions: Charge Carriers That Mediate the Electron Capture Dissociation Pathways of Peptides. *J. Am. Soc. Mass Spectrom.*, **2011**, *22*, 2232–2245.
[30] Flick, T.G.; Donald, W.A.; Williams, E.R. Electron Capture Dissociation of Trivalent Metal Ion-Peptide Complexes. *J. Am. Soc. Mass Spectrom.*, **2013**, *24*, 193–201.

Chapter 3

Mobile Proton Control for Improved Sulfopeptide Stability and Tandem Mass Spectrometry Behavior in Positive Ion Mode

3.1 Introduction

Tyrosine sulfation is a posttranslational modification (PTM) that occurs in the trans-Golgi network and is catalyzed by two membrane bound tyrosylprotein sulfotransferases (TPSTs) [1]; TPST-1 and TPST-2. Tyrosine sulfated proteins are involved in several biological functions, including blood coagulation, leukocyte rolling, hormonal regulation, immunity, and G-protein coupled receptors for chemokines [2,3]. Mass spectrometry (MS) is a powerful analytical tool for characterizing protein PTMs; however, there are severe analytical challenges in the identification of tyrosine sulfation. Sulfonate groups (SO_3) are labile under acidic conditions, and facile SO_3 loss occurs during both electrospray ionization (ESI) and tandem MS (MS/MS) activation in positive ion mode [4,5], including radical-driven MS/MS, e.g., electron capture and transfer dissociation (ECD/ETD) [6] that can effectively retain other labile PTMs such as phosphorylation. Thus, sulfation sites cannot be directly determined and limited sequence information is typically generated for the corresponding peptides. This facile sulfonate loss in sulfopeptide cations has been proposed to be due to mobile proton-mediated elimination [5]. Another challenge is that

phosphorylation (HPO_3) has the same nominal mass, 80 Da, as sulfation (SO_3), with the exact mass difference being only 9.5 mDa [7]. Without using FT-based instruments such as FT-ICR or Orbitrap mass spectrometers, this mass difference is difficult to detect with certainty. Also, due to the acidic nature of the sulfate group, negative ion mode MS is preferred due to improved ionization efficiency and higher gas-phase stability of deprotonated sulfate groups. Negative ion mode MS/MS approaches, including negative ion electron capture dissociation (niECD) [8,9], negative ion mode ultraviolet photodissociation [10], negative electron transfer dissociation [8], and negative ion mode free radical initiated peptide sequencing (FRIPS)[11] demonstrated limited sulfonate loss during peptide dissociation. However, negative ion mode tandem MS data can be difficult to interpret [12], experimental time scales may not be compatible with liquid chromatography (LC) separation [8,9], and MS-based bioinformatics tools are optimized for positive ion mode [13].

Our group previously showed that divalent metal charge carriers can stabilize sulfate groups in positive ion mode. ECD of such metal-adducted sulfopeptides resulted in *c*- and *z*-type ions retaining sulfation [4]. A recent study by McLuckey and co-workers showed that guanidinium adducts can also stabilize sulfation [14]. Chen et al. reported that tyrosine sulfated peptides could be directly characterized by ETD and ETD followed by collision induced dissociation (ETciD) [5]; however, sequence coverage was low and significant sulfonate loss still occurred. Yagami et al. demonstrated that sulfated peptides containing arginine residues or intermolecularly complexed with an arginine-rich peptide were more stable in both liquid secondary ion MS^1 and MALDI MS^1 compared with sulfopeptides lacking arginine [5]. These authors proposed that sulfate-arginine conjugate acid-base pairs were responsible for this stabilization. Similarly, we recently found that tryptic sulfopeptides, i.e., lysine- or arginine-containing peptides, from rat liver Golgi membrane

appeared more stable in ESI than standard, acidic sulfopeptides [15]. Here, we examine the influence of basic amino acid side chains on the ESI-MS and MS/MS stability of sulfopeptide cations in the absence of adducts. Several radical-driven tandem MS techniques are explored, including ECD, ETD, and FRIPS. In addition, we further evaluate the influence of high proton affinity chemical groups and fixed positive charging on sulfopeptide cation stability through peptide chemical derivatization with the goal of establishing a proteomics compatible workflow for global analysis of protein tyrosine sulfation.

3.2 Experimental

3.2.1 Materials

Synthetic peptides (H-DRVY(SO_3)IHPFHL-OH), (H-DLVY(SO_3)IHPFHK-OH), (H-TDVCY(SO3)YHQK-OH) and (H-TDVCYY(SO_3)HQK-OH), were obtained from Genscript Corp (Piscataway, NJ). Cholecystokinin fragment 26-33 (CCKS, DY(SO_3)MGWMDF-NH_2), and hirudin fragment 55-65 (H-DFEEIPEEY(SO_3)LQ-OH) were purchased from Sigma-Aldrich (St. Louis, MO). Water, methanol, triethylamine (TEA), trifluoroacetic acid (TFA), phosphate buffered saline (PBS) pH 7.2, and formic acid of LC-MS grade were purchased from Fisher chemical (Fair Lawn, NJ). *o*-TEMPO-Bz-C(O)-NHS was acquired from FutureChem (Seoul, Korea). Triethylamine bicarbonate (TEAB), iodoacetamide (IAM), *N*-ethylmaleimide (NEM), 1-Methyl-2-vinylpyridinium triflate (VP), dimethyl sulfoxide (DMSO), *O*-methylisothiourea hemisulfate, 1H-pyrazole-1-carboxamidine hydrochloride (HPCA), and C18 Ziptips were purchased from Sigma Aldrich.

3.2.2 Peptide Chemical Derivatization

Lysine and N-terminal Guanidination

Lysine guanidination reactions were carried out as previously described [16] with some modifications. *O*-methylisothiourea hemisulfate, 15 mg in 15 µL of 10 % TEA, was prepared. Three µL of 100 mM peptide solution (in water) was mixed with 2 µL of the *O*-methylisothiourea hemisulfate solution. This mixture was combined with 5 µL of 10 % TEA, followed by incubation for 30 min at 65 °C. The reaction mixture was acidified with 10 % TFA and guanidinated peptides were desalted by C18 ziptips.

The procedure for N-terminal guanidination was slightly modified from a previously described protocol[17]. Two µL of 2 mM HPCA in 10 % TEA was added to 2 µL of 1 mM peptide (in water), followed by addition of 2 µL, 10 % TEA. The reaction solution was incubated at 95 °C for 1 h, acidified with 10 % TFA and resulting guanidinated peptides were desalted by C18 ziptips.

Cysteine alkylation

Cysteine residues in sulfopeptides were modified with either IAM, NEM, or VP. For IAM modification, three µL of 100 mM TEAB buffer was added to 3 µL of 1 mM peptide solutions (in water). Iodoacetamide was prepared at 100 mM in 100 mM TEAB. Three µL of this solution was added to the peptide solution, which was then vortexed briefly. This reaction solution was incubated at 45 °C for 45 min in the dark. The sample was then incubated at room temperature for 15 min, acidified with 1.5 µL of 10 % TFA, and purified with C18 ziptips.

NEM solution was prepared by adding 50 µL of PBS, pH 7.2, to 1 mg of NEM. Two µL of NEM solution was added to 2 µL of 1 mM peptide in PBS, pH 7.2,. The mixture was vortexed briefly and incubated at room temperature for 1 hour. One µL of 100 mM TEAB buffer was then

added to the mixture, followed by adding 3 μL of 10 % TFA. This sample was purified using C18 ziptips.

Cysteine modification with quaternized vinyl pyridine was performed as previously described [18] with some modifications. Sodium phosphate (NaPi), 100 mM, pH 8 buffer was prepared. Eight μL DMSO was added to 90 μL of NaPi buffer solution. This mixture was added to 1 μL of 1 mM peptide (in water). 1-methyl-2-vinylpyridinium triflate was dissolved in DMSO to 10 mM. The peptide/buffer mixture was added to 2 μL of 1-methyl-2-vinylpyridinium triflate buffer. The reaction solution was briefly vortexed and incubated for ~1-2 hours at 37 °C. The reaction was quenched by adding 15 μL of 10 % TFA. The sample was desalted by C18 microspin column (Harvard apparatus, Holliston, MA).

o-TEMPO-Bz-NHS Peptide Conjugation Reaction

The conjugation reaction is described in Chapter 2. Briefly, a peptide N-terminus was conjugated with *o*-TEMPO-Bz-C(O)-NHS at a 1:25 ratio. The reaction solution was incubated at room temperature overnight, followed by C18 reversed phase solid phase extraction with a Vac cartridge (Sep-Pak C18 1 cc Vac Cartridge: Waters Corp., Miliford, MA, USA) and drying by SpeedVac.

3.2.3 Mass Spectrometry

CID and ECD experiments were performed in positive ion mode on a 7 T SolariX quadrupole Fourier transform ion cyclotron resonance (FT-ICR) mass spectrometer (Bruker Daltonics, Billerica, MA, USA) equipped with an Apollo II ESI source. The samples were directly infused at a flow rate of 120 μL/h. The capillary voltage, capillary exit voltage, funnel 1 voltage, drying gas flow rate, and drying gas temperature were set to 3,900 V, 270 V, 150 V, 3.8 L/min, and 180 ºC, respectively. Precursor ions were selected by the quadrupole using an 8-12 m/z

isolation window, then accumulated for 0.1-0.5 s in the hexapole collision cell. For CID experiments, 1-10 V of collision voltage was applied. CID spectra were averaged over 10-20 scans with 256 k data points per spectrum. ECD experiments were performed in the ICR cell at a cathode heating current of 1.6 A. The ECD bias, ECD lens, and irradiation time were set to 1-2 V, 8-10 V, and 150-500 ms, respectively. ECD spectra were averaged over 20-30 scans.

ETD experiments were performed in positive ion mode on an Orbitrap Fusion Lumos Tribrid Mass Spectrometer (Thermo Scientific, San Jose, CA) equipped with a nanospray Flex ion source. The samples were directly infused at a flow rate of 0.5 μL/min. The ESI voltage was 1700 V, the ion transfer tube temperature was 160 ºC, and a resolution of 50,000 was used for MS^1 scans. For MS^2, the ETD reaction time was adjusted between 10 and 50 ms, and the ETD spectra were averaged over 50-100 scans.

Data analysis was performed manually using Bruker Data Analysis 5.0, and Thermo Xcalibur Qual Browser Theoretical masses of precursor and fragment ions were predicted by the MS product function in Protein prospector (http://prospector.ucsf.edu/prospector/cgi-bin/msform.cgi?form=msproduct).
An in-house Excel macro was used for analysis of the FRIPS experimental data.

3.3 Results and Discussion

3.3.1 Influence of Basic Amino Acid Residues on Sulfopeptide Stability in ESI-MS

The standard acidic sulfopeptides cholecystokinin fragment 26-33 (CCKS, H-DY(SO_3)MGWMDF-NH_2), hirudin fragment 55-65 (H-DFEEIPEEY(SO_3)LQ-OH), and synthetic sulfoangiotensin I (H-DRVY(SO_3)IHPFHL-OH) were subjected to ESI-FT-ICR MS. Based on known sulfotyrosine-containing proteins, consensus features for tyrosine sulfation have been proposed: acidic amino acids, i.e., aspartic and glutamic acid, is usually present at position -5 to

+5 from the sulfated tyrosine, no cysteine residues or N-linked glycosylation are located from the -7 to +7 position, and turn-inducing amino acids such as proline, glycine, serine, asparagine, and glutamine are typically present at the -7 to +7 position [1,19,20]. Accordingly, the standard sulfopeptides CCKS and hirudin lack basic amino acid residues. By contrast, our first model sulfopeptide, synthetic sulfoangiotensin I, contains three basic amino acid residues. Positive ion mode ESI-FT-ICR mass spectra of singly protonated CCKS and hirudin as well as doubly protonated sulfoangiotensin I at 2V collision energy are shown in Figure 3.1a-c. This low collision energy does not typically induce peptide fragmentation. However; CCKS and hirudin show significant sulfonate (SO_3) loss (Figures 3.1a, b). By contrast, sulfonate loss was not observed for doubly protonated sulfoangiotensin I (Figure 3.1c),despite the higher charge state. At 7 V, a relatively mild collision energy, the acidic sulfopeptides were completely desulfated (Figures 3.1d, e) while sulfoangiotensin I began to undergo sulfonate loss (Figure 3.1f). These results are in good agreement with the findings of Yagami et al for LSIMS and MALDI. At even higher CID voltage, sulfoangiotensin I also showed complete desulfation; however, as expected, no sulfated fragment ions were observed in CID.

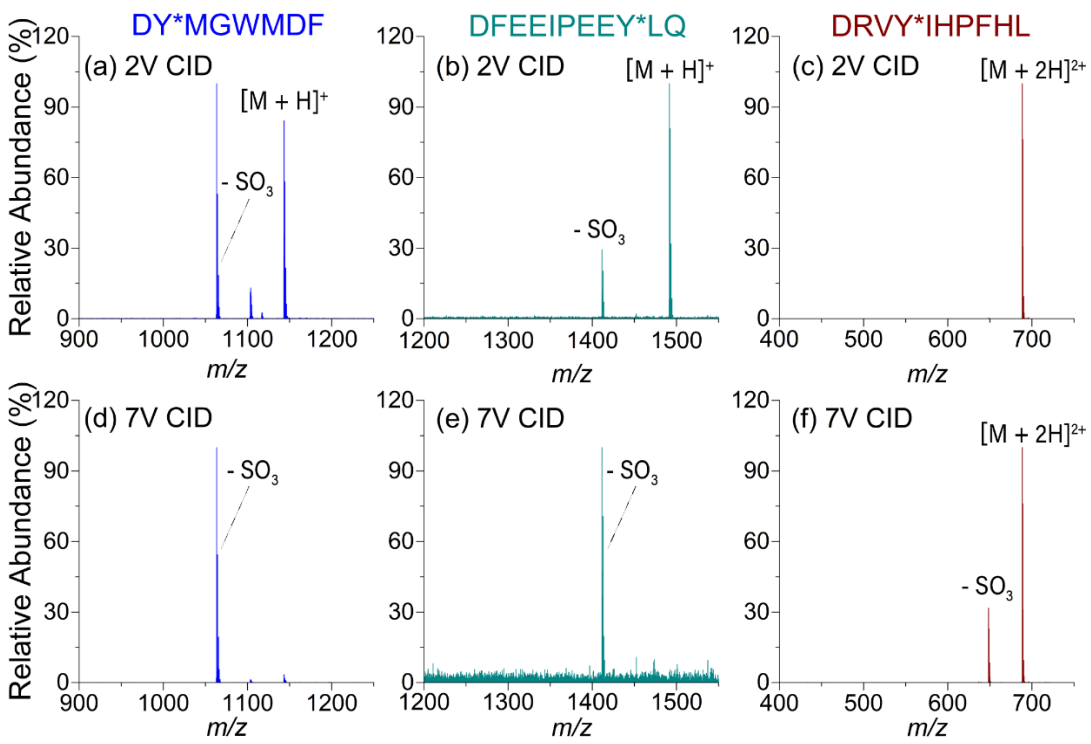

Figure 3.1 Positive ion mode ESI-FT-ICR mass spectra of sulfated peptides: singly charged CCKS 26-33 (a, d), singly charged hirudin 54-65 (b, e), and doubly charged synthetic sulfoangiotensin I (c, f), at two collision voltages. Asterisks (*) denote sulfated tyrosine.

To more accurately mimic a tryptic sulfopeptide, we modified the sulfoangiontensin I sequence to contain a lysine residue at the C-terminal end: H-DVY(SO_3)IHPFHLK-OH. We also generated the lysine-guanidinated, homoarginine, version of this peptide for comparison. Figure 3.2 shows the positive ion mode ESI-FT-ICR mass spectra at 2 V and 7 V collision energy for these sulfoangiotensin I-derived tryptic-like peptides as well as the original sulfoangiotensin for comparison. At 2 V collision energy, all three basic residue-containing sulfopeptides show complete sulfate retention (Figures 3.2 a-c) whereas, at 7 V, the original arginine- (Fig. 3.2d) and the homoarginine- (Fig. 3.2f) containing peptides showed similar stability (~30% SO_3 loss). By contrast, the lysine-containing peptide (Fig. 3.2e) showed a higher degree of SO_3 loss. This result may be explained by the lower propensity of lysine to form a salt bridge with the sulfate group, or

based on the lower proton affinity of lysine, thus enabling more facile mobile proton-driven SO_3 loss.

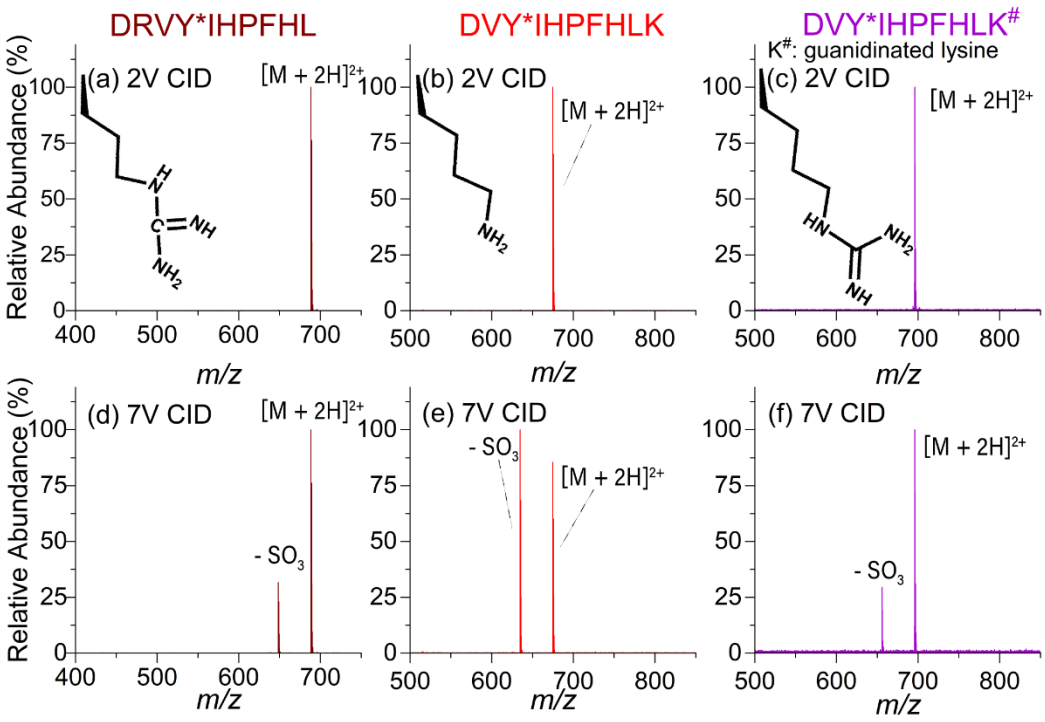

Figure 3.2 Positive ion mode ESI FT-ICR mass spectra of doubly protonated sulfoangiotensin I (a, d), modified (lysine-containing, tryptic-like) sulfoangiotensin I (b, e), and guanidinated modified sulfoangiotensin I (c, F). Asterisks (*) denote sulfation, and pound (#) denotes guanidination.

3.3.2 Influence of Basic Amino Acid Residues on Sulfopeptide Stability in Radical-Driven MS/MS

Encouraged by the observed significantly higher positive ion mode stability of sulfopeptides containing basic amino acid residues, we hypothesized that radical-driven MS/MS techniques may be more successful for such peptides than previously reported for acidic sulfopeptides, particularly under careful mobile proton control. Figure 3.3 shows the ECD MS/MS spectra of doubly- and triply protonated sulfoangiotensin I. As hypothesized, significant sulfate retention was observed for the doubly charged precursor ion (Figure 3.3 a). By contrast, abundant sulfonate loss from the precursor ions as well as the charged reduced species, $[M + 3H]^{2+\bullet}$, were

observed for triply charged sulfoangiotensin I (Figure 3.3b). Furthermore, no sulfated fragment ions were observed in ECD of the higher sulfopeptide charge state.

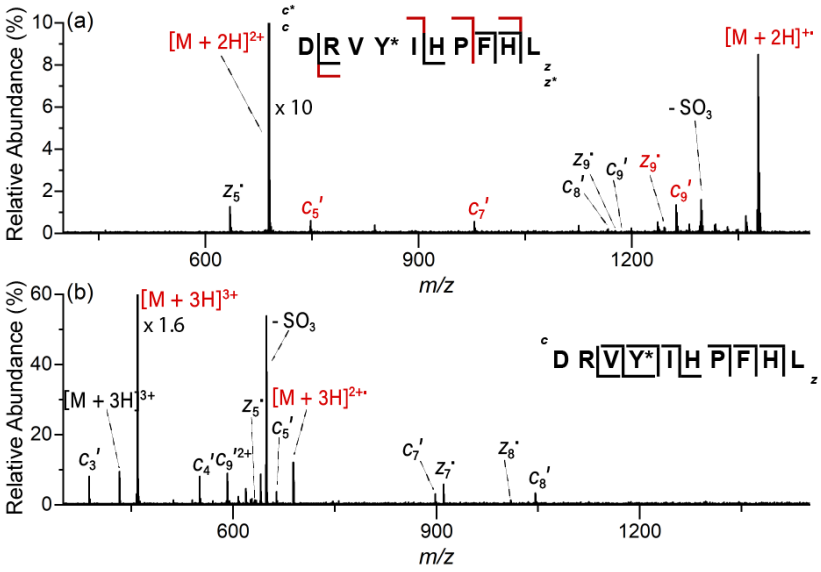

Figure 3.3 ECD spectra of doubly- (a) and triply- (b) protonated sulfoangiotensin I. Precursor and fragment ions retaining sulfation are highlighted in red.

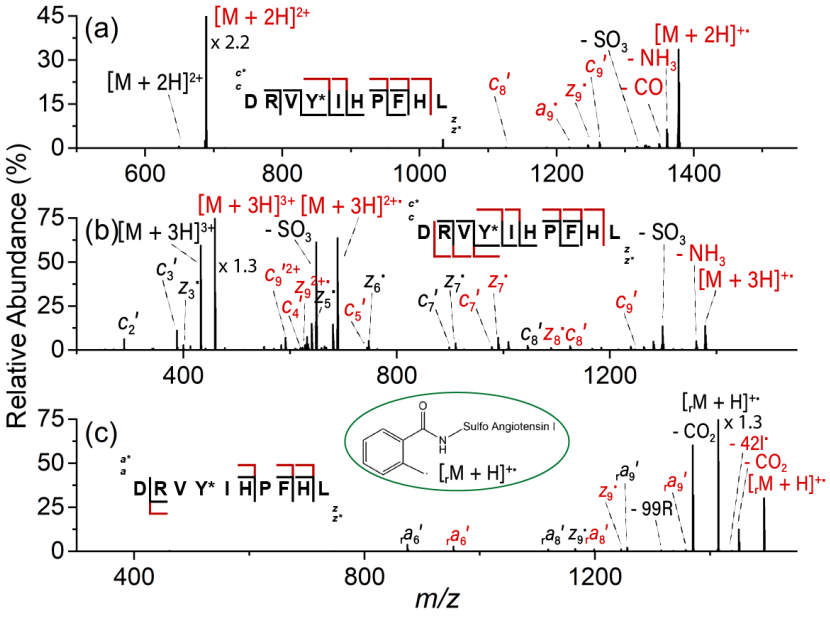

Figure 3.4 ETD of doubly- (a) and triply- (b) protonated sulfoangiotensin I as well as FRIPS MS3 of the singly protonated peptide (c). Lower case 'r' denotes truncated FRIPS tag [21]. Precursor and fragment ions retaining sulfation are highlighted in red.

Figure 3.4 shows the ETD MS/MS and FRIPS MS^3 spectra of sulfoangiotensin I. In ETD sulfated fragment ions were observed for both doubly- (Fig. 3.4a) and triply- (Fig. 3.4b) protonated precursor ions. We propose that the difference between ECD and ETD of triply protonated sulfoangiotensin I is due to the internal energy difference following electron-ion and ion-ion recombination, respectively, as well as the different pressure and temperature regimes where these reactions take place. In ECD, electron capture occurs under ultrahigh vacuum in the immediate vicinity of a hot cathode [22], whereas electron transfer occurs in an ion trap at orders of magnitude higher pressure at which precursor ions are collisionally cooled [22].

Intriguingly, in FRIPS MS^3 of sulfoangiotensin I, homolytic cleavage to yield the truncated radical initiator $[_rM + H]^{+\bullet}$ (shown in the inset of Fig. 3.4c) was observed with only partial sulfonate loss. Thus, sulfate-containing $[_rM + H]^{+\bullet}$ ions could be further isolated and subjected to higher energy collision dissociation (HCD) to propagate the radical site and induce the backbone fragmentation shown in Fig. 3.4c, including several sulfate-retaining fragment ions. Unlike ECD/ETD, FRIPS is compatible with singly charged precursor ions, i.e., the sole proton charge carrier is likely located on the arginine residue, which partially prevents mobile proton-driven sulfonate loss. However, sequence coverage was lower in FRIPS compared with ETD, and more substantial sulfonate loss was observed in FRIPS due to collisional activation.

3.3.3 N-terminal Guanidination for Enhanced MS and MS/MS Stability of an Acidic Sulfopeptide

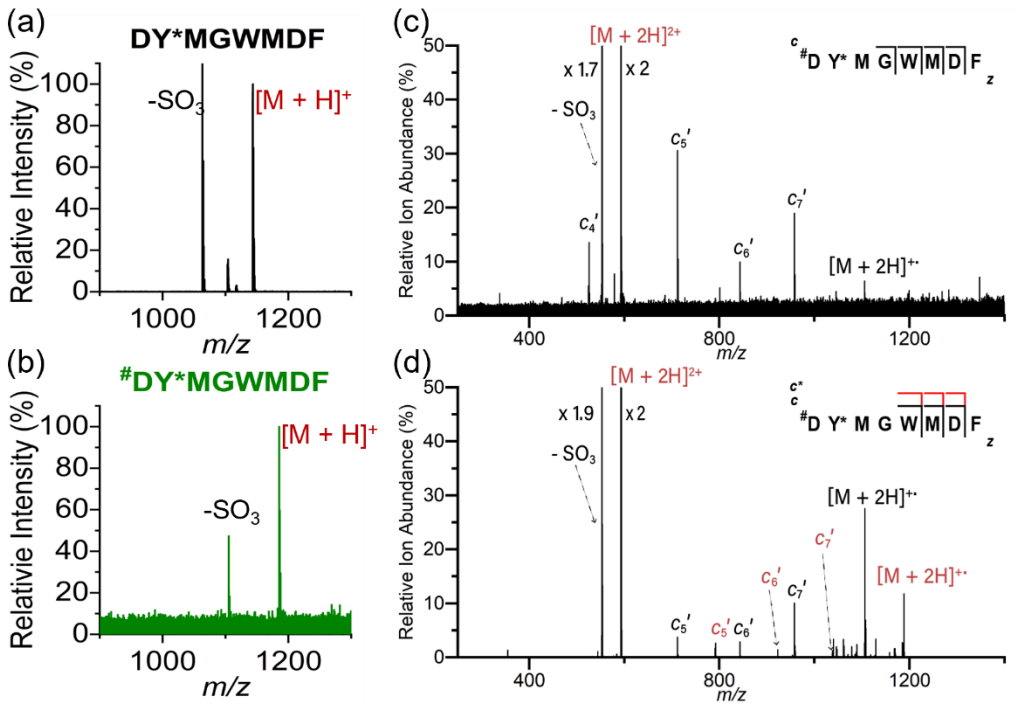

Figure 3.5 Positive ion mode ESI-FT-ICR mass spectra of singly protonated CCKS 26-33 (a), singly protonated, N-terminally guanidinated CCKS 26-33 (b) at 2V collision voltage. ECD(c), and ETD (d) of doubly protonated, N-terminally guanidinated CCKS 26-33. Asterisks (*) denote sulfated tyrosines, and pound (#) denotes guanidination. Precursor and fragment ions retaining sulfation are highlighted in red.

In order to reduce proton mobility in sulfopeptides lacking basic residues, N-terminal guanidination was attempted based on a recently published guanidination strategy involving HPCA reagent [17]. Following successful N-terminal guanidination of CCKS 26-33, the ESI stability of the modified peptide was first examined. Interestingly, N-terminal guanidination shifted the most abundant charge state from 1+ to 2+ (Data not shown), i.e., the abundance of the singly protonated peptide was lower for the modified peptide (Fig. 3.5b) compared with the unmodified peptide (Figure 3.5a). Both the modified and unmodified peptide showed sulfonate loss at the extremely low CID voltage of 2 V (Figs. 3.5a, b). However, the degree of desulfation was significantly reduced for the N-terminally guanidinated peptide(Figure 3.5b). Because, relatively abundant doubly protonated CCKS 26-33 was observed following guanidination, both

ECD and ETD were feasible for the modified sulfopeptide. Similar to triply protonated sulfoangiotensin I and our earlier ECD work [4], no sulfate retention was observed in ECD of unmodified CCKS (Fig. 3.5c). By contrast, ETD of doubly protonated, N-terminally guanidinated CCKS 26-33 (Fig. 3.5d) showed fragment ions with partial sulfate retention. Again, we propose that the observed differences between ECD and ETD are due to the different energetics of these two radical-driven MS/MS approaches.

3.3.4 Effects of Cysteine Modification on Sulfopeptide Stability in Radical-Driven MS/MS

In previous work, our group found that the *ST6GAL1* tryptic peptide, TDVCYYHQK, from digested rat liver Golgi membrane was singly sulfated based on its MS^1 accurate mass and complete PTM loss during HCD MS/MS [15]. However, the sulfation site could not be inferred because this peptide contains two adjacent tyrosine residues. To elucidate whether radical-driven MS/MS rather than HCD would be able to accomplish sulfation site determination in this tryptic peptide, we synthesized two isomeric sulfopeptides with sulfotyrosine in either location:: TDVCY(SO_3)YHQK and TDVCYY(SO_3)HQK. Figure 3.6 shows the ECD and ETD mass spectra of the doubly protonated forms of these two sulfopeptides.

To differentiate TDVCY(SO_3)YHQK from TDVCYY(SO_3)HQK, the following characteristic fragment ions should ideally be observed in ECD/ETD MS/MS spectra: c_5' and c_6', or $z_4^{\bullet}$ and $z_5^{\bullet}$. As shown in Figure 3.6, both ECD and ETD resulted in *c*-, *z*-, and *y*-type ions that retained sulfation. The desired fragment ions $z_4^{\bullet}$ and $z_5^{\bullet}$ were observed in the ECD spectra for both peptides (Figures 3.6 a, c), whereas these characteristic fragment ions were only observed for TDVCY(SO_3)YHQK in ETD (Figure 3.6b). Thus, the sulfotyrosine location could not be identified in ETD of the TDVCYY(SO_3)HQK peptide (Figure 3.6d). While promising, these experiments were carried out with non-modified cysteine (free cysteine), which is unusual in

proteomic workflows because cysteine alkylation is typically performed following disulfide bond reduction.

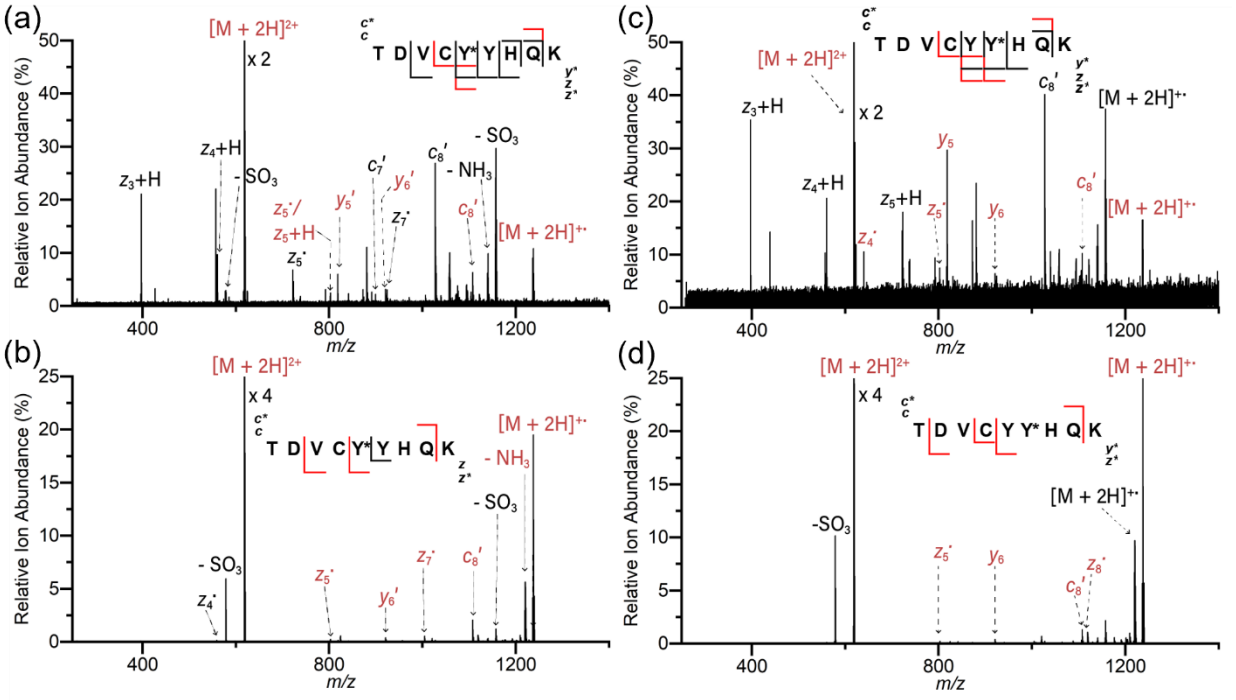

Figure 3.6 Tandem mass spectra of the doubly protonated synthetic sulfopeptide TDVCY*YHQK (a), (b), and the doubly protonated synthetic sulfopeptide TDVCYY*HQK (c), (d). ECD spectra (a, c), and ETD spectra (b, d). Asterisks (*) denote sulfated tyrosines. Precursor and fragment ions retaining sulfation are highlighted in red.

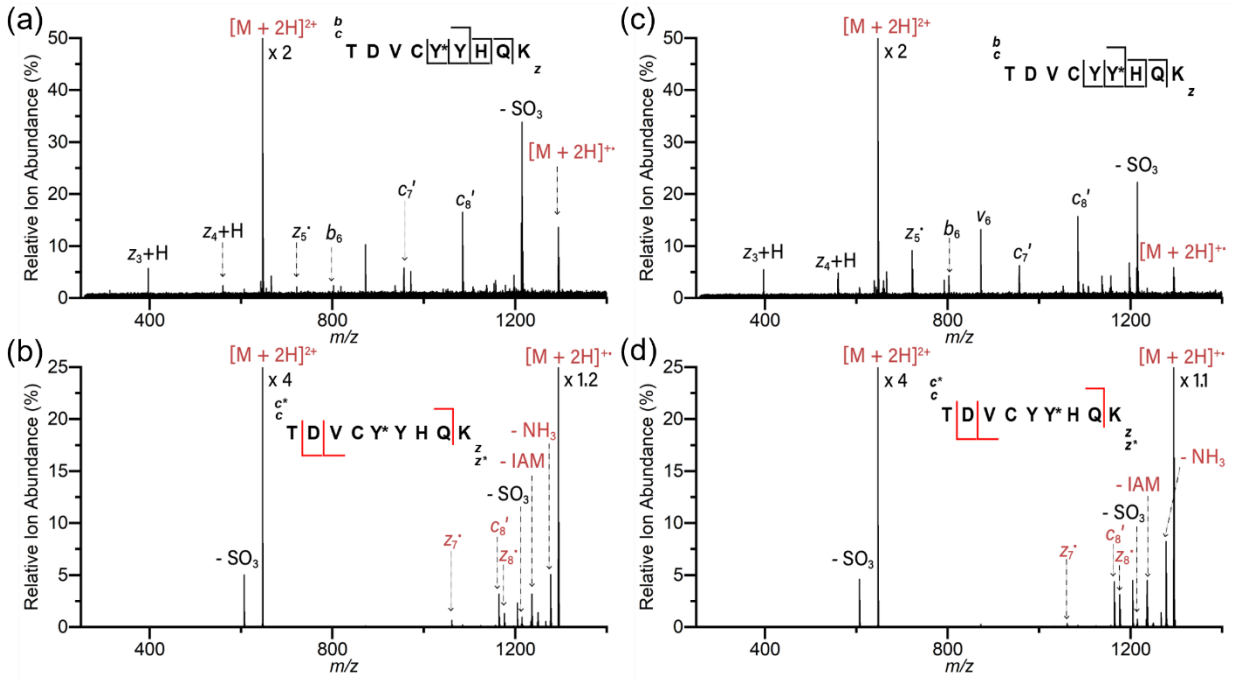

Figure 3.7 Tandem mass spectra of doubly protonated, IAM-modified TDVCY(SO_3)YHQK (a, b), and IAM-modified TDVCYY(SO_3)HQK (c, d). ECD spectra (a, c), and ETD spectra (b, d), asterisks (*) denote sulfated tyrosines. Precursor and fragment ions retaining sulfation are highlighted in red.

To better mimic a proteomic workflow, we alkylated the sulfopeptide isomers with iodoacetamide, the most common alkylation reagent. Figure 3.7 shows the ECD and ETD mass spectra of IAM-modified TDVCY(SO_3)YHQK and TDVCYY(SO_3)HQK. In ECD of IAM-modified peptides, no fragment ions retained sulfation and significant sulfonate loss was observed from the charged reduced precursor ion, $[M + 2H]^{+\bullet}$ (Figures 3.7a, c). Following ETD, the same sulfate-containing fragment ions, $z_7^{\bullet}$, $z_8^{\bullet}$, *and* c_8', were observed for both peptides, as well as neutral losses of the cysteine alkyl group and ammonia (Figure 3.7b, d). The desired characteristic fragment ions were not generated by ECD, nor ETD. In addition, IAM modification resulted in lower sequence coverage. These results suggested that other cysteine modifications may be necessary to differentiate these two sulfopeptide isomers. Based on the results described in previous sections, we were particularly interested in exploring more basic chemical groups.

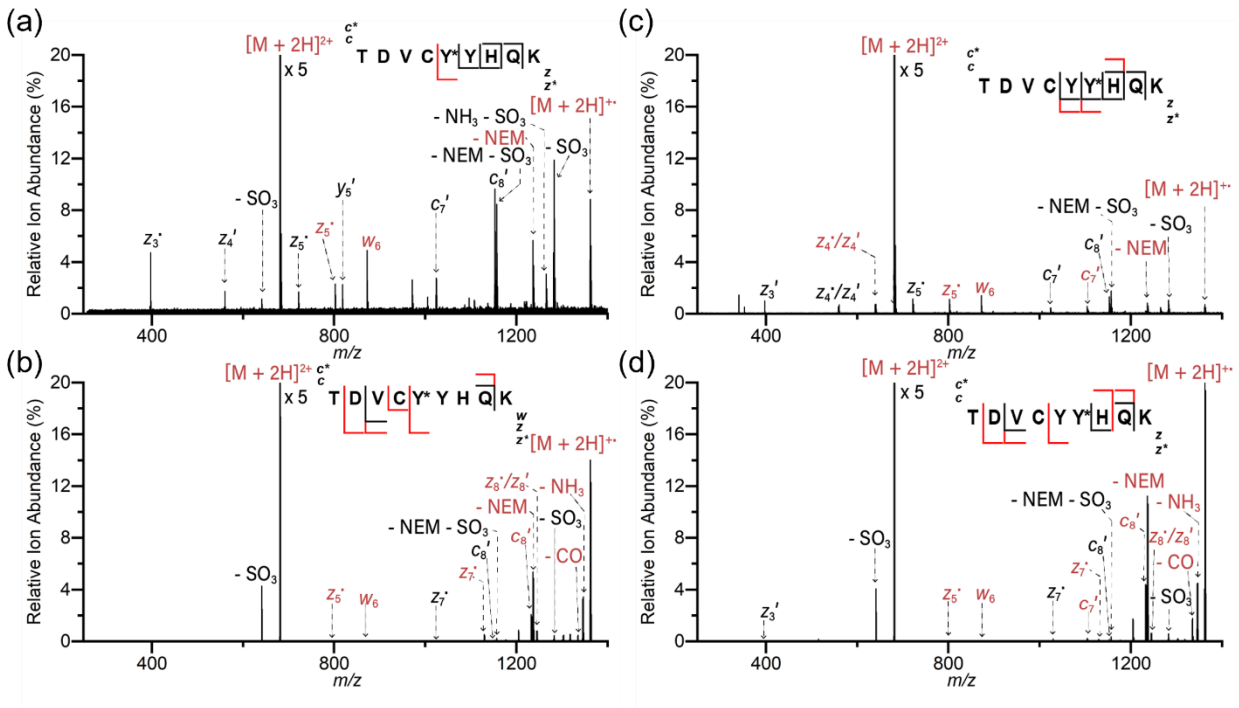

Figure 3.8 Tandem mass spectra of doubly protonated, NEM-modified TDVCY(SO_3)YHQK (a, b), and doubly protonated, NEM-modified TDVCYY(SO_3)HQK (c, d). ECD spectra (a, c) and ETD spectra (b, d), asterisks (*) denote sulfated tyrosines. Precursor and fragment ions retaining sulfation are highlighted in red.

N-ethylmaleimide is another commonly used alkylating agent for cysteine modification. Nadler et al. demonstrated via density functional theory calculations that the gas phase basicity of NEM-modified cysteine is higher than for IAM modification [23]. Therefore, we hypothesized that NEM modification would improve sulfopeptide stability in ECD/ETD compared with IAM modification. Figure 3.8 shows ECD and ETD tandem mass spectra of doubly protonated, NEM-modified TDVCY(SO_3)YHQK and TDVCYY(SO_3)HQK. Overall, improved sulfate retention was indeed observed compared with IAM modification, including several sulfated fragment ions from both ECD and ETD. Neutral losses of the NEM modification and ammonia are also observed from both ECD and ETD (Figure 3.8). Interestingly, ECD of NEM-modified peptides provided site specific information, including the characteristic fragment ions $z_4^{\bullet}$ *and* $z_5^{\bullet}$, for both peptides

(Figures 3.8a, c). ETD yielded a higher number of sulfated fragment ions than ECD; however, the tyrosine sulfation site could not be determined due to the absence of the $z_4^{\bullet}$ ion (Figures 3.8b, d).

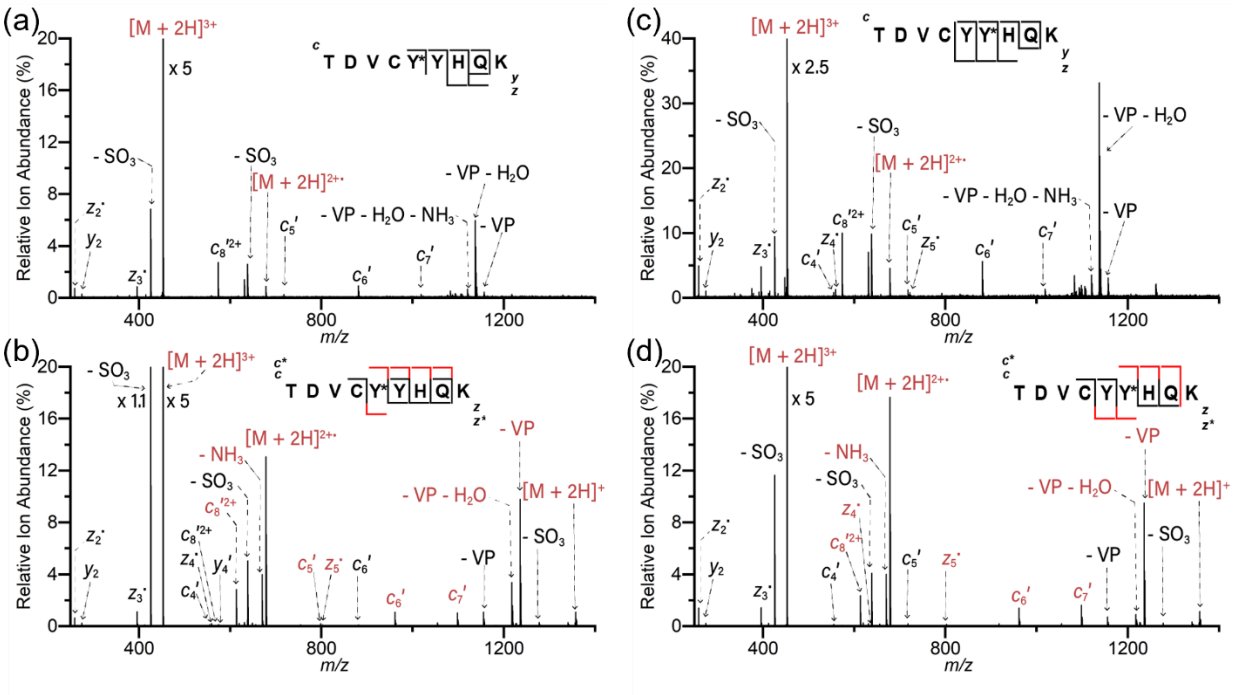

Figure 3.9 Tandem mass spectra of triply charged, VP-modified TDVCY(SO_3)YHQK (a, b), and triply charged, VP-modified TDVCYY(SO_3)HQK (c, d). ECD spectra (a, c) and ETD spectra (b, d), asterisks (*) denote sulfated tyrosines. Precursor and fragment ions retaining sulfation are highlighted in red.

To further instill mobile proton control, 1-methyl-2-vinylpyridinium, containing a fixed positive charge through a quaternized vinyl pyridine, was used for cysteine modification. This cysteine reagent was shown to enable selective and ultrafast cysteine modification with charge modulation [18]. Nadler et al., determined that VP has an even higher gas-phase basicity than NEM [23]. Based on these findings, we expected that VP modification may enable even higher sulfopeptide stability due to greater charge localization. Following VP modification, the dominant charge state for the two sulfopeptide isomers shifted from 2+ to 3+ (data not shown). In ECD of such triply charged precursor ions, no sulfated fragment ions were observed. Furthermore, abundant VP loss from the charged reduced precursor ions, $[M + 2H]^{2+\bullet}$, were observed (Figures

3.9a, c). On the other hand, ETD of VP-modified peptides (Figures 3.9b, d) generated all four characteristic fragment ions, $z_4^{\bullet}$, $z_5^{\bullet}$, c_5' and c_6', and showed a higher number of fragment ions retaining sulfation.

3.4 Conclusion

In this Chapter, we demonstrated the influence of peptide derivatization strategies, including guanidination and cysteine modification, to instill mobile proton control and thus enhance sulfopeptide stability during ECD and ETD. Sulfopeptides containing arginine or homoarginine show significantly higher stability in positive ion mode compared with acidic, native sulfopeptides. The presence of lysine also improves stability but to a lesser extent than arginine/guanidinium. This higher stability may be due to salt bridge interactions with a deprotonated sulfate. Fragment ions retaining sulfation were observed for an arginine-containing sulfopeptide in ETD (3+ and 2+ charge states), ECD (2+ charge state), and FRIPS (1+ charge state), consistent with the corresponding peptide internal energy increase in these three MS/MS techniques. Among these activation methods, ETD appears most suitable to identify tyrosine sulfation sites in tryptic peptides.

N-terminal guanidination of an acidic standard sulfopeptide resulted in higher stability in positive ion mode compared with the unmodified peptide. The dominant charge state of the unmodified sulfopeptide CCKS 26-33 was 1+, which is incompatible with ETD. N-terminal guanidination shifted the dominant charge state to 2+, thus allowing efficient ETD that yielded sulfate-retaining fragment ions. ETD of sulfopeptides modified with the typical alkylation reagent iodoacetamide showed fragments retaining sulfation but could not differentiate two sulfopeptide isomers. By contrast, ETD of cysteine-containing sulfopeptides modified with 1-methyl-2-vinyl-pyridine yielded sequence informative fragments retaining sulfation. According to Matos et al.,

proteome-wide cysteine modification with quaternary vinyl pyridine showed a reaction yield greater than 95%, as confirmed by LC-MS, and a high reaction specificity toward cysteine residues [18]. Sun et al. also described the incorporation of N-terminal and lysine guanidination into a proteomics workflow; for example, a whole cell lysate was guanidinated with HPCA, digested with trypsin, and analyzed with LC-MS [17]. Therefore, we expect that the demonstrated sulfopeptide modification strategies can be employed in sulfoproteomics workflows to enable global analysis of tyrosine sulfation.

3.5 Acknowledgement

This work was supported by the National Science Foundation CHE 2004043 and the University of Michigan. The Thermo Scientific Orbitrap Fusion Lumos was acquired via National Institutes of Health grant S10 OD021619. I would like to thank Dr. Brent Martin for the suggestion of cysteine fixed charge modification.

3.6 References

[1] Monigatti, F.; Hekking, B.; Steen, H. Protein Sulfation Analysis-A Primer. *Biochim. Biophys. Acta - Proteins Proteomics*, **2006**, *1764*, 1904–1913.

[2] Moore, K.L. Protein Tyrosine Sulfation: A Critical Posttranslation Modification in Plants and Animals. *Proc. Natl. Acad. Sci. U. S. A.*, **2009**, *106*, 14741–14742.

[3] Sasaki, N. Current Status and Future Prospects for Research on Tyrosine Sulfation. *Curr. Pharm. Biotechnol.*, **2015**, *13*, 2632–2641.

[4] Liu, H.; Håkansson, K. Electron Capture Dissociation of Tyrosine O-Sulfated Peptides Complexed with Divalent Metal Cations. *Anal. Chem*, **2006**, *78*, 7570–7576.

[5] Yagami, T.; Kitagawa, K.; Aida, C.; Fujiwara, H.; Futaki, S. Stabilization of a Tyrosine O-Sulfate Residue by a Cationic Functional Group: Formation of a Conjugate Acid-Base Pair. *J. Pept. Res.*, **2000**, *56*, 239–249.

[6] Medzihradszky, K.F.; Guan, S.; Maltby, D.A.; Burlingame, A.L. Sulfopeptide Fragmentation in Electron- Capture and Electron-Transfer Dissociation. *J. Am. Soc. Mass Spectrom.*, **2007**, *18*, 1617–1624.

[7] Yang, Y.S.; Wang, C.C.; Chen, B.H.; Hou, Y.H.; Hung, K.S.; Mao, Y.C. Tyrosine Sulfation as a Protein Post-Translational Modification. *Molecules*, **2015**, *20*, 2138–2164.

[8] Hersberger, K.E.; Håkansson, K. Characterization of O-Sulfopeptides by Negative Ion Mode Tandem Mass Spectrometry: Superior Performance of Negative Ion Electron

Capture Dissociation. *Anal. Chem.*, **2012**, *84*, 6370–6377.
[9] Yoo, H.J.; Wang, N.; Zhuang, S.; Song, H.; Håkansson, K. Negative-Ion Electron Capture Dissociation: Radical-Driven Fragmentation of Charge-Increased Gaseous Peptide Anions. *J. Am. Chem. Soc.*, **2011**, *133*, 16790–16793.
[10] Robinson, M.R.; Moore, K.L.; Brodbelt, J.S. Direct Identification of Tyrosine Sulfation by Using Ultraviolet Photodissociation Mass Spectrometry. *J. Am. Soc. Mass Spectrom.*, **2014**, *25*, 1461–1471.
[11] Borotto, N.B.; Ileka, K.M.; Tom, C.A.T.M.B.; Martin, B.R.; Håkansson, K. Free Radical Initiated Peptide Sequencing for Direct Site Localization of Sulfation and Phosphorylation with Negative Ion Mode Mass Spectrometry. *Anal. Chem.*, **2018**, *90*, 9682–9686.
[12] Riley, N.M.; Rush, M.J.P.; Rose, C.M.; Richards, A.L.; Kwiecien, N.W.; Bailey, D.J.; Hebert, A.S.; Westphall, M.S.; Coon, J.J. The Negative Mode Proteome with Activated Ion Negative Electron Transfer Dissociation (AI-NETD). *Mol. Cell. Proteomics*, **2015**, *14*, 2644–2660.
[13] Nefedov, A. V.; Gilski, M.J.; Sadygov, R.G. Bioinformatics Tools for Mass Spectrometry-Based High Throughput Quantitative Proteomics Platforms. *Curr. Proteomics*, **2011**, *8*, 125–137.
[14] Shih, M.; McLuckey, S.A. Ion/Ion Charge Inversion/Attachment in Conjunction with Dipolar DC Collisional Activation as a Selective Screen for Sulfo- and Phosphopeptides. *Int. J. Mass Spectrom.*, **2019**, *444*, 116–181.
[15] Kweon, H.K.; Kong, A.T.; Hersberger, K.E.; Huang, S.; Nesvizhskii, A.I.; Wang, Y.; Håkansson, K.; Andrews, P.C. A Novel Analytical Framework for Sulfoproteomics Reveals Tyrosine Sulfation and Phosphorylation Crosstalk in the Golgi. *Manuscr.*
[16] Beardsley, R.L.; Reilly, J.P. Optimization of Guanidination Procedures for MALDI Mass Mapping. *Anal. Chem.*, **2002**, *74*, 1884–1890.
[17] Sun, M.; Liang, Y.; Li, Y.; Yang, K.; Zhao, B.; Yuan, H.; Li, X.; Zhang, X.; Liang, Z.; Shan, Y.; Zhang, L.; Zhang, Y. Comprehensive Analysis of Protein N-Terminome by Guanidination of Terminal Amines. *Anal. Chem.*, **2020**, *92*, 567–572.
[18] Matos, M.J.; Navo, C.D.; Hakala, T.; Ferhati, X.; Guerreiro, A.; Hartmann, D.; Bernardim, B.; Saar, K.L.; Compañón, I.; Corzana, F.; Knowles, T.P.J.; Jiménez-Osés, G.; Bernardes, G.J.L. Quaternization of Vinyl/Alkynyl Pyridine Enables Ultrafast Cysteine-Selective Protein Modification and Charge Modulation. *Angew. Chemie*, **2019**, *131*, 6712–6716.
[19] Huttner, W.B. Tyrosine Sulfation and the Secretory Pathway. *Annu. Rev. Physiol.*, **1988**, *50*, 363–376.
[20] Stone, M.J.; Chuang, S.; Hou, X.; Shoham, M.; Zhu, J.Z. Tyrosine Sulfation: An Increasingly Recognised Post-Translational Modification of Secreted Proteins. *N. Biotechnol.*, **2009**, *25*, 299–317.
[21] Lee, M.; Kang, M.; Moon, B.; Oh, H. Bin. Gas-Phase Peptide Sequencing by TEMPO-Mediated Radical Generation. *Analyst*, **2009**, *134*, 1706–1712.
[22] Zhurov, K.O.; Fornelli, L.; Wodrich, M.D.; Laskay, Ü.A.; Tsybin, Y.O. Principles of Electron Capture and Transfer Dissociation Mass Spectrometry Applied to Peptide and Protein Structure Analysis. *Chem. Soc. Rev.*, **2013**, *42*, 5014–5030.
[23] Nadler, W.; Berg, R.; Walch, P.; Hanke, S.; Baalmann, M.; Kerner, A.; Trumpp, A.; Roesli, C. Ion Source-Dependent Performance of 4-Vinylpyridine, Iodoacetamide, and N-Maleoyl Derivatives for the Detection of Cysteine-Containing Peptides in Complex

Proteomics. *Anal. Bioanal. Chem.*, **2016**, *408*, 2055–2067.

Chapter 4

Radical-Driven Tandem Mass Spectrometry for Sulfotyrosine Site Determination in Peptides with Multiple Tyrosine Residues

4.1 Introduction

Tyrosyl protein sulfotransferases (TPSTs) are located in the *trans* Golgi with the enzyme active site oriented towards the Golgi lumen [1]. Two homologous TPST enzymes, TPST1 and TPST2, are found in vertebrate and invertebrate species. TPSTs use the sulfonate (SO_3) donor, adenosine 3'-phosphate 5'-phosphosulfate (PAPS) to catalyze sulfation of tyrosine hydroxyl groups [2]. TPSTs are type II integral membrane proteins with a size of about 54 kDa. In addition to the aforementioned luminal catalytic domain, which is glycosylated, these enzymes consist of a single transmembrane domain, and a short N-terminal cytoplasmic domain [3]. TPSTs are stimulated by Mn^{2+} ions, and their activity is highest at pH 6-6.5 [3]. Tyrosine sulfation, catalyzed by TPSTs, majorly occurs on secreted and transmembrane proteins that transit the *trans* Golgi network [4]. Tyrosine sulfated proteins are involved in several functions in the body, including hemostasis, blood anticoagulation, rolling and adhesion of leukocytes on endothelial cells, and chemokine receptor ligand binding [5].

Radioactive and non-radioactive methods have been used for the detection of tyrosine sulfation. In radioactive labeling, ^{35}S-containing sodium sulfate is used for metabolic labeling via PAPS [6]. However, the complex regulations [5], and the requirement for large amounts of radioactivity due to dilution by the presence of endogenous sulfate are major disadvantages [7]. Also, this method provides monitoring and quantification of total sulfation in proteins, thus the exact sulfation location cannot be determined [8]. For non-radioactive methods, mass spectrometry has been widely used for the analysis of tyrosine sulfation. However, there are several challenges, including facile desulfation and poor sulfopeptide ionization efficiency in positive ion mode, which is typically used in proteomics workflows. In collision induced dissociation (CID), the most common activation method for tandem mass spectrometry (MS/MS), complete SO_3 loss is observed from fragment ions [9], thus precluding CID-based sulfation site determination. Alternative radical-driven MS/MS techniques, such as electron capture dissociation (ECD) showed retention of tyrosine sulfation during MS/MS [10], while extensive sulfonate loss from fragment ions was also reported depending on the sulfopeptide sequence [11]. Chen et al. demonstrated that electron transfer dissociation (ETD) can generate sulfate-retaining fragment ions, albeit with poor sequence coverage [12]. Unlike positive ion mode, negative ion mode analysis shows improved sulfopeptide ionization due to the acidic nature of the sulfate group [13] and deprotonated sulfate groups also have higher gas-phase stability. Several negative ion mode MS/MS approaches have been demonstrated to allow sulfate retention in fragment ions, including negative ion ECD (niECD) [13,14], negative free radical initiated peptide sequencing (nFRIPS) [15], and negative ultraviolet photodissociation (nUVPD) [16] techniques have demonstrated the localization of tyrosine sulfation with limited loss of SO_3. However, these techniques are not directly compatible with typical proteomics workflows.

Our group recently performed higher energy collision dissociation (HCD) MS/MS-based label-free quantitative sulfoproteomics analysis of rat liver Golgi membrane [17]. One tryptic peptide from TPST1, H-LGYDPYANPPNYGKPDPK-OH, was identified as sulfated through accurate mass MS^1. However, the exact tyrosine sulfation site was undetermined because this peptide contains three tyrosine residues and HCD, as expected, resulted in complete desulfation. Here, we explore a plethora of alternative MS/MS approaches to determine the optimum strategy for sulfotyrosine site localization in this peptide. Three synthetic sulfopeptides, TPST1_A-C with sulfotyrosine located in the three different positions, respectively, was subjected to MS/MS with and without chemical derivatization to improve gas-phase sulfate stability through mobile proton control.

4.2 Experimental

4.2.1 Materials

Synthetic peptides TPST1_A (H-LGY(SO_3)DPYANPPNYGKPDPK-OH), TPST1_B (H-LGYDPY(SO_3)ANPPNYGKPDPK-OH), and TPST1_C (H-LGYDPYANPPNY(SO_3)GKPDPK-OH) were obtained from Genscript Corp (Piscataway, NJ). Water, methanol, triethylamine (TEA), trifluoroacetic acid (TFA), pH 6 MES buffer, and formic acid of LC-MS grade were purchased from Fisher chemical (Fair Lawn, NJ). *o*-TEMPO-Bz-C(O)-NHS was acquired from FutureChem (Seoul, Korea). Triethylamine bicarbonate (TEAB), dimethyl sulfoxide (DMSO), O-methylisothiourea hemisulfate, 1H-pyrazole-1-carboxamidine hydrochloride (HPCA), and C18 Ziptips were purchased from Sigma Aldrich (St. Louis, MO). Methyl-DABCO (1,4-diazabicyclo[2.2.2]octane)-*N*-hydroxysuccinimide (NHS) ester reagent was obtained from Dr. Philip Andrews' lab at the University of Michigan.

4.2.2 Peptide Modification

Lysine Guanidination

Lysine guanidination reactions were carried out as previously described[18] with some modifications. O-methylisothiourea hemisulfate, 15 mg in 15 μL of 10 % TEA, was prepared. Three μL of 100 mM peptide solution (in water) was mixed with 2 μL of the *O*-methylisothiourea hemisulfate solution. This mixture was further combined with 5 μL of 10 % TEA, followed by incubation for 30 min at 65 °C. The reaction mixture was acidified with 10 % TFA and peptides were desalted by C18 ziptips.

N-terminal and Lysine Guanidination

N-terminal and lysine guanidination was performed based on a previously described protocol[19] with slight modifications. Two μL of 2 mM HPCA in 10 % TEA was added to 2 μL of 1 mM peptide (in water), followed by addition of 2 μL, 10 % TEA. The reaction solution was incubated at 95 °C for 1 h, acidified with 10 % TFA, and modified peptides were desalted by C18 ziptips.

N-terminal Fixed Charge Modification

Methyl-DABCO-NHS (Mw 518.19 g/mol) and peptide (5:1 ratio) were reacted in pH 6 MES buffer. The reaction solution was incubated at room temperature for 30 minutes. Then the solution was acidified with 10% TFA, followed by C18 Ziptip desalting.

o-TEMPO-Bz-NHS Peptide Conjugation Reaction

The conjugation reaction is described in Chapter 2. Briefly, a peptide N-terminus was conjugated with *o*-TEMPO-Bz-C(O)-NHS at a 1:25 ratio. The reaction solution was incubated at room temperature overnight, followed by C18 reversed phase solid phase extraction with a Vac

cartridge (Sep-Pak C18 1 cc Vac Cartridge: Waters Corp., Miliford, MA, USA) and drying by SpeedVac.

4.2.3 Mass Spectrometry

A 7 T SolariX quadrupole Fourier transform ion cyclotron resonance (FT-ICR) mass spectrometer (Bruker Daltonics, Billerica, MA, USA) equipped with an Apollo II ESI source was used for sulfopeptide ECD experiments. The samples were directly injected to the source at a flow rate of 120 μL/h. The capillary voltage, capillary exit voltage, funnel 1 voltage, drying gas flow rate, and drying gas temperature were set to 3,900 V, 270 V, 150 V, 3.8 L/min, and 180 ºC, respectively. Precursor ions were selected with a quadrupole isolation window of 8-12 m/z, then accumulated for 0.1-0.5 s in the hexapole collision cell. For ECD experiments, performed in the ICR cell,the cathode heating current was kept at 1.6 A, and the ECD bias, ECD lens, and irradiation time were set to 1-2 eV, 8-10 V, and 150-500 ms, respectively. ECD spectra were averaged over 20-30 scans.

An Orbitrap Fusion Lumos Tribrid Mass Spectrometer (Thermo Scientific, San Jose, CA) with a nanospray Flex ion source was used for FRIPS and ETD experiments. The samples were directly infused to the source at a flow rate of 0.5 μL/min. The ESI voltage was 1700 V, the ion transfer tube temperature was 150-180 ºC, and the MS^1 resolution was set to 50,000. For ETD experiments, the ETD reaction time was adjusted between 10 and 50 ms, and the ETD spectra were averaged over 50-100 scans. For EThcD, the ETD reaction time was set to 15-25 ms and a supplemental activation HCD voltage of 15 (arbitrary unit) was applied. For negative ion mode FRIPS, doubly deprotonated, *o*-TEMPO-Bz-C(O)-tagged precursor ions were selected and fragmented by gentle CID to homolytically cleave the radical initiator, followed by HCD MS^3 at a resolution of 120,000.

Data analysis was performed manually using Bruker Data Analysis 5.0, and Thermo Xcalibur Qual Browser. Theoretical fragment ion masses were determined by the MS product function in Protein prospector

(http://prospector.ucsf.edu/prospector/cgi-bin/msform.cgi?form=msproduct) and the FRIPS experimental data were manually compared with theoretical fragment ion masses through an in-house Excel macro.

4.3 Results and Discussion

4.3.1 ETD and ECD of Unmodified TPST1 Sulfopeptides

ETD and ECD MS/MS were performed to elucidate whether the sulfation site could be determined in the three TPST1_A-C sulfopeptide isomers. ETD experiments were carried out with an Orbitrap Fusion Lumos mass spectrometer and ECD experiments were performed with an FT-ICR mass spectrometer.

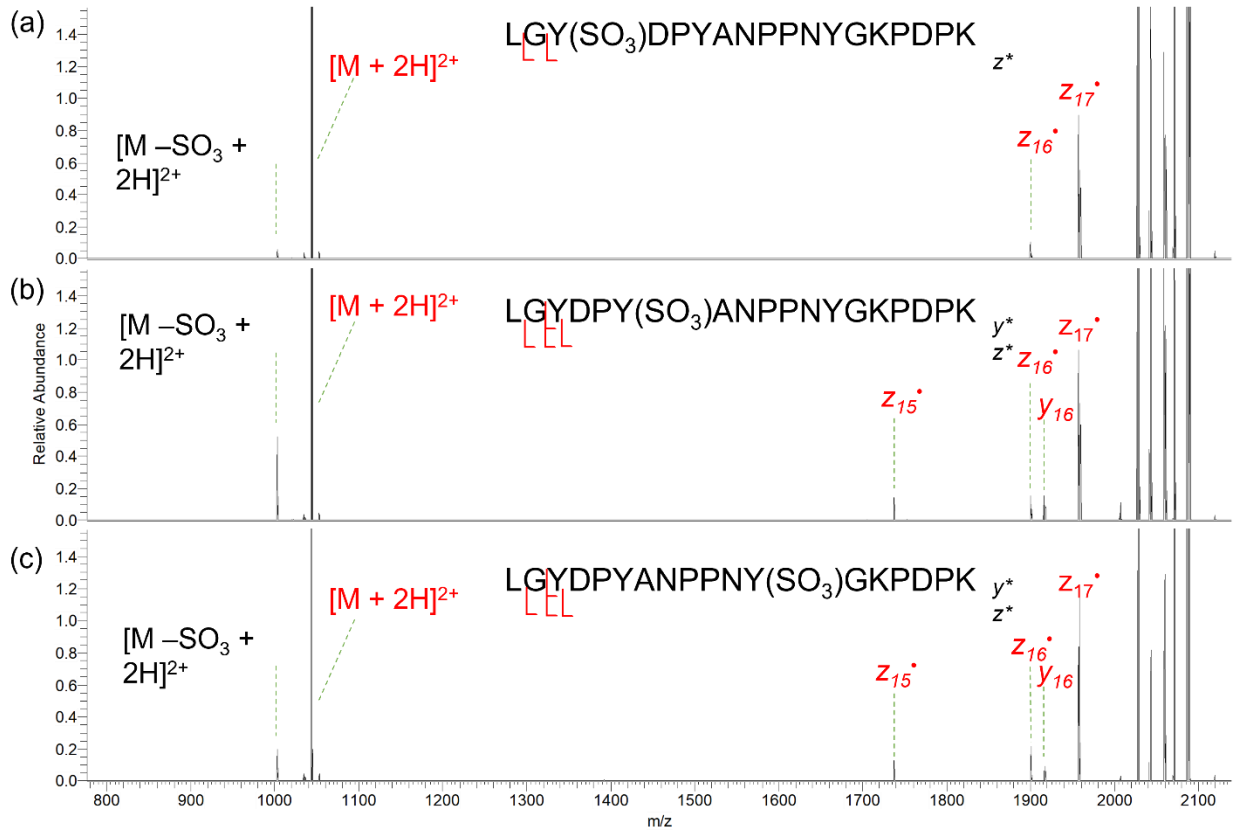

Figure 4.1 ETD spectra of doubly protonated TPST1_A (a), TPST1_B (b), and TPST1_C (c). Precursor and fragment ions retaining sulfation are highlighted in red.

Both doubly and triply protonated precursor ions were dominantly observed in positive ion mode ESI-MS for all three TPST1 peptide isomers. Figure 4.1 shows ETD spectra of the doubly protonated peptides. Desulfation, i.e., generation of $[M - SO_3 + 2H]^{2+}$, was minimum (approximately 0.4% relative ion abundance) and sulfated *c′*- and *z*•-type backbone fragments ions were detected upon ETD. However, as typically observed [20], doubly charged peptides generated low sequence coverage. ETD of TPST1_A generated $z_{16}^{\bullet}$ and $z_{17}^{\bullet}$, whereas $z_{15}^{\bullet}$, $z_{16}^{\bullet}$, y_{16}, and $z_{17}^{\bullet}$ fragment ions were observed for TPST1_B and C. Although these fragment ions retained sulfation, they provide insufficient information to determine the tyrosine sulfation site.

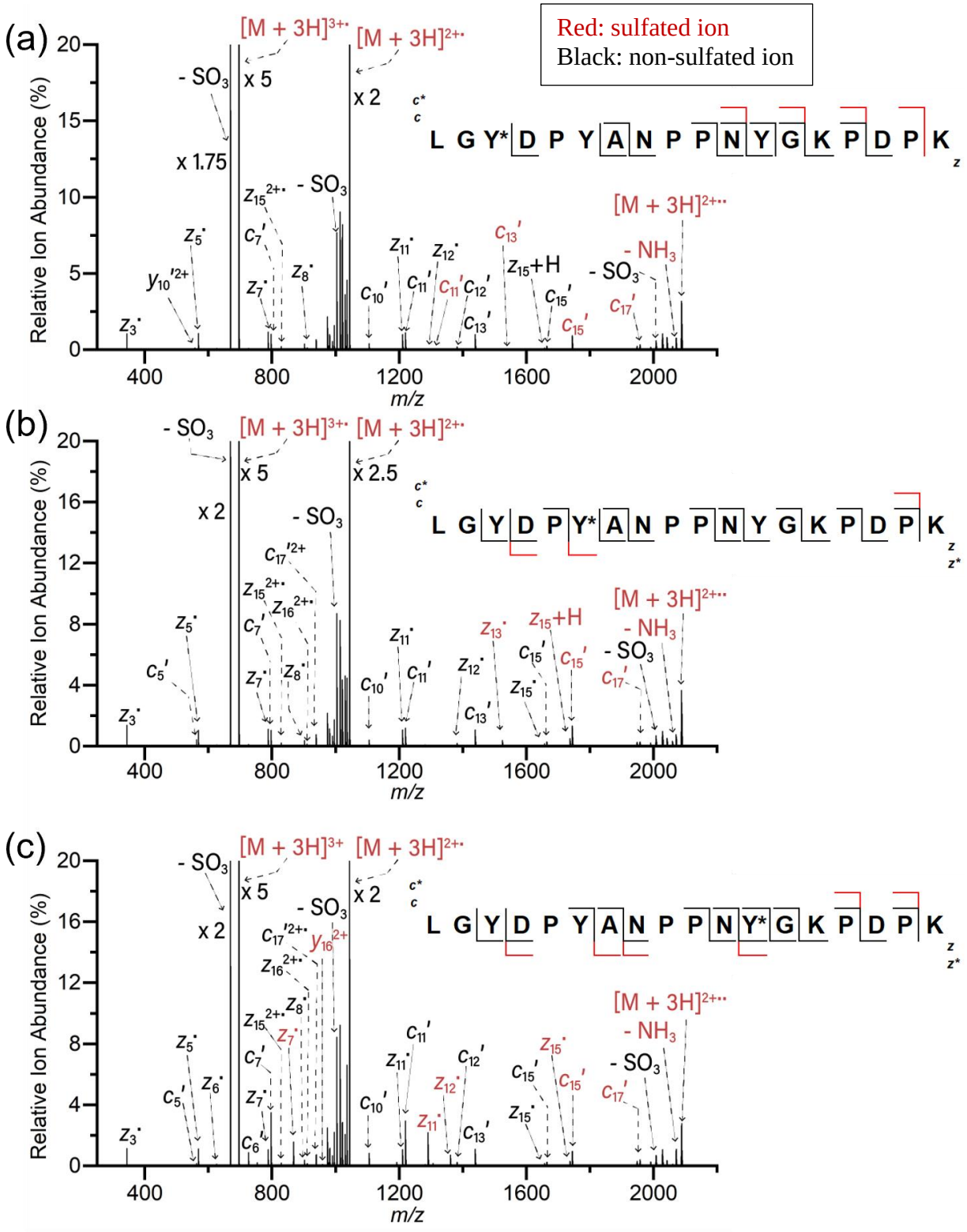

Figure 4.2 ETD spectra of triply protonated TPST1_A (a), TPST1_B (b), and TPST1_C (c). Precursor and fragment ions retaining sulfation are highlighted in red. Asterisks (*) denote sulfated tyrosine.

Figure 4.2 shows the ETD spectra of triply protonated TPST1_A-C peptides. As expected [20,21], greatly improved sequence coverage was obtained for each sulfopeptide isomer. ETD of triply protonated TPST1_A-C showed partial sulfate retention with a mixture of sulfate-retaining and desulfated backbone fragment ions. For TPST1_C, the sulfate location among the three tyrosine residues can be determined from the observed sulfated fragment ions $z_7^{\bullet}$, $z_{10}^{\bullet}$, and $z_{11}^{\bullet}$, which unambiguously show that the third tyrosine is sulfated. Interestingly, the doubly charged y_{16}^{2+} fragment ion also retained sulfation, suggesting that it originated from a radical-driven dissociation pathway. Formation of *a*• and their complementary *y*′-type ions has been described as an alternative pathway in ECD [22]. Unlike TPST1_C, the tyrosine sulfation sites in TPST1_A and B could not be unambiguously determined due to the absence of characteristic, sulfated fragment ions.

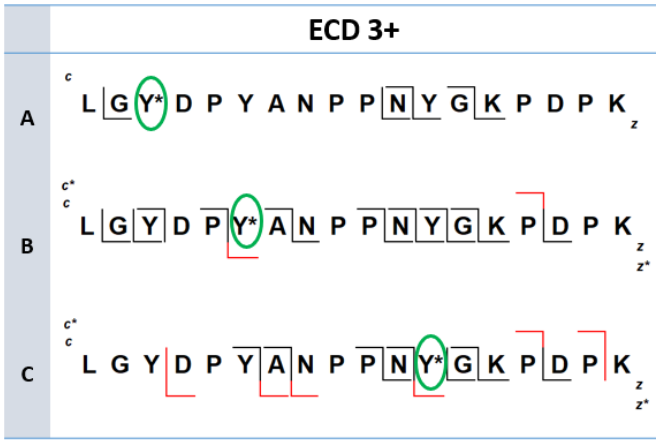

Table 4.1 Backbone fragmentation from ECD of triply protonated TPST1_A, B, and C peptides. Backbone fragments retaining sulfation are highlighted in red. Only *c*- and *z*-type ions are included in this table. Sulfated tyrosines are highlighted with asterisks and green circles.

The results from ECD of triply protonated TPST1 sulfopeptides are summarized in Table 4.1. No sulfated fragment ions were observed for TPST1_A, therefore information on the tyrosine sulfation site was not obtained. ECD of TPST1_B and C, on the other hand, showed sulfated fragment ions. In particular, the sequence informative $z_7^{\bullet}$, $z_{10}^{\bullet}$, and $z_{11}^{\bullet}$ fragment ions, which were

also observed in ETD spectra, were also detected in ECD of TPST1_C. Thus, the tyrosine sulfation site in TPST1_C could be determined by both ETD and ECD. However, again, insufficient fragmentation/sulfate retention was seen in ECD of TPST1_A and B. We speculate that TPST1_C has a more favorable gas-phase confirmation for optimum ETD/ECD, possibly involving sulfate stabilizing interactions between a lysine sidechain and the tyrosine sulfate group. Because trypsin does not cleave lysines on the N-terminal side of proline, these peptides contain two lysine residues.

4.3.2 ECD and ETD of Guanidinated TPST1_A and TPST1_B Sulfopeptides

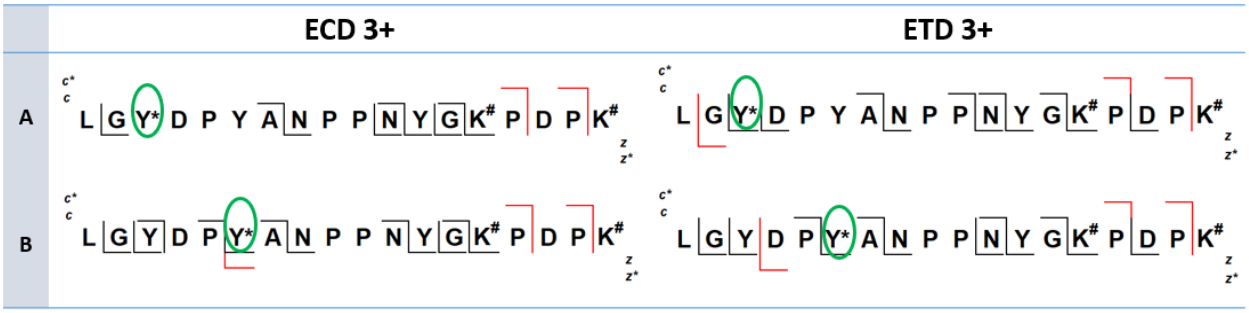

Table 4.2 ECD vs. ETD of triply protonated, guanidinated TPST1_A and B. Backbone fragments retaining sulfation are highlighted in red. Number signs (#) represent guanidinated lysine. Only *c*- and *z*-type ions are included in this table. Sulfated tyrosines are highlighted with asterisks and green circles.

To further explore the differentiation between TPST1_A and TPST1_B, the peptide modification strategy for mobile proton control, discussed in Chapter 3, was employed. First, lysine guanidination was performed. While no sulfated fragment ions were generated in ECD of unmodified TPST1_A, lysine-guanidinated TPST1_A showed improved gas-phase stability, including generation of sulfated *c*-type fragment ions (Table 4.2, top left). Also, improved sequence coverage (24% → 47%) was obtained from ECD upon lysine guanidination. Lysine-guanidinated TPST1_B also showed additional sulfated fragment ions compared with the unmodified peptide upon ECD (Table 4.2, bottom left). ETD of these guanidinated peptides yielded the same sequence coverage as the unmodified sulfopeptides but with slight differences in

the observed backbone N-Cα cleavage sites. However, ECD/ETD of lysine-guanidinated TPST1_A and B still did not allow sulfation site determination.

We further modified these two sulfopeptides by adding an N-terminal guanidinium group. Unexpectedly, the number of observed fragment ions remained the same or decreased upon N-terminal guanidination in both ECD and ETD (Table 4.3). It is well established that observation of backbone N-Cα bond cleavage is hindered if precursor ions contain intramolecular non-covalent bonding, e.g., hydrogen bonding or salt bridging [23,24]. Because such non-covalent interactions can remain upon backbone dissociation [20,25], complementary fragment ions remain bound and, thus, are not individually observed. We expect the introduction of an additional guanidinium group to alter the peptide conformation, possibly resulting in more extensive intramolecular non-covalent bonding and thus leading to the observed lower sequence coverage.

	ECD 3+	ETD 3+
A		
B		

Table 4.3 ECD vs. ETD of triply protonated N-terminally and lysine-guanidinated TPST1_A and B. Backbone fragments retaining sulfation are highlighted in red.. Number signs (#) represent guanidinium groups on the N-terminus and lysine side chains. Sulfated tyrosines are highlighted with asterisks and green circles.

4.3.3 EThcD of Fixed Charge-Modified TPST1_A and TPST1_B Sulfopeptides

To introduce additional mobile proton control, we attached a fixed positive charge-tag, 1,4-diazabicyclo[2.2.2]octane (DABCO), to TPST1_A and B. This DABCO tag (Figure 4.3) contains two quaternary amine, fixed positive charges. Because the DABCO reagent is an NHS ester, conjugation can occur with both lysine side chain free amines and the N-terminal free amine in

TPST1 peptides. In order to promote conjugation at the N-terminus only, lysine side chains were first guanidinated. The resulting conjugated peptides appeared as triply- and quadruply-charged upon ESI-MS[1] (data not shown). The triply-charged precursor ions showed highly enhanced stability compared with the unmodified sulfopeptides with sulfonate loss being completely absent in ETD. Furthermore, only partial SO_3 loss was observed upon further HCD activation, i.e., EThcD, at moderate normalized collision energy (15-20%). It was previously reported that EThcD caused significant desulfation, even for arginine-containing sulfopeptides [12]. However, it appears that the elimination of mobile protons through fixed charging affords additional sulfopeptide stability, thus reducing SO_3 loss upon supplementary collisional activation of sulfopeptides. EThcD fragmentation of TPST1_A and TPST1_B are summarized in Table 4.4. N-terminal *c*-type fragment ions from both peptides all completely retained the sulfate group, presumably because they contain the DABCO fixed charge moiety and thus accrue positive charge with limited protonation. Interestingly, peptide backbone cleavages were only observed in the C-terminal halves of the peptides with the exception of complementary c_7/z_{11} fragments for TPST1_B.. Cooper and co-workers have demonstrated that it is unlikely to observe ECD fragment ions from the sequence region between a lysine and a phosphorylated residue due to salt bridge formation [26]. Similarly, we propose that the absence of shorter *c*-type ions and longer *z*-type ions in EThcD of DABCO-modified TPST1_A and B is due to strong salt bridge formation between the N-terminal DABCO group and sulfotyrosine. The sulfotyrosine residues are located in the N-terminal half of the peptide in both TPST1_A and B and, thus, such salt bridge formation can prevent generation of fragment ions from the N-terminal sequence regions. Due to the absence of such fragments, sulfation site determination was also unattainable from EThcD of TPST1_A and B.

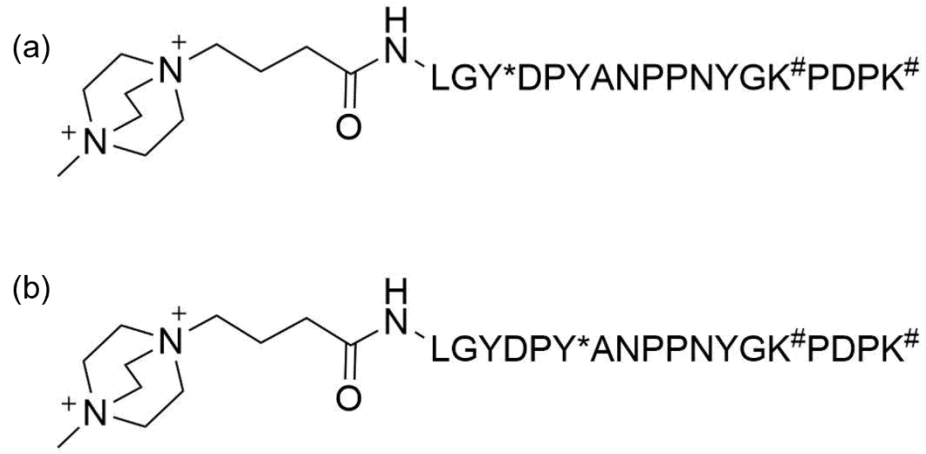

Figure 4.3 DABCO-conjugated TPST1_A (a) and TPST1_B (b).

	TPST1_A	TPST1_B
EThcD 3+	□LGY*DPYANPPNYGK#PDPK#	□LGYDPY*ANPPNYGK#PDPK#

Table 4.4 EThcD of triply charged, N-terminally DABCO fixed charge-modified and lysine guanidinated TPST1_A and B. Backbone fragments retaining sulfation are highlighted in red. Squares (□) denote the DABCO fixed charge group and number signs (#) represent lysine guanidination. Sulfated tyrosines are highlighted with asterisks and green circles.

4.3.4 Positive and Negative ion mode FRIPS of TPST1_A and TPST1_B Sulfopeptides

Free radical initiated peptide sequencing is an alternative tandem mass spectrometry technique that utilizes radical-driven fragmentation from the introduction of a CID-cleavable radical initiator tag. Previously, our group demonstrated that negative ion mode FRIPS can characterize tyrosine sulfated peptides with limited SO_3 loss [15]. In Chapter 3, I showed that sulfoangiotensin I, which contains several basic amino acid residues, could be characterized by positive ion mode FRIPS to yield sulfated fragment ions. To further explore the differentiation of TPST1_A and B, we employed TEMPO-based FRIPS [27] in both positive and negative ion mode. Similar to the DABCO tag experiments described above, the TEMPO-based NHS ester reagent

can conjugate to both the peptide N-termini and the lysine side chains [28]. Thus lysine guanidination was again conducted prior to o-TEMPO-Bz-C(O) conjugation with the peptide N-termini. Positive ion mode FRIPS was first performed with doubly protonated TPST1_A and B sulfopeptides; however, near complete SO_3 loss was observed upon CID MS/MS aimed at promoting homolytic cleavage, i.e., initial radical site generation, within the radical initiator tag [27]. Therefore, we attempted negative ion mode FRIPS of doubly deprotonated TPST1_A and B. This charge state was dominant in negative ion mode MS^1 of o-TEMPO-Bz-C(O) conjugated peptides (data not shown). Abundant free radical formation from radical TEMPO loss was observed upon CID in negative ion mode. The resulting truncated radical tag-containing peptides (Figure 2.1) were further isolated and subjected to HCD MS^3 to promote backbone dissociation through radical propagation. The subscript "r" in, e.g., $[_rM - 2H]^{2-\bullet}$ and $_ra_4'$ refers to the truncated radical initiator at the peptide N-terminus, resulting in a mass increase of 117 Da from the unmodified peptide [27]. The Zubarev nomenclature was used for peak annotation. In this system, "•" denotes a hydrogen atom [29] whereas "H" denotes a proton. The proposed nomenclature by Julian and co-workers was used for annotating side chain losses [30]. FRIPS typically yields a variety of fragment ion types, e.g., *a*-, *c*-, *x*-, *y*-, and *z*-type ions [27,31], as well as side chain losses from the precursor ions. TPST1_A and B showed similar behavior in nFRIPS (Figure 4.4). Intriguingly, no SO_3 loss from neither the precursor ions, nor the fragment ions was observed. Similar to previous FRIPS observations, neutral CO_2 loss from the precursor ions was dominant for both sulfopeptides [32]. Also, similar to the results presented in Chapter 3, tyrosine side chain loss ($C_7H_6O^{\bullet}$) [32,33] was abundant (Figure 4.4). The nFRIPS MS^3 spectrum of lysine-guanidinated TPST1_A (Figure 4.4a) reveals the exact tyrosine sulfation site because $_ra_3'$, $_ra_4'$,

and $_{r}a_{5}$' fragment ions are all sulfated. Similarly, for TPST1_B, sulfated $_{r}a_{6}$' *and* y_{14} fragment ions unambiguously locate the sulfated tyrosine.

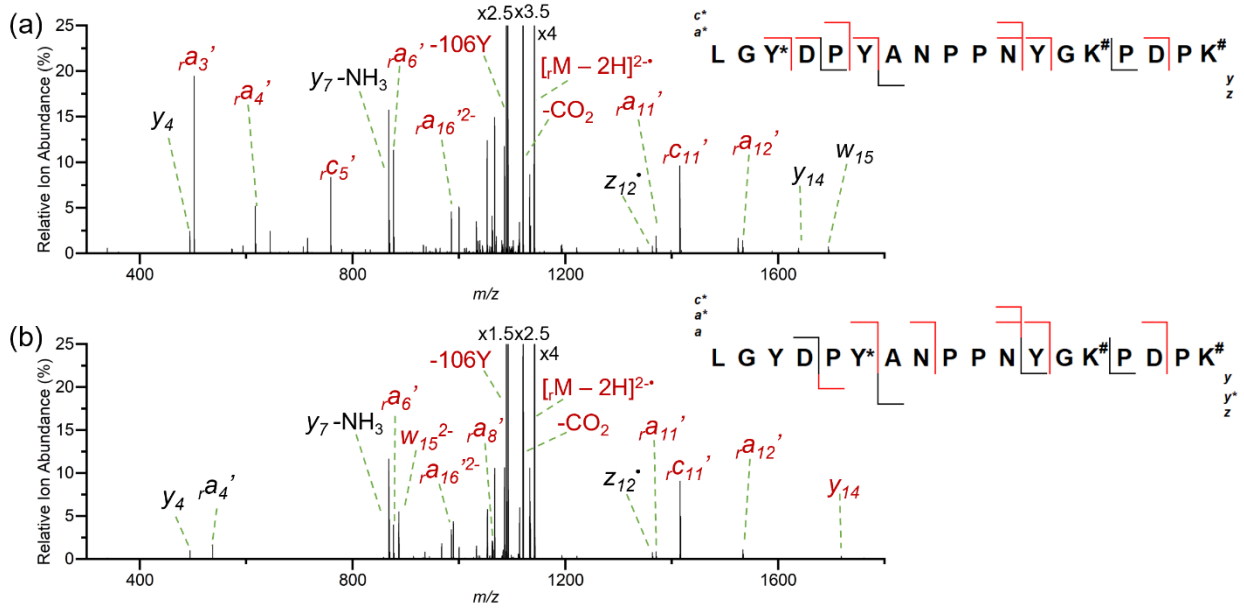

Figure 4.4 Negative ion mode FRIPS MS^3 spectra of doubly deprotonated lysine-guanidinated TPST1_A (a) andTPST1_B (b). Asterisks (*) denote tyrosine sulfation. Precursor and fragment ions retaining sulfation are highlighted in red.

4.4 Conclusion

In this work, we employed peptide N-terminal and lysine derivatization strategies to differentiate three isomeric TPST1 sulfopeptides containing three possible tyrosine sulfation sites. These peptides were subjected to a variety of radical-driven tandem mass spectrometry methods, including ECD, ETD, EThcD, and FRIPS. In the absence of peptide derivatization, both ECD and ETD of triply protonated TPST1_C, with sulfation on the third tyrosine residue, unambiguously revealed the tyrosine sulfation site. On the other hand, sulfation site determination in TPST1_A and B, with sulfation on the first and second tyrosine residue, respectively, was unattainable both in the absence and presence of various modifications, including lysine guanidination, N-terminal+lysine guanidination, and N-terminal fixed charge derivatization+guanidination. For the

fixed charge-containing peptides, a significant increase in sulfate stability was demonstrated, allowing several sulfate-containing fragments ions to be generated from EThcD. However, insufficient generation of characteristic fragment ions precluded sulfation site determination in TPST1_ A and B. ECD/ETD data of modified peptides show evidence of altered gas-phase peptide structures upon derivatization, indicating strong intramolecular interactions that prevent generation of sufficient backbone fragmentation. FRIPS MS^3 in positive ion mode was not feasible as extensive sulfonate loss occurred during the MS^2 CID step, aimed at homolytically cleaving the radical initiator. However, negative ion mode FRIPS [15,31] of lysine-guanidinated TPST1_A and B resulted in sequence informative, sulfate-retaining fragment ions, which allowed tyrosine sulfation site determination in both peptides. Overall, these results imply that negative ion mode MS/MS methods may be required for complete tyrosine sulfation analysis. While FRIPS MS^3 has not ye been employed in an LC-MS-compatible proteomic workflow, isobaric tags for relative and absolute quantitation (iTRAQ)- and tandem-mass-tag (TMT)-based methods, which often involve MS^3 approaches [34] are compatible with proteome-wide analysis. Thus we expect that LC-FRIPS MS^3 will also be feasible for large scale sulfoproteomics.

4.5 Acknowledgement

This work was supported by the National Science Foundation CHE 2004043 and the University of Michigan. The Thermo Scientific Orbitrap Fusion Lumos was acquired via National Institutes of Health grant S10 OD021619. I would like to thank Dr. Hye Kyong Kweon for the help acquiring the DABCO tag from Dr. Philip Andrews' lab.

4.6 References

[1] Huttner, W.B. Tyrosine Sulfation and the Secretory Pathway. *Annu. Rev. Physiol.*, **1988**, *50*, 363–376.

[2] Seibert, C.; Sakmar, T.P. Toward a Framework for Sulfoproteomics: Synthesis and Characterization of Sulfotyrosine-Containing Peptides. *Pept. Sci.*, **2008**, *90*, 459–477.
[3] Bundgaard, J.R.; Rehfeld, J.F. Tyrosylprotein Sulfotransferases. In *Handbook of Biologically Active Peptides*; Kastin, A.J., Ed.; Elsevier Inc., **2013**; pp. 1829–1834.
[4] Moore, K.L. The Biology and Enzymology of Protein Tyrosine O-Sulfation. *Journal of Biological Chemistry*, **2003**, *278*, 24243–24246.
[5] Yang, Y.S.; Wang, C.C.; Chen, B.H.; Hou, Y.H.; Hung, K.S.; Mao, Y.C. Tyrosine Sulfation as a Protein Post-Translational Modification. *Molecules*, **2015**, *20*, 2138–2164.
[6] Lee, R.W.H.; Huttner, W.B. Tyrosine-O-Sulfated Proteins of PC12 Pheochromocytoma Cells and Their Sulfation by a Tyrosylprotein Sulfotransferase. *J. Biol. Chem.*, **1983**, *258*, 11326–11334.
[7] Monigatti, F.; Hekking, B.; Steen, H. Protein Sulfation Analysis-A Primer. *Biochim. Biophys. Acta - Proteins Proteomics*, **2006**, *1764*, 1904–1913.
[8] Danan, L.M.; Yu, Z.; Hoffhines, A.J.; Moore, K.L.; Leary, J.A. Mass Spectrometric Kinetic Analysis of Human Tyrosylprotein Sulfotransferase-1 and -2. *J. Am. Soc. Mass Spectrom.*, **2008**, *19*, 1459–1466.
[9] Önnerfjord, P.; Heathfield, T.F.; Heinegård, D. Identification of Tyrosine Sulfation in Extracellular Leucine-Rich Repeat Proteins Using Mass Spectrometry. *J. Biol. Chem.*, **2004**, *279*, 26–33.
[10] Haselmann, K.F.; Budnik, B.A.; Olsen, J. V.; Nielsen, M.L.; Reis, C.A.; Clausen, H.; Johnsen, A.H.; Zubarev, R.A. Advantages of External Accumulation for Electron Capture Dissociation in Fourier Transform Mass Spectrometry. *Anal. Chem.*, **2001**, *73*, 2998–3005.
[11] Liu, H.; Håkansson, K. Electron Capture Dissociation of Tyrosine O-Sulfated Peptides Complexed with Divalent Metal Cations. *Anal. Chem*, **2006**, *78*, 7570–7576.
[12] Chen, G.; Zhang, Y.; Trinidad, J.C.; Dann III, C. Distinguishing Sulfotyrosine Containing Peptides from Their Phosphotyrosine Counterparts Using Mass Spectrometry. *J. Am. Soc. Mass Spectrom.*, **2018**, *29*, 455–462.
[13] Hersberger, K.E.; Håkansson, K. Characterization of O-Sulfopeptides by Negative Ion Mode Tandem Mass Spectrometry: Superior Performance of Negative Ion Electron Capture Dissociation. *Anal. Chem.*, **2012**, *84*, 6370–6377.
[14] Yoo, H.J.; Wang, N.; Zhuang, S.; Song, H.; Håkansson, K. Negative-Ion Electron Capture Dissociation: Radical-Driven Fragmentation of Charge-Increased Gaseous Peptide Anions. *J. Am. Chem. Soc.*, **2011**, *133*, 16790–16793.
[15] Borotto, N.B.; Ileka, K.M.; Tom, C.A.T.M.B.; Martin, B.R.; Håkansson, K. Free Radical Initiated Peptide Sequencing for Direct Site Localization of Sulfation and Phosphorylation with Negative Ion Mode Mass Spectrometry. *Anal. Chem.*, **2018**, *90*, 9682–9686.
[16] Robinson, M.R.; Moore, K.L.; Brodbelt, J.S. Direct Identification of Tyrosine Sulfation by Using Ultraviolet Photodissociation Mass Spectrometry. *J. Am. Soc. Mass Spectrom.*, **2014**, *25*, 1461–1471.
[17] Kweon, H.K.; Kong, A.T.; Hersberger, K.E.; Huang, S.; Nesvizhskii, A.I.; Wang, Y.; Håkansson, K.; Andrews, P.C. A Novel Analytical Framework for Sulfoproteomics Reveals Tyrosine Sulfation and Phosphorylation Crosstalk in the Golgi. *Manuscr.*
[18] Beardsley, R.L.; Reilly, J.P. Optimization of Guanidination Procedures for MALDI Mass Mapping. *Anal. Chem.*, **2002**, *74*, 1884–1890.
[19] Sun, M.; Liang, Y.; Li, Y.; Yang, K.; Zhao, B.; Yuan, H.; Li, X.; Zhang, X.; Liang, Z.;

Shan, Y.; Zhang, L.; Zhang, Y. Comprehensive Analysis of Protein N-Terminome by Guanidination of Terminal Amines. *Anal. Chem.*, **2020**, *92*, 567–572.
[20] Good, D.M.; Wirtala, M.; McAlister, G.C.; Coon, J.J. Performance Characteristics of Electron Transfer Dissociation Mass Spectrometry. *Mol. Cell. Proteomics*, **2007**, *6*, 1942–1951.
[21] Liu, J.; Mcluckey, S.A. International Journal of Mass Spectrometry Electron Transfer Dissociation : Effects of Cation Charge State on Product Partitioning in Ion / Ion Electron Transfer to Multiply Protonated Polypeptides. *Int. J. Mass Spectrom.*, **2012**, *330–332*, 174–181.
[22] Zubarev, R.A.; Kruger, N.A.; Fridriksson, E.K.; Lewis, M.A.; Horn, D.M.; Carpenter, B.K.; McLafferty, F.W. Electron Capture Dissociation of Gaseous Multiply-Charged Proteins Is Favored at Disulfide Bonds and Other Sites of High Hydrogen Atom Affinity. *J. Am. Chem. Soc.*, **1999**, *121*, 2857–2862.
[23] Adams, C.M.; Kjeldsen, F.; Zubarev, R.A.; Budnik, B.A.; Haselmann, K.F. Electron Capture Dissociation Distinguishes a Single D-Amino Acid in a Protein and Probes the Tertiary Structure. *J. Am. Soc. Mass Spectrom.*, **2004**, *15*, 1087–1098.
[24] Zubarev, R.A. Electron-Capture Dissociation Tandem Mass Spectrometry. *Curr. Opin. Biotechnol.*, **2004**, *15*, 12–16.
[25] Lopez-Clavijo, A.F.; Duque-Daza, C.A.; Creese, A.J.; Cooper, H.J. Electron Capture Dissociation Mass Spectrometry of Phosphopeptides: Arginine and Phosphoserine. *Int. J. Mass Spectrom.*, **2015**, *390*, 63–70.
[26] Creese, A.J.; Cooper, H.J. The Effect of Phosphorylation on the Electron Capture Dissociation of Peptide Ions. *J. Am. Soc. Mass Spectrom.*, **2008**, *19*, 1263–1274.
[27] Lee, M.; Kang, M.; Moon, B.; Oh, H. Bin. Gas-Phase Peptide Sequencing by TEMPO-Mediated Radical Generation. *Analyst*, **2009**, *134*, 1706–1712.
[28] Jeon, A.; Hwangbo, S.; Ryu, E.S.; Lee, J.; Yun, K.N.; Kim, J.Y.; Moon, B.; Oh, H. Bin. Guanidination of Lysine Residue Improves the Sensitivity and Facilitates the Interpretation of Free Radical Initiated Peptide Sequencing (FRIPS) Mass Spectrometry Results. *Int. J. Mass Spectrom.*, **2015**, *390*, 110–117.
[29] Kjeldsen, F.; Haselmann, K.F.; Budnik, B.A.; Jensen, F.; Zubarev, R.A. Dissociative Capture of Hot (3–13 EV) Electrons by Polypeptide Polycations: An Efficient Process Accompanied by Secondary Fragmentation. *Chem. Phys. Lett.*, **2002**, *356*, 201–206.
[30] Sun, Q.; Nelson, H.; Ly, T.; Stoltz, B.M.; Julian, R.R. Side Chain Chemistry Mediates Backbone Fragmentation in Hydrogen Deficient Peptide Radicals. *J. Proteome Res.*, **2009**, *8*, 958–966.
[31] Lee, J.; Park, H.; Kwon, H.; Kwon, G.; Jeon, A.; Kim, H.I.; Sung, B.J.; Moon, B.; Oh, H. Bin. One-Step Peptide Backbone Dissociations in Negative-Ion Free Radical Initiated Peptide Sequencing Mass Spectrometry. *Anal. Chem.*, **2013**, *85*, 7044–7051.
[32] Lee, C.S.; Jang, I.; Hwangbo, S.; Moon, B.; Oh, H. Bin. Side Chain Cleavage in TEMPO-Assisted Free Radical Initiated Peptide Sequencing (FRIPS): Amino Acid Composition Information. *Bull. Korean Chem. Soc.*, **2015**, *36*, 810–814.
[33] Hage, C.; Ihling, C.H.; Götze, M.; Schäfer, M.; Sinz, A. Dissociation Behavior of a TEMPO-Active Ester Cross-Linker for Peptide Structure Analysis by Free Radical Initiated Peptide Sequencing (FRIPS) in Negative ESI-MS. *J. Am. Soc. Mass Spectrom.*, **2017**, *28*, 56–68.
[34] Erickson, B.K.; Jedrychowski, M.P.; McAlister, G.C.; Everley, R.A.; Kunz, R.; Gygi, S.P.

Evaluating Multiplexed Quantitative Phosphopeptide Analysis on a Hybrid Quadrupole Mass Filter/Linear Ion Trap/Orbitrap Mass Spectrometer. *Anal. Chem.*, **2015**, *87*, 1241–1249.

Chapter 5

Peptide Size Effect on the Degree of Hydrogen/Deuterium Scrambling During Mass Spectrometry Ionization and Ion Transfer: a Case for a Middle-Down Approach

5.1 Introduction

Amide hydrogen/deuterium exchange (HDX) provides information on protein structure and dynamics. HDX methodology has been combined with nuclear magnetic resonance (NMR) spectroscopy [1] and with mass spectrometry (MS). While NMR spectroscopy can provide atomic resolution, MS has gained attention as an alternative structural elucidation tool in recent years due to its higher sensitivity less stringent sample purity requirements, and compatibly with larger proteins [2]. HDX-MS has been employed to probe protein folding [3], protein oligomerization [4], protein-protein complexes [5], protein-ligand binding [6], and protein-membrane interaction [7].

HDX-MS is typically implemented in a bottom-up approach in which proteins of interest are incubated in deuterated buffer for fixed time points, followed by HDX quenching and proteolytic digestion. The generated peptides are subjected to liquid chromatography separation/desalting and their deuterium levels are determined by the observed mass shifts in the corresponding mass spectra [8]. Pepsin is widely used for proteolytic cleavage of deuterated

proteins because it is compatible with the quenching conditions, typically low pH and temperature. Peptic peptide LC-MS analysis allows determination of the global amide hydrogen deuterium level for each observed peptide as amide hydrogens have relatively slow HDX back exchange rates [9]. By contrast, deuterated termina and side chains are back exchanged during LC. In this approach, spatial resolution is dependent on the length of the proteolytic peptides, typically 5-20 amino acid residues for peptic peptides [10], with smaller peptides providing the most localized deuterium information. Peptides with overlapping sequences allow further localization of deuterated sites and a high level of overlapping peptides thus results in improved spatial resolution [11]. One approach to increase the number of overlapping peptides is to employ multiple, complementary proteases [12]. However, HDX-MS is typically performed with short LC separation to minimize back-exchange (deuterium to hydrogen), thus more complex peptide mixtures are challenging to analyze due to signal overlap in the resulting mass spectra, a problem exacerbated by the broadened isotopic distributions form deuterium uptake [13].

A potential alternative approach to enhance spatial resolution in HDX-MS is gas-phase fragmentation of deuterated peptides via tandem mass spectrometry (MS/MS). In theory, such fragmentation can provide deuterium level information at individual amide groups [13]. However, collision induced dissociation (CID), the most common and effective MS/MS activation technique, has been shown to promote intramolecular hydrogen/deuterium migration during activation, thus erasing the original deuterium labeling pattern [14,15]. This behavior is consistent with the mobile proton model [16] for amide backbone cleavage in CID. In this model, proton charge carriers located at sites of high proton affinity transfer to the amide nitrogen upon collisional heating. Such protonation weakens amide bonds which become susceptible to nucleophilic attack from a nearby carbonyl oxygen, resulting in bond dissociation to form N-terminal *b*- and C-terminal *y*-type ions.

By contrast, electron capture dissociation (ECD) and electron transfer dissociation (ETD) are radical-driven activation techniques that do not involve significant vibrational excitation. Accordingly, limited amide hydrogen migration occurs and solution-phase deuterium labeling patterns can be preserved [15,17]. Thus, single residue spatial resolution is feasible with ECD/ETD. However, H/D scrambling can occur prior to MS/MS activation during peptide ion transfer through a mass spectrometer. Rand et al. showed that the magnitude of electrospray ion source voltages and the width of the quadrupole ion selection window prior to MS/MS can impart excess vibrational energy prior to ECD of peptide ions [15]. Careful tuning of such instrument parameters can reduce this undesired vibrational excitation; however, such tuning for "soft" conditions typically results in significant signal intensity decrease, requiring higher protein amounts and rendering acquisition of high quality ECD/ETD data challenging.

Because internal energy increase, originating from kinetic energy conversion during ion-neutral collisions, is distributed among all vibrational modes in a peptide (intramolecular vibrational energy redistribution (IVR) [18]), the amount of energy per bond decreases as molecular size increases [19]. Thus, we hypothesized that larger peptides may be more tolerant to typical ion source and ion isolation conditions, which allow higher ion transmission. In this Chapter, we explore this hypothesis with peptides of varying length, designed around the peptide P1 probe, developed by Rand and Jørgensen [20], that can be regioselectively deuterium labeled.

5.2 Experimental

5.2.1 Materials

Synthetic peptides P1 (H-HHHHHHIIKIIK-OH), P1S (H-HHHHHIIKIK-OH), and P1L2 (H-HHHHHHHHIIKIIKII-OH), were obtained from Genscript Corp (Piscataway, NJ). Water,

methanol, and formic acid of LC-MS grade were purchased from Fisher chemical (Fair Lawn, NJ). Deuterium oxide (D_2O), 99.9 atom % D, was purchased from Sigma-Aldrich (St. Louis, MO).

5.2.2 Hydrogen/Deuterium Exchange

Two mM peptide in H_2O was diluted into D_2O 20-fold at 4 ºC for 18 hours. Deuterated peptides were further diluted into electrospray ionization (ESI) solvent of 49:49:2 (v/v) methanol:water:formic acid, precooled to 4 ºC. This solution was immediately frozen with liquid nitrogen and stored at -80 ºC. The frozen sample was thawed in a 0 ºC ice bath and the solution was quickly transferred to a precooled syringe (Hamilton Co., Reno, NV) connected to precooled PEEK tubing. Too keep the syringe cool, the syringe and syringe pump were covered with an ice bag.

5.2.3 Mass Spectrometry

A 7 T SolariX quadrupole-Fourier transform ion cyclotron resonance (FT-ICR) mass spectrometer (Bruker Daltonics, Billerica, MA, USA), equipped with an Apollo II ESI source was used for ECD experiments. Sample loaded syringe was mounted on the instrument syringe pump and infused at a flow rate of 120 μL/h. Experiments were performed at three different ion source and ion isolation settings; “medium”, “harsh”, and “soft”. The corresponding instrument settings are listed in Table 5.1. Triply protonated precursor ions were selected by the quadrupole mass filter and accumulated for 0.4-0.8 s in the hexapole collision cell. For ECD, the cathode heating current was kept at 1.6 A. The ECD bias, ECD lens, and irradiation time were set to 0.8-1.5 V, 8-12 V, and 150-500 ms, respectively. ECD spectra were averaged over 20-50 scans for the m/a range of 200-1800.

Instrumental parameters	“Medium” conditions	"Harsh" conditions	"Soft" conditions
Drying gas flow	1.5 L/min	3.0 L/min	2.0 L/min
Nebulizing gas flow	0.8 bar	1.0 bar	1.1 bar
Drying gas temperature	120 °C	200 °C	40 °C
Capillary voltage (inlet)	-2.5 kV	-3.8 kV	-2.0 kV
Capillary exit voltage	200 V	280 V	50 V
Deflector plate voltage	170 V	265 V	40 V
Funnel 1 voltage	100 V	100 V	11 V
Skimmer 1 voltage	10 V	44 V	4 V
Funnel 2 voltage	8.0 V	8.0 V	5.5 V
Skimmer 2 voltage	4.0 V	4.0 V	4.0 V
Quadrupole isolation width	15 Da	10 Da	25 Da
Collision voltage	-0.8 V	-4.0 V	-0.5 V

Table 5.1 Instrument parameters for “medium”, “harsh”, and “soft” ion source and ion isolation conditions of a 7T SolariX FT-ICR mass spectrometer.

5.2.4 Data Analysis

The mass spectra were processed with DataAnalysis software (Bruker). The average masses of deuterated fragment ions and the charge-reduced species were calculated using Excel. Scrambling analysis was carried out as previously described [21]. Briefly, intrinsic exchange rates at each amide bond were calculated by HXPep software [22], kindly provided by Dr. Z. Zhang. This software is based on the intrinsic HDX rates established by Bai et al. [23]. These intrinsic rate constants provided the theoretical deuterium level for each ECD fragment ion under 0% scrambling conditions. A correction term was applied to account for additional deuterium incorporation into fast-exchanging sites due to the residual D_2O in the ESI solvent.

P1S Residues	k(1/min)	$t_{1/2}$(min)	pH_{min}
H2	7.425783	0.093343	-0.01
H3	0.178802	3.876619	1.46
H4	0.178802	3.876619	1.46
H5	0.178802	3.876619	1.46
I6	0.005777	119.9882	2.17
I7	0.00089	778.7176	2.66
K8	0.00321	215.9168	2.49
I9	0.001887	367.2332	2.64
K10	**0.003735**	**185.5602**	**2.62**

Table *5.2* Predicted intrinsic amide exchange rates for the peptide P1S (HHHHHIIKIK). The rate constants were calculated at 0 °C, pH 2.5 using HXPep software.

P1 Residues	k(1/min)	$t_{1/2}$(min)	pH_{min}	P1L2 Residues	k(1/min)	$t_{1/2}$(min)	pH_{min}
H2	7.425783	0.093343	-0.01	H2	7.425783	0.093343	-0.01
H3	0.178802	3.876619	1.46	H3	0.178802	3.876619	1.46
H4	0.178802	3.876619	1.46	H4	0.178802	3.876619	1.46
H5	0.178802	3.876619	1.46	H5	0.178802	3.876619	1.46
H6	0.178802	3.876619	1.46	H6	0.178802	3.876619	1.46
I7	0.005777	119.9882	2.17	H7	0.178802	3.876619	1.46
I8	0.00089	778.7176	2.66	H8	0.178802	3.876619	1.46
K9	0.00321	215.9168	2.49	I9	0.005777	119.9882	2.17
I10	0.001887	367.2332	2.64	I10	0.00089	778.7176	2.66
I11	0.00089	778.7176	2.66	K11	0.00321	215.9168	2.49
K12	0.003735	185.5602	2.62	I12	0.001887	367.2332	2.64
				I13	0.00089	778.7176	2.66
				K14	0.00321	215.9168	2.49
				I15	0.001887	367.2332	2.64
				I16	0.001164	595.4417	2.79

Table 5.3 *Predicted intrinsic amide exchange rates for the peptides P1(HHHHHHIIKIIK) and P1L2 (HHHHHHHHIIKIIKII). The rate constants were calculated at 0 °C, pH 2.5 using HXPep software.*

The total number of deuterium, D_{tot}, experimentally incorporated into a peptide was determined by measuring the difference in average mass of deuterated and non-deuterated charge reduced species following ECD of deuterated and non-deuterated peptide, respectively. The difference in average mass (Δm_{exp}) observed between analogous fragment ions from ECD of deuterated and non-deuterated peptide, respectively, was used for calculation of each fragment's experimental deuteration degree, d_{exp}:

Equation 5.1

$$d_{exp} = \Delta m_{exp} / D_{tot}$$

The theoretical deuterium level under 0% scrambling conditions, $d_{0\%}$, for each ECD fragment ion was predicted by the pseudo-first order kinetic model and the rate constants obtained by HXPep software. Theoretical 100% scrambling conditions, $d_{100\%}$, for each ECD fragment ion was calculated by the following equation:

Equation 5.2

$$d_{100\%} = {H_{Frag}}\Big/{H_{Pre}}$$

where H_{Frag} is the number of exchangeable hydrogen atoms in each fragment ion and H_{Pre} is the number of exchangeable hydrogens in the entire precursor ion. Both the charge state and sequence of fragment ions were taken into consideration when calculating H_{Frag} and H_{Pre} [24]. The percent H/D scrambling for each fragment ion was then calculated by the following equation:

Equation 5.3

$$\%\, Scrambling = \frac{(d_{exp} - d_{0\%})}{(d_{100\%} - d_{0\%})} \times 100\%$$

where d_{exp}, $d_{0\%}$, and $d_{100\%}$ indicate the experimentally observed deuteration level and the predicted deuteration level for 0% and 100% scrambling, respectively. Each H/D scrambling experiment was performed in triplicate.

5.3 Results and Discussion

Jørgensen and co-workers previously showed that the vibrational internal energy uptake during ionization and ion transmission of the deuterated 12-mer peptide P1 (HHHHHHIIKIIK) prior to ECD/ETD must be minimized to limit H/D scrambling[15].To examine our hypothesis that peptide length should impact H/D scrambling levels, we designed a shorter and a longer model peptide, P1S (HHHHHIIKIK) and P1L2 (HHHHHHHHHIIKIIKII), around the sequence of the P1 peptide [20]while maintaining the ability for regioselective deuterium labeling. P1S contains 10 amino acids and the intrinsic HDX rate constants for each amide bond, calculated using HXPep software, are listed in Table 5.2. P1L2 contains 16 amino acid residues and its intrinsic HDX rate constants, along with those of P1, are listed in Table 5.3. All three peptides were deuterated and back-exchanged into H_2O. The triply protonated charge states of these peptides were selected and subjected to ECD following the “medium”, “harsh”, and “soft” ion source and transfer conditions described in Table 5.1, respectively. ECD-generated singly-charged *c*-type fragment ions were used for H/D scrambling level calculations.

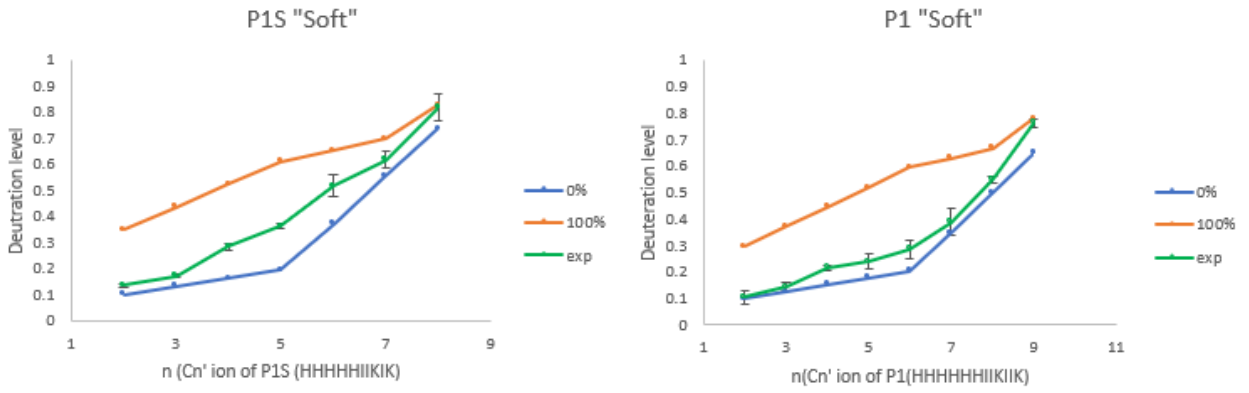

Figure 5.1 Deuteration levels of ECD-generated c-type fragment ions from P1S and P1 peptides under "soft" ion source and ion transfer conditions. Data were collected on a Bruker SolariX FT-ICR mass spectrometer.

Figure 5.1 illustrates observed deuteration levels for ECD-generated *c*-type fragment ions (in green), along with the theoretical levels for 0% (in blue) and 100% (in orange) scrambling, respectively, under "soft" ion transfer conditions. Error bars represent a single standard deviation for triplicate measurements. Instrument tuning to achieve such soft ion source conditions was based on previous work by Wang et al.[21] with some modifications. Similar to previous work, ion transfer conditions for which minimum H/D scrambling is observed was attained for most fragments from the P1 peptide (Fig. 5.1, right panel) [15,21]. However, these instrument settings results in 5-fold loss of signal and, thus, poor abundance of ECD fragment ions. For the shorter P1S peptide, the smallest observed *c*-type ions, c_2 and c_3, show a low degree (<15%) of H/D scrambling; however, this level of scrambling is higher than for the same ions generated from the P1 peptide. For larger fragment ions, a more noticeable difference is observed between the two peptides with a significant (but not complete) degree of scrambling observed for the shorter peptide (Fig. 5.1, left panel), even under "soft" ion transfer conditions. In particular, 89% scrambling was observed for the c_8 fragment from the P1S peptide. Similarly, the c_9 fragment ion from P1 shows

87% scrambling under these conditions. However, overall, significantly less scrambling is observed for the longer P1 peptide.

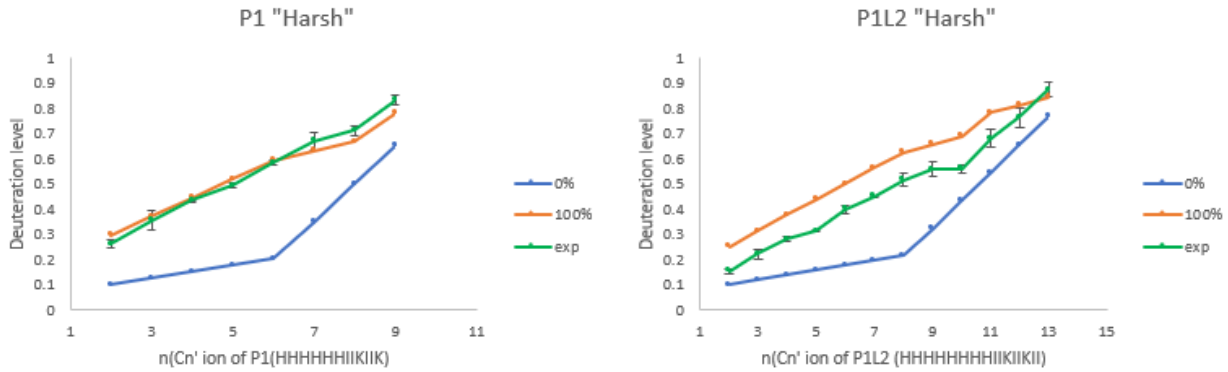

Figure 5.2 Deuteration levels of ECD-generated c-type fragment ions from P1 and P1L2 peptides under "Harsh" ion source and ion transfer conditions. Data were collected on a Bruker SolariX FT-ICR mass spectrometer.

Next, we tuned the ion source and ion transfer parameters to promote "harsh" conditions (Table 5.1) at which peptide signal abundance is high but P1 is known to undergo significant scrambling. Accordingly, nearly complete scrambling was observed for the P1 peptide (Figure 5.2, left panel). The experimentally observed deuteration levels of *c*-type fragment ions from the P1 peptide are in good agreement with previously reported data [15]. By contrast, interestingly, only partial scrambling was observed for the longer P1L2 peptide, even at these "harsh" conditions with an H/D scrambling of 35-75% for *c*-type fragment ions (Figure 5.2, right panel). These data are consistent with our hypothesis that larger peptides are more tolerant to typical "harsh" source conditions.

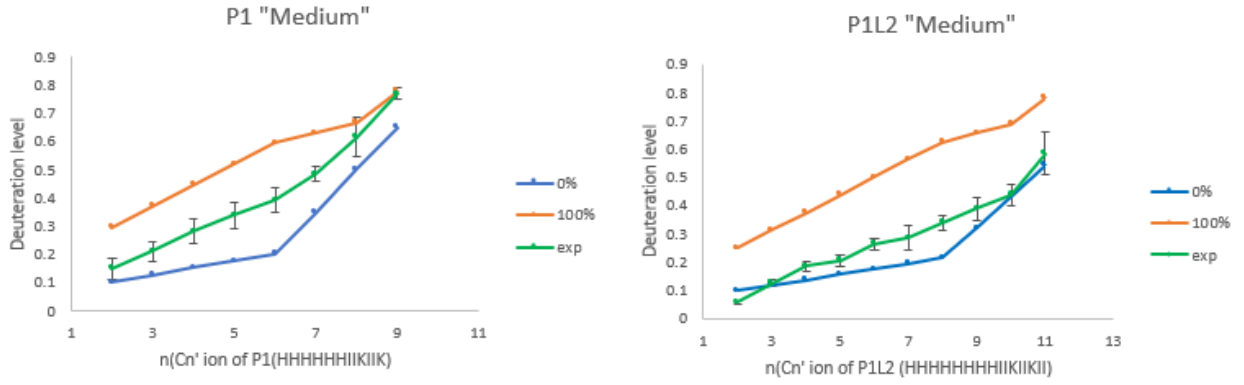

Figure 5.3 Deuteration levels of ECD-generated c-type fragment ions from P1S and P1 peptides under "Medium" ion source and ion transfer conditions. Data were collected on a Bruker SolariX FT-ICR mass spectrometer.

To further examine the tolerance of more "harsh" conditions at which higher signal abundance can be generated, we explored "medium" conditions, more gentle than those in Fig. 5.2 but harsher than those in Fig. 5.1. For P1, as expected, only partial scrambling was observed for ECD-generated *c*-type ions under these "medium" ion source and ion transfer conditions (Figure 5.3, left panel). Under these source settings, moderate signal abundance was achieved for each examined *c*-type ion compared with the poor abundance observed under "soft" conditions. For P1L2, experimentally observed deuteration levels under "medium" conditions show smaller deviations from the 0% scrambling curve, i.e., an overall lower degree of scrambling, again consistent with our hypothesis. However, there were some limitations to these experiments, including relatively low ionization efficiency for P1L2. The increased number of fragmentation channels for the larger peptide also results in the available total signal being more diluted. The P1L2 c_2 fragment ion showed a significantly lower deuteration level than the theoretical 0% scrambling curve, which may be due to the low ion abundance. Nevertheless, the overall trends in the presented data support our hypothesis that longer peptides are less likely to undergo H/D scrambling prior to ECD/ETD under more typical ion source and transfer conditions.

5.4 Conclusion

Under “soft” ion source and transfer conditions, the 10 amino acid residue peptide P1S showed significantly more scrambling than the original 12 amino acid residue P1 peptide. In addition, under “harsh” conditions, where P1 shows nearly 100% scrambling, the 16 amino acid residue P1L2 underwent only partial scrambling. Under “medium” ion source and ion transfer conditions at which improved signal abundance is achieved, P1 showed partial scrambling. On the other hand, the longer P1L2 peptide showed only limited scrambling under the same conditions. Overall, we found a correlation between the degree of H/D scrambling and peptide length. Further studies are needed to establish the optimum peptide size for maximum ion abundance and sequence coverage while maintaining low scrambling levels; however our preliminary findings strongly suggest a sweet spot for middle-down HDX implementations.

5.5 Acknowledgement

This work was supported by the National Science Foundation CHE 1609840 and the University of Michigan. I would like to thank Dr. Qingyi Wang for H/D scrambling calculation help. I would also like to thank Dr. Zhang for kindly providing the HXPEP software.

5.6 References

[1] Molday, R.S.; Englander, S.W.; Kallen, G. Primary Structure Effects on Peptide Group Hydrogen Exchange*. *Biochemistry*, **1972**, *11*, 150–158.

[2] Pan, J.; Han, J.; Borchers, C.H.; Konermann, L. Hydrogen/Deuterium Exchange Mass Spectrometry with Top-down Electron Capture Dissociation for Characterizing Structural Transitions of a 17 KDa Protein. *J. Am. Chem. Soc.*, **2009**, *131*, 12801–12808.

[3] Suchanova, B.; Tuma, R. Folding and Assembly of Large Macromolecular Complexes Monitored by Hydrogen-Deuterium Exchange and Mass Spectrometry. *Microb. Cell Fact.*, **2008**, *7*.

[4] Mysling, S.; Betzer, C.; Jensen, P.H.; Jørgensen, T.J. Characterizing the Dynamics of α-Synuclein Oligomers Using Hydrogen/Deuterium Exchange Monitored by Mass Spectrometry. *Biochemistry*, **2013**, *52*, 9097–9103.

[5] Houde, D.; Arndt, J.; Domeier, W.; Berkowitz, S.; Engen, J.R. Characterization of IgG1

Conformation and Conformational Dynamics by Hydrogen/Deuterium Exchange Mass Spectrometry. *Anal. Chem.*, **2009**, *81*, 2644–2651.
[6] Garcia, R.A.; Pantazatos, D.; Villarreal, F.J. Hydrogen/Deuterium Exchange Mass Spectrometry for Investigating Protein-Ligand Interactions. *Assay Drug Dev. Technol.*, **2004**, *2*, 81–91.
[7] Burke, J.E.; Hsu, Y.; Deems, R.A.; Li, S.; Woods, V.L.; Dennis, E.A. A Phospholipid Substrate Molecule Residing in the Membrane Surface Mediates Opening of the Lid Region in Group IVA Cytosolic Phospholipase A2. *J. Biol. Chem.*, **2008**, *283*, 31227–31236.
[8] Wales, T.E.; Engen, J.R. Hydrogen Exchange Mass Spectrometry for the Analysis of Protein Dynamics. *Mass Spectrom. Rev.*, **2006**, *25*, 158–170.
[9] Woods, V.L.; Hamuro, Y. High Resolution, High-Throughput Amide Deuterium Exchange-Mass Spectrometry (DXMS) Determination of Protein Binding Site Structure and Dynamics: Utility in Pharmaceutical Design. *J. Cell. Biochem.*, **2001**, *84*, 89–98.
[10] Karch, K.R.; Coradin, M.; Zandarashvili, L.; Kan, Z.Y.; Gerace, M.; Englander, S.W.; Black, B.E.; Garcia, B.A. Hydrogen-Deuterium Exchange Coupled to Top- and Middle-Down Mass Spectrometry Reveals Histone Tail Dynamics before and after Nucleosome Assembly. *Structure*, **2018**, *26*, 1651-1663.e3.
[11] Wei, H.; Tymiak, A.A.; Chen, G. Introduction Hydrogen/Deuterium Exchange Mass Spectrometry for Protein Higher-Order Structure Characterization. In *Characterization of Protein Therapeutics using Mass Spectrometry*; Chen, G., Ed.; Springer: New York, **2013**; pp. 305–341.
[12] Rand, K.D. Pinpointing Changes in Higher-Order Protein Structure by Hydrogen/Deuterium Exchange Coupled to Electron Transfer Dissociation Mass Spectrometry. *Int. J. Mass Spectrom.*, **2013**, *338*, 2–10.
[13] Jensen, P.F.; Rand, K.D. Gas-Phase Fragmentation of Peptides to Increase the Spatial Resolution of the Hydrogen Exchange Mass Spectrometry Experiment. In *Hydrogen Exchange Mass Spectrometry of Proteins*; Weis, D.D., Ed.; John Wiley & Sons, Ltd, **2016**; pp. 127–147.
[14] Demmers, J.A.A.; Rijkers, D.T.S.; Haverkamp, J.; Killian, J.A.; Heck, A.J.R. Factors Affecting Gas-Phase Deuterium Scrambling in Peptide Ions and Their Implications for Protein Structure Determination. *J. Am. Chem. Soc.*, **2002**, *124*, 11191–11198.
[15] Rand, K.D.; Adams, C.M.; Zubarev, R.A.; Jørgensen, T.J.D. Electron Capture Dissociation Proceeds with a Low Degree of Intramolecular Migration of Peptide Amide Hydrogens. *J. Am. Soc. Mass Spectrom.*, **2008**, *130*, 1341–1349.
[16] Wysocki, V.H.; Tsaprailis, G.; Smith, L.L.; Breci, L.A. Mobile and Localized Protons: A Framework for Understanding Peptide Dissociation. *J. Mass Spectrom.*, **2000**, *35*, 1399–1406.
[17] Zehl, M.; Rand, K.D.; Jensen, O.N.; Jørgensen, T.J.D. Electron Transfer Dissociation Facilitates the Measurement of Deuterium Incorporation into Selectively Labeled Peptides with Single Residue Resolution. *J. Am. Chem. Soc*, **2008**, *130*, 17453–17459.
[18] Lifshitz, C. Intramolecular Vibrational Energy Redistribution and Ergocity of Biomolecular Dissociation. In *Principle of Mass Spectrometry Applied to Biomolecules*; Laskin, J.; Lifshitz, C., Eds.; John Wiley and Sons, Inc, **2006**; pp. 239–275.
[19] Sleno, L.; Volmer, D.A. Ion Activation Methods for Tandem Mass Spectrometry. *J. Mass Spectrom.*, **2004**, *39*, 1091–1112.

[20] Rand, K.D.; Jørgensen, T.J.D. Development of a Peptide Probe for the Occurrence of Hydrogen (1 H/ 2 H) Scrambling upon Gas-Phase Fragmentation. *Anal. Chem.*, **2007**, *79*, 8686–8693.
[21] Wang, Q.; Borotto, N.B.; Håkansson, K. Gas-Phase Hydrogen/Deuterium Scrambling in Negative-Ion Mode Tandem Mass Spectrometry. *J. Am. Soc. Mass Spectrom.*, **2019**.
[22] Zhang, Z.; Li, W.; Logan, T.M.; Li, M.; Marshall, A.G. Human Recombinant [C22A] FK506-Binding Protein Amide Hydrogen Exchange Rates from Mass Spectrometry Match and Extend Those from NMR. *Protein Sci.*, **1997**, *6*, 2203–2217.
[23] Bai, Y.; Milne, J.S.; Mayne, L.; Englander, S.W. Primary Structure Effects Hydrogen Exchange on Peptide Group. *Proteins Struct. Funct. Genet.*, **1993**, *17*, 75–86.
[24] Petrotchenko, E. V.; Borchers, C.H. HDX Match Software for the Data Analysis of Top-Down ECD-FTMS Hydrogen/Deuterium Exchange Experiments. *J. Am. Soc. Mass Spectrom.*, **2015**, *26*, 1895–1898.

Chapter 6

Conclusions and Future Directions

6.1 Dissertation Summary

In this dissertation, we presented novel mechanistic insights for improved characterization of protein structure through radical-driven tandem mass spectrometry techniques. In Chapter 2, the influence of charge state on FRIPS dissociation pathways and the effects of replacing proton charge carriers to promote radical-driven pathways in FRIPS were discussed. As the charge state increases, fragment ions generated by undesired mobile proton-driven pathways increase. Peptides lacking basic amino acid residues predominantly dissociate via mobile proton pathways in their protonated states. We showed that alternative metal ion charge carriers such as sodium and calcium ions can promotes radical-driven pathways.

Peptide derivatization strategies for tyrosine sulfation identification are described in Chapters 3 and 4. In Chapter 3, guanidination and cysteine modification approaches to enhance the stability of sulfated peptides in positive ion mode are discussed. Arginine- or guanidinated lysine-containing sulfopeptides showed higher stability in positive ion mode MS due to lower proton mobility afforded by these high proton affinity groups. Such chemical moieties may also form salt bridges with the sulfated tyrosine, further stabilizing this group. For standard, acidic

sulfopeptides, N-terminal guanidination was shown to improve the gas-phase stability. ECD at lower charge state and ETD at higher charge state allowed localization of tyrosine sulfation with limited sulfonate loss for these modified peptides. ETD of sulfopeptides with the fixed charge cysteine modification 1-methyl-2-vinyl-pyridine- generated informative, sulfate-containing fragment ions, allowing determination of the tyrosine sulfation site in a peptide with multiple tyrosine residues.

Sulfotyrosine site determination in peptides with multiple tyrosine residues was further explored in Chapter 4 via a variety of radical-driven MS/MS methods along with peptide derivatization strategies. This work aimed to determine the feasibility of characterizing the sulfation site in a tyrosylprotein sulfotransferase 1 (TPST1) tryptic sulfopeptide, detected in in a proteomic analysis of rat liver Golgi. This peptide is singly sulfated but contains three tyrosine residues for three possible sulfation sites. For the synthetic TPST1 peptide with sulfation on the third tyrosine, TPST1_C, the sulfation site could be determined via either ECD or ETD without chemical derivatization. However, synthetic peptides sulfated on the first and second tyrosine, respectively, (TPST1_A and TPST1_B) could not be differentiated due to lack of characteristic fragment ions in ECD/ETD. Lysine guanidination and N-terminal+lysine guanidination did not overcome this issue for these two peptides, possibly because chemical derivatization alters the peptide conformations to include more intramolecular interactions, preventing detection of fragment ions from those areas of the peptides. N-terminal fixed charge modification with a DABCO-based tag greatly improved the stability of these sulfopeptides and resulted in limited SO_3 loss, even in EThcD. However; observed sulfated fragment ions were insufficient to unambiguously determine the sulfation site. By contrast, negative ion mode FRIPS resulted in

characteristic, sulfated fragment ions that revealed the exact tyrosine sulfation sites in TPST1_A and B.

In Chapter 5, the extent of H/D scrambling as a function of peptide length was examined. ECD was used to probe the degree of scrambling for three regioselective model peptides, P1S (10-mer), P1 (12-mer), and P1L2 (16-mer) under three ion source and ion transfer conditions, “soft”, “medium”, and “harsh”. Even at the “soft” conditions, P1S showed considerable scrambling compared with P1, which underwent minimum scrambling. Under “harsh” conditions, P1L2 showed partial scrambling whereas P1 showed complete scrambling. Finally, under “medium” ion source and ion transfer conditions, both P1 and P1L2 showed partial scrambling but a lower degree of scrambling was observed for P1L2. These data confirm our hypothesis that longer peptides are more tolerant to harsher source conditions where improved signal abundance is observed. This work suggests that a middle-down approach to protein HDX-MS/MS is preferred to maximize spatial resolution.

6.2 Future Directions

6.2.1 Identification of the Structural Difference Between TPST1 Peptides through Ion Mobility-Mass spectrometry

In Chapter 4, highly different fragmentation behaviors were observed for the TPST1_A, B, and C sulfopeptide isomers. In addition chemical derivatization further altered fragmentation with extensive guanidination decreasing ECD and ETD fragmentation efficiency. It has been reported that ECD/ETD dissociation efficiency depends on protein/peptide conformation; for example, peptide backbone bond dissociation in the protein interior is not observed. This behavior has been proposed to be due to intramolecular hydrogen bonding preventing complementary product ions

from separating but can also be explained through lack of nearby protons for electron recombination [1,2]. In order to understand structural effects influencing the fragmentation patterns between sulfopeptide isomers and between modified- and unmodified sulfopeptides, their collisional cross section (CCS) can be measured by ion mobility separation coupled with mass spectrometry [3]. Figure 6.1 shows preliminary raw ion mobility data for unmodified TPST1_A, acquired with an Agilent 6560 c IM-Q-TOF instrument. Two to three drift time values are observed in these data; however, due to insufficient tuning optimization and high peptide concentration, poor IM resolution was obtained. the ion source and drift tube parameters will require particular tuning to minimize loss of the highly labile sulfate group. With careful tuning and proper concentration, we expect that accurate CCS values for the modified- and unmodified peptides can be measured to revealing their conformational differences.

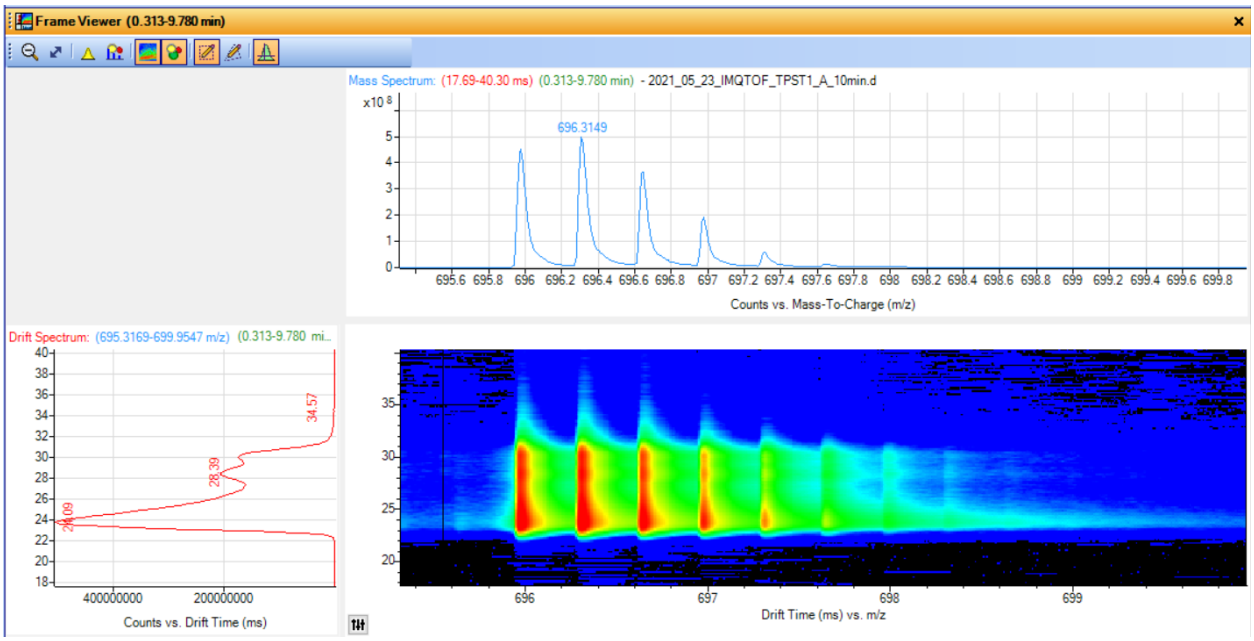

Figure 6.1 Raw ion mobility data for doubly protonated TPST1_A.

6.2.2 Automated HDX Coupled with LC-IM-ECD-MS/MS

In Chapter 5, longer peptides showed less scrambling under the same ion source and ion transfer conditions compared with shorter peptides. Therefore, we expect that a middle-down approach will minimize H/D scrambling under typical instrument conditions, without compromising ion signal. Borchers and co-workers recently developed an HDX-MS/MS middle-down approach [4]. With offline pepsin digestion, larger peptides, between 12 and 25 kDa, were obtained and ETD resulted in ~95% sequence coverage [4]. However, offline pepsin digestion typically leads to a higher level of back exchange and lower reproducibility than online digestion. We anticipate that a fully automated HDX platform, LEAP HDX PAL, coupled with an Agilent LC-IM-Q-TOF system will improve reproducibility and throughput [5]. Figure 6.2 shows an LC chromatogram of online pepsin-digested PikAIII module 5, a protein with a molecular weight around 163 kDa. Extensive digestion is observed for this relatively larger protein, i.e., observed peptides are too short to be considered "middle-down" level. However, with the automated system, the online pepsin digestion time can be conducted under controlled settings, including control of flow rate, pressure, and online digestion time. The Agilent 6560 IM Q-TOF mass spectrometer is equipped with an e-MSion ExD cell that will improve spatial resolution of larger peptides from such experiments.

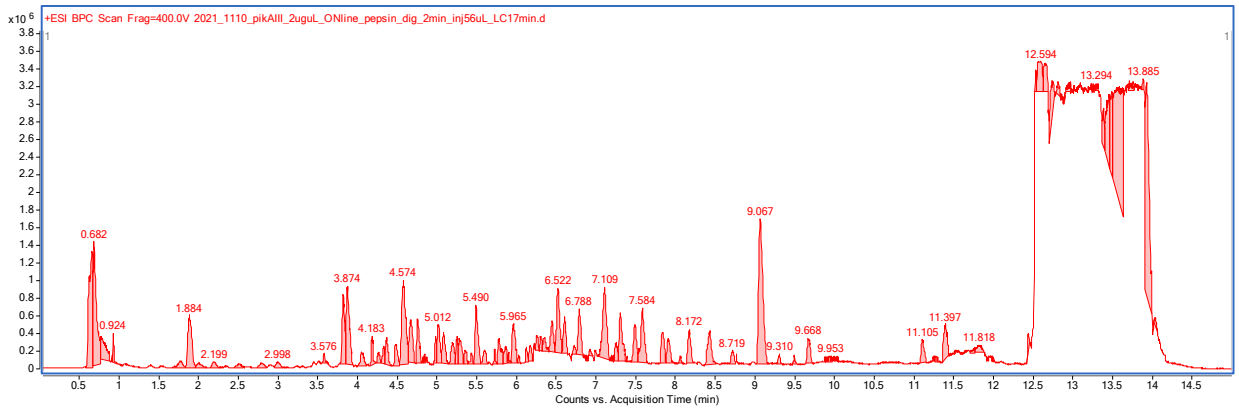

Figure 6.2 LC chromatogram of online pepsin digested PikAIII module 5 protein. Digestion time was 2 minutes and the total LC elution time was 17 minutes.

6.2.3 Sulfopeptide Enrichment and Peptide Derivatization for Proteomic Analysis

In Chapters 3 and 4, peptide derivatization strategies were employed for synthetic sulfopeptides to improve sulfopeptide stability during MS and MS/MS. These strategies improved the elucidation of tyrosine sulfation sites, even in peptides with multiple tyrosine residues. Application of these strategies at the proteome level would transform tyrosine sulfation analysis [6]. In future work, proteins purified from rat Golgi membrane will be tryptically digested and chemically derivatized. Similar to common proteomics workflows, cysteine alkylation will be performed prior to trypsin digestion. To minimize ion suppression from non-sulfopeptides, immobilized metal affinity chromatography (IMAC) [7] or metal oxide affinity chromatography (MOAC) [6] can be employed to enrich tryptic sulfopeptides. N-terminal and/or lysine modification of enriched sulfopeptides will both be explored to improve sulfate stability. We propose that a decision tree-tandem mass spectrometry method [8], implemented on an Orbitrap Fusion Lumos mass spectrometery coupled with an nLC system may maximize sulfopeptide identification. In this method (Figure 6.3), HCD activation is performed at the MS^2 level. Based on the outcome of this MS^2 event, a decision tree [8,9] will trigger a subsequent ETD event when HCD MS/MS mass spectra exhibit neutral sulfonate loss (80 Da) from the precursor ion. In the

absence of this neutral loss, ETD will not be triggered for maximum throughput. As described in Chapters 3 and 4, ETD is a suitable method for localizing tyrosine sulfation as limited SO_3 loss can occur.

Figure 6.3 Proposed experimental workflow for tyrosine sulfation identification by decision tree-driven tandem mass spectrometry. Red triangle represents labile PTM.

Mass spectra may be processed by either Thermo Proteome Discoverer or MaxQuant as illustrated by Kweon et al. [6]. We anticipate that the integration of chemical derivatization, enrichment, and decision tree-tandem mass spectrometry will greatly enhance tyrosine sulfation analysis, including unambiguous identification of tyrosine sulfation sites. Furthermore, this approach can be further adapted for identification of other labile PTMs or protein adducts, such as benzo[a]pyrene diol epoxide (BPDE) [10].

6.2.4 Peptide Size Effect on the Degree of Hydrogen/Deuterium Scrambling

In the work described in Chapter 5, the H/D scrambling degree as function of peptide length was determined for three model regioselective peptides. Further studies are required to fully understand the deuterium uptake and gas-phase structure of each model peptide. For example, peptides ending in lysine, such as the -IIK end pattern in peptides P1 and P1S, are known to adopt helical structures in the gas phase [11]. Such structures may show different scrambling behavior than less structures peptides. For consistency, P1L2 should be modified to also end with lysine. Furthermore, sequences could be scrambled to avoid the lysine capping effect.

Insights into the gas-phase structures of these peptides can be obtained via IM-MS experiments and molecular dynamics (MD) simulations. The combination of IM-MS and MD simulation will deepen our insights into H/D scrambling behavior as function of peptide length.

6.3 References

[1] Adams, C.M.; Kjeldsen, F.; Zubarev, R.A.; Budnik, B.A.; Haselmann, K.F. Electron Capture Dissociation Distinguishes a Single D-Amino Acid in a Protein and Probes the Tertiary Structure. *J. Am. Soc. Mass Spectrom.*, **2004**, *15*, 1087–1098.

[2] Lopez-Clavijo, A.F.; Duque-Daza, C.A.; Creese, A.J.; Cooper, H.J. Electron Capture Dissociation Mass Spectrometry of Phosphopeptides: Arginine and Phosphoserine. *Int. J. Mass Spectrom.*, **2015**, *390*, 63–70.

[3] May, J.C.; Mclean, J.A. Ion Mobility-Mass Spectrometry: Time-Dispersive Instrumentation. *Anal. Chem.*, **2015**, *87*, 1422–1436.

[4] Pan, J.; Zhang, S.; Chou, A.; Borchers, C.H. Higher-Order Structural Interrogation of Antibodies Using Middle-down Hydrogen/Deuterium Exchange Mass Spectrometry. *Chem. Sci.*, **2016**, *7*, 1480–1486.

[5] Hamuro, Y.; Coales, S.J.; Woods, V. Protein-Targeting Drug Discovery Guided by Hydrogen/Deuterium Exchange Mass Spectrometry (DXMS). *Mass Spectrom. Med. Chem.*, **2007**, *36*, 377–398.

[6] Kweon, H.K.; Kong, A.T.; Hersberger, K.E.; Huang, S.; Nesvizhskii, A.I.; Wang, Y.; Håkansson, K.; Andrews, P.C. A Novel Analytical Framework for Sulfoproteomics Reveals Tyrosine Sulfation and Phosphorylation Crosstalk in the Golgi. *Manuscr.*

[7] Capriotti, A.L.; Cerrato, A.; Laganà, A.; Montone, C.M.; Piovesana, S.; Zenezini Chiozzi, R.; Cavaliere, C. Development of a Sample-Preparation Workflow for Sulfopeptide Enrichment: From Target Analysis to Challenges in Shotgun Sulfoproteomics. *Anal. Chem.*, **2020**, *92*, 7964–7971.

[8] Swaney, D.L.; McAlister, G.C.; Coon, J.J. Decision Tree-Driven Tandem Mass Spectrometry for Shotgun Proteomics. *Nat. Methods*, **2008**, *5*, 959–964.

[9] Ferries, S.; Perkins, S.; Brownridge, P.J.; Campbell, A.; Eyers, P.A.; Jones, A.R.; Eyers, C.E. Evaluation of Parameters for Confident Phosphorylation Site Localization Using an Orbitrap Fusion Tribrid Mass Spectrometer. *J. Proteome Res.*, **2017**, *16*, 3448–3459.

[10] Chung, M.K.; Regazzoni, L.; McClean, M.; Herrick, R.; Rappaport, S.M. A Sandwich ELISA for Measuring Benzo[a]Pyrene-Albumin Adducts in Human Plasma. *Anal. Biochem.*, **2013**, *435*, 140–149.

[11] Hudgins, R.R.; Jarrold, M.F. Helix Formation in Unsolvated Alanine-Based Peptides: Helical Monomers and Helical Dimers. *J. Am. Chem. Soc*, **1999**, *121*, 3494–3501.